THERMODYNAMIC AND DYNAMIC EVALUATIONS ON THE MISCIBILITY OF GAS INJECTION FOR ENHANCED OIL RECOVERY

Tetsuo Mineiro Miyakawa

Dissertação de Mestrado apresentada ao Programa de Pós-graduação em Engenharia Química, COPPE, da Universidade Federal do Rio de Janeiro, como parte dos requisitos necessários à obtenção do título de Mestre em Engenharia Química.

Orientadores: Frederico Wanderley Tavares
Victor de Souza Rios

Rio de Janeiro
Abril de 2023

THERMODYNAMIC AND DYNAMIC EVALUATIONS ON THE MISCIBILITY OF GAS INJECTION FOR ENHANCED OIL RECOVERY

Tetsuo Mineiro Miyakawa

DISSERTAÇÃO SUBMETIDA AO CORPO DOCENTE DO INSTITUTO ALBERTO LUIZ COIMBRA DE PÓS-GRADUAÇÃO E PESQUISA DE ENGENHARIA (COPPE) DA UNIVERSIDADE FEDERAL DO RIO DE JANEIRO COMO PARTE DOS REQUISITOS NECESSÁRIOS PARA A OBTENÇÃO DO GRAU DE MESTRE EM CIÊNCIAS EM ENGENHARIA QUÍMICA.

Examinada por:

Prof. Frederico Wanderley Tavares, D.Sc.

Eng. Victor de Souza Rios, D.Sc.

Eng. Rogério de Oliveira Espósito, D.Sc

Eng. José Sérgio de Araujo Cavalcante Filho, D.Sc.

Prof. Frederico de Araujo Kronemberger, D.Sc.

Prof. Márcio Luis Lyra Paredes, D.Sc.

RIO DE JANEIRO, RJ – BRASIL
ABRIL DE 2023

Miyakawa, Tetsuo Mineiro

THERMODYNAMIC AND DYNAMIC EVALUATIONS ON THE MISCIBILITY OF GAS INJECTION FOR ENHANCED OIL RECOVERY/Tetsuo Mineiro Miyakawa. – Rio de Janeiro: UFRJ/COPPE, 2023.

XX, 118 p.: il.; 29,7cm.

Orientadores: Frederico Wanderley Tavares

Victor de Souza Rios

Dissertação (mestrado) – UFRJ/COPPE/Programa de Engenharia Química, 2023.

Referências Bibliográficas: p. 93 – 99.

1. Miscibility. 2. Gas Injection. 3. EOR. 4. Reservoir Simulation. I. Tavares, Frederico Wanderley *et al.* II. Universidade Federal do Rio de Janeiro, COPPE, Programa de Engenharia Química. III. Título.

This thesis is dedicated in memory of my mother, whose unwavering commitment, hard work, and determination served as a model for me throughout my life, including in my academic pursuits.

Acknowledgments

Words cannot express my appreciation for Dr. Victor Rios, whose immeasurable patience, commitment, and involvement contributed significantly to this research. I could not have proceeded on this path without the guidance and knowledge freely supplied by Drs. Rogério Espósito and Sergio Cavalcante Filho. I would also like to convey my sincere appreciation to Dr. Frederico Tavares for his instruction, discussion, and patience during the development of this work. Additionally, these professionals, whom I am pleased to call my friends, have contributed significantly to the progression of this thesis and my personal growth.

I would like to also thank Dr. Frederico Kronemberger for his valuable comments and contributions to the qualifying and examination committees. And also for Dr. Márcio Paredes for his inputs and suggestions on the examination committees.

The professors from COPPE/PEQ deserve my thanks for sharing their expertise, as well as the personnel whose willingness and assistance made administrative work and lessons simpler.

Furthermore, I am grateful to my peers from PEQ, especially the 2018 and 2019 students who share this route, for their support, feedback sessions, and countless hours spent studying together.

I am also grateful to Petrobras (Petróleo Brasileiro S.A.) and my former immediate managers, MSc. Luciana Santos, MSc. Bruno Moczydlower, Thiago Coutinho, and Tiago Homem, for investing in my development and providing the necessary support for my part-time research. In addition, I am indebted to numerous colleagues at this great company, whose advice, training, and support have had a direct impact on my professional trajectory; however, I will not make the mistake of attempting to name each and every one of these brilliant professionals.

Lastly, I would be remiss not to mention my spouse, Kalenne Brilhante. Your belief in me has kept my spirits and motivation strong throughout this endeavor.

All models are wrong, but some are useful (George E. P. Box)

Resumo da Dissertação apresentada à COPPE/UFRJ como parte dos requisitos necessários para a obtenção do grau de Mestre em Ciências (M.Sc.)

AVALIAÇÃO TERMODINÂMICA E DINÂMICA DA MISCIBILIDADE NA INJEÇÃO DE GÁS PARA RECUPERAÇÃO AVANÇADA

Tetsuo Mineiro Miyakawa

Abril/2023

Orientadores: Frederico Wanderley Tavares
Victor de Souza Rios

Programa: Engenharia Química

O período de injeção de gás no método WAG aumenta a eficiência de deslocamento do óleo para os poços produtores por, dentre vários fatores, reduzir a viscosidade do óleo, acessar poros de menor diâmetro e remover/reduzir tensão interfacial entre o gás injetado e o óleo deslocado na rocha porosa. Avaliar a efetividade da injeção de gás ou WAG como método de recuperação é complexa pela indisponibilidade de medições no meio poroso e ausência de medições diretas de subsuperfície, pelos seus altos custos. Sendo assim, algumas informações de campo podem ser adquiridas em superfície para avaliar seu desempenho, como injetar traçadores químicos e monitorar sua produção ou, como este trabalho propõe, análises laboratoriais do óleo produzido.

Este trabalho analisou minuciosamente a composição do óleo produzido sob injeção de gás em condições miscível e imiscível. O objetivo foi identificar padrões de alteração na composição do óleo em cada condição de miscibilidade e identificar como as medições de superfície podem trazer informações do deslocamento do fluido no meio poroso. Os indicadores encontrados foram capazes de distinguir os cenários de miscibilidade e foram submetidos a testes de sensibilidade em relação aos principais parâmetros do escoamento, como formato da permeabilidade relativa, quantidade de óleo móvel e alteração de viscosidade. Adicionalmente, o efeito da alteração da composição no meio poroso foi avaliado durante o escoamento através das alterações dos envelopes de fases. Os indicadores se mostraram uma valiosa e pouco dispendiosa forma de adquirir informações relevantes para monitoramento da injeção de gás como método de recuperação.

Abstract of Dissertation presented to COPPE/UFRJ as a partial fulfillment of the requirements for the degree of Master of Science (M.Sc.)

THERMODYNAMIC AND DYNAMIC EVALUATIONS ON THE MISCIBILITY OF GAS INJECTION FOR ENHANCED OIL RECOVERY

Tetsuo Mineiro Miyakawa

April/2023

Advisors: Frederico Wanderley Tavares
Victor de Souza Rios

Department: Chemical Engineering

The gas injection period in the WAG method increases the efficiency of oil displacement to the producing wells by reducing oil viscosity, accessing smaller pores, and removing/reducing the interfacial tension between the injected gas and the displaced oil in porous rock, among other factors. However, evaluating the effectiveness of gas injection or WAG as a recovery method is complex due to the unavailability of measurements in the porous medium and the high costs of direct subsurface measurements. Therefore, some field information can be acquired on the surface to evaluate its performance, such as injecting chemical tracers and monitoring production, or, as proposed in this work, analyzing the composition of the produced oil through laboratory chromatography.

This work has thoroughly analyzed the composition of oil produced under gas injection, under miscible and immiscible conditions. The objective was to identify patterns of change in oil composition in each miscibility condition and to identify how surface measurements can provide information on the displacement occurring in the porous medium. The indicators found were able to distinguish the miscibility scenarios and were submitted to sensitivity tests in relation to the main flow parameters, such as the relative permeability format, the amount of mobile oil, and changes in the phases' viscosity. Additionally, the composition alteration in the porous medium was evaluated during the flow analysis by analyzing the changes in two-phase envelopes. The indicators proved valuable and inexpensive to acquire relevant information for monitoring gas injection as a recovery method.

Contents

List of Figures

List of Tables

List of Abbreviations

A_t	Cross sectional area, p. 24
E_A	Areal Sweep Efficiency, p. 21
E_D	Displacement Efficiency, p. 21
E_H	Vertical Sweep Efficiency, p. 21
E_R	Recovery Efficiency, p. 21
E_V	Volumetric Sweep Efficiency, p. 21
$MMP2_2$	Minimum Miscibility Pressure for ResFluid2 and Mix2, p. 87
$MMP3_2$	Minimum Miscibility Pressure for ResFluid2 and Mix3, p. 87
S_g	Gas Saturation, p. 13
S_{or}	Residual oil saturation, p. 19
S_o	Oil Saturation, p. 13
S_{wi}	Irreducible water saturation, p. 19
S_w	Water Saturation, p. 13
V_B	Bulk Volume, p. 13
V_p	Porous Volume, p. 13
V_b	Bulk volume of a given control volume, p. 23
Φ_{ij}	Fugacity Coefficient of component i in j phase, p. 7
γ	Specific weight, p. 24
μ	Viscosity, p. 24
μ_g	Gas Viscosity, p. 11

μ_i	Chemical Potential of *i*, p. 5
μ_i^0	Chemical Potential Pure substance, p. 7
μ_o	Oil Viscosity, p. 11
$\overline{\kappa_{ij}}$	Dispersion tensor for component i for phase j, p. 23
ϕ	Porosity, p. 13
ρ	density, p. 11
σ	Interfacial Tension, p. 15
$\widehat{f}_i$	Fugacity of component *i* in mixture, p. 7
ξ_j	molar density of the phase j, p. 23
k_j	Effective Permeability of phase "j", p. 17
k_{rg}	Relative Permeability of gas phase, p. 18
k_{rj}	Relative Permeability of phase "j", p. 17
k_{ro} at S_{wi}	Oil relative permeability at water irreducible saturation, p. 20
k_{ro}	Relative Permeability of oil phase, p. 18
k_{rw} at S_{or}	Water relative permeability at oil residual saturation, p. 20
k_{rw}	Relative Permeability of water phase, p. 18
m_j	Mass of phase *j*, p. 25
n_c	Number of components, p. 22
n_p	Number of phases, p. 22
q_j	Molar flow rate of component i on well, p. 23
q_m	Mass flow rate, p. 22
u_a	Apparent velocity of flow, p. 24
u_j	Superficial velocity (flux) of phase j, p. 23
x_{ij}	Mole fraction of component i in phase j, p. 23
x_i	Mole fraction of component *i* in liquid phase, p. 7

y_i	Mole fraction of component i in vapor phase, p. 7
ANP	Agência Nacional do Petroleo - National Petroleum Agency, p. 2
A	Helmholtz free energy, p. 5
BIC	Binary Interaction Coefficient, p. 9
Bg	Gas Formation Volume Factor, p. 11
Bo	Oil Formation Volume Factor, p. 11
CCE	Constant Composition Expansion, p. 11
Diflib	Differential Liberation, p. 11
EOR	Enhanced Oil Recovery, p. 1
EOS	Equation of State, p. 8
FAWAG	Foam Assisted-WAG, p. 1
FCM	First-Contact Miscible, p. 29
GOR	Gas Oil Ratio, p. 11
G	Gibbs free energy, p. 5
HCPV	Hydrocarbon Pore Volume, p. 32
HWAG	Hybrid-Water Alternating Gas, p. 1
H	Enthalpy, p. 5
IFT	Interfacial tension, p. 29
IPV	Injected Pore Volume, p. 53
K	Permeability, p. 13
MCM	Multiple-Contact Miscible, p. 29
MMP	Minimum Miscibility Pressure, p. 29
M	Mobility Ratio, p. 20
Mix1	Injected Gas Composition with 50% CO_2 and 50% of C_1, p. 49
Mix2	Injected Gas Composition with 100% of C_1, p. 49

Mix3	Injected Gas Composition with 10% CO_2 and 90% of C_1, p. 50
N	Number of mols, p. 5
OOIP	Original Oil In Place, p. 32
PWAG	Polymer-Water Alternating Gas, p. 1
P	Pressure, p. 5
Q	Volumetric rate, p. 24
RF	Recovery Factor, p. 53
R	Universal Gas Constant, p. 8
SG	Specific Gravity, p. 11
SRK	Soave-Redlich-Kwong Equation, p. 8
SWAG	Simultaneous Water and Gas Injection, p. 1
S	Entropy, p. 5
T	Temperature, p. 5
U	Internal Energy, p. 5
WAG	Water Alternating Gas, p. 1
Z	Compressibility factor of gas, p. 11
Z	Elevation, p. 24
a	van der Walls attractive factor, p. 8
b	van der Walls covolume, p. 8
std	Standard condition: 1 atm 60^{o}F, p. 11
u	Fluid (Apparent) velocity, p. 24
vdW	van der Walls, p. 8

Chapter 1

Introduction

Water Alternating Gas (WAG) is the most applied enhanced oil recovery (EOR) method on reservoirs worldwide, according to CHEN *et al.* (2010). WAG benefits from combining the macroscopic sweep efficiency of water flooding and the high microscopic displacement efficiency of gas injection (CHRISTENSEN *et al.*, 2001).

There are several WAG methods described in the literature. AFZALI *et al.* (2018) have reviewed many of them, including Simultaneous Water and Gas Injection (SWAG), in which gas and water are mixed on the surface and injected into a reservoir; Hybrid-WAG (HWAG) in which CO_2 cycles are hybridized with conventional WAG; Foam Assisted-WAG (FAWAG) that aims to reduce gas mobility (AARRA *et al.* (2002)); and Polymer-WAG (PAG or PWAG) that aims to control the mobility of water.

On classical WAG, CHEN *et al.* (2010) list some parameters to design and optimize the method, such as WAG ratios, cycles period, and injection rates. For a HWAG, the CO_2 amount must be included in the optimization since this component tends to improve miscibility and account for WAG ratio.

According to AFZALI *et al.* (2018), one of the best WAG strategies was applied in the Brent reservoir of Stafjord field. CROGH *et al.* (2002) report this project from its conception up to 5 years of WAG injection. The key of WAG was surveillance, which was based in acquiring pressure data, saturation and production logs, and tracer technology. This collected data served to ensure WAG was increasing oil production and to estimate the amount of additional oil production.

Since offshore field logging is an expensive data to get, especially if an offshore drilling rig is required, we propose other data that could be acquired in order to ensure that the WAG method is improving recovery, consequently enhancing the economical indicators. To perform this, the present work proposes to develop an alternative methodology to measure gas injection effectiveness in regard to the phase behavior of injected gas and crude oil during displacement, by adding this information to surveillance of gas injection purely or in gas injection periods on WAG.

1.1 Motivation

Recently, discoveries on the pre-salt layer showed its outstanding potential. Nowadays, oil production from pre-salt fields accounts for more than 70% of the Brazilian oil production and more than half of its reserves, according to Brazil's National Petroleum Agency (ANP). The huge volumes and CO_2 content of carbonate reservoirs make them an ideal scenario for the WAG method to improve oil recovery. As a surveillance method, logging and fluid sampling constitutes a hefty cost, easily a multi-million dollar undertaking, becoming unprofitable. A cheaper and more prompt alternative to rise the same information may enable the WAG project by increasing its value.

1.2 Objectives

The main objective of this work is to test the hypothesis that oil composition varies depending on the mechanism of gas displacement (miscible or immiscible) and to develop an alternative methodology capable of measuring the effectiveness of gas displacement with commonly acquired data from offshore projects, such as dead-oil composition analysis.

To accomplish this general objective, three specific objectives were drawn as follows:

- Develop a methodology to test the hypothesis that miscibility, either attained by pressure or enrichment, influenced by gas injection, can be identified using oil production composition data.
- Evaluate the proposed methodology using numerical simulation studies.
- Identify key markers for when a gas displacement is likely to promote a very efficient sweep, as in a miscible gas injection, and for a low-efficiency sweep, as in an immiscible gas injection.

1.3 Structure

In the following section, we present the structure of this work and what is discussed in each chapter.

Chapter 2 presents a brief review of theory on the main topics related to the objectives of this thesis. We begin with a brief overview of the main thermodynamic concepts applied to reservoir engineering. We then present fundamental knowledge

of reservoir engineering on flow dynamics and important factors that influence flooding and its performance. Finally, we demonstrate the mathematical model of numerical simulators for both formulations used in the reservoirs in the petroleum industry: black oil and compositional.

Chapter 3 introduces a literature review on WAG, focusing on the gas injection period in each cycle, after the water flood. Despite the focus of this work on gas injection, as WAG is the most applied EOR method, more studies have been carried out on its monitoring and surveillance. The evolution of this method, its expected improvements in a robust design project of WAG during the gas injection time, and main parameters for a successful design method are presented, followed by a review of field project cases reported in the literature. The chapter ends with a section dedicated to an analysis of the main surveillance parameters and their objectives.

Chapter 4 discusses the main hypotheses of this work and proposes a methodology to evaluate them. The fluid selection and modelling, and the reservoir model are presented to formulate the case studies of this work.

In Chapter 5, the investigation of the hypothesis that, depending on the miscible condition of gas injection, oil composition alters differently, and the indicators found in this work are presented. A series of studies to investigate the main mechanisms and parameters that influence indicator response are discussed: such as the influence of pressure, gas composition, mobile oil, relative permeability shape, and viscosity. Also, an analysis of the reservoir fluid composition as drainage occurs is done to evaluate the influence on the two-phase envelope in different miscibility conditions.

Chapter 6 summarizes the conclusion of the evaluation and the recommendations for future work.

In Appendix A, a stepwise procedure for EOS tuning is structured, and in Appendix B, a mathematical approach and coding of Gauss-Laguerre Quadrature Points technique are discussed and presented.

Chapter 2

Theoretical Fundamentals

In this chapter, we present some fundamentals of thermodynamics, reservoir engineering, and reservoir simulation. The main objective is to review the fundamental knowledge available in the literature for a better understanding of the concepts required to comprehend gas injection in an enhanced oil recovery strategy and its particularities.

2.1 Thermodynamics

This subject focuses on the study of driving forces to evaluate whether a state is more stable than others. In other words, its objective is to find the most stable state allowed for a system, which is known as the **equilibrium state**. Despite the term "dynamics" in its name, the kinetics, or the amount of time necessary to reach an equilibrium state, is not the main objective, as it requires the evaluation of some transport phenomena or entropy balance, which is beyond the scope of this work.

The behavior of a phase at local equilibrium is crucial in many fields, especially for flow in porous rocks, as it determines whether the flowing mixture is segregated into two phases with different behaviors and properties or if it is monophasic. This affects the recovery mechanism and how the injected fluid will flow in the reservoir.

The equilibrium state is the condition of a system where the properties are constant through time since no work, heat, or mass crosses the boundary of the system. Hence, there is no tendency for a spontaneous change in the system properties PEREIRA (2018). The fundamental laws of thermodynamics are necessary to determine the conditions that define the equilibrium state.

2.1.1 Equilibrium State

The First Law of Thermodynamics focuses on the study of internal energy (U) and how heat and work affect the amount of energy stored as thermal and bond energy. The

Second Law of Thermodynamics defines entropy (S) and provides the system with a condition to reach equilibrium since the global entropy is not allowed to decrease and always goes to the maximum at equilibrium. Coupling the First and Second Laws of Thermodynamics results in the fundamental equation of Thermodynamics (Equation 2.1):

$$dU = TdS - PdV + \sum_{i=1}^{Nc} \mu_i dN_i \tag{2.1}$$

From Equation 2.1 and by applying Legendre transforms, other fundamental equations are defined for Enthalpy (H) (Equation 2.2), Helmholtz (A) free energy (Equation 2.3), and Gibbs free energy (G) (Equation 2.4).

$$dH = TdS + VdP + \sum_{j=1}^{Nc} \mu_i dN_i \tag{2.2}$$

$$dA = -SdT - PdV + \sum_{i=1}^{Nc} \mu_i dN_i \tag{2.3}$$

$$dG = -SdT + VdP + \sum_{i=1}^{Nc} \mu_i dN_i \tag{2.4}$$

Isolating the first derivative of entropy from Equation 2.1 for any α phase, the expression is:

$$dS^{\alpha} = \frac{1}{T^{\alpha}} dU^{\alpha} + \frac{P^{\alpha}}{T^{\alpha}} dV^{\alpha} + \frac{1}{T^{\alpha}} \sum_{i=1}^{Nc} \mu_i^{\alpha} dN_i^{\alpha} \tag{2.5}$$

For a two-phase (α and β) isolated system, with no mass, heat, or work crossing the boundaries, the following holds: $dN = 0 = dN^{\alpha} + dN^{\beta}$, $dV = 0 = dV^{\alpha} + dV^{\beta}$, and $dU = 0 = dU^{\alpha} + dU^{\beta}$. By adding the expressions for entropy in each phase, we obtain an equation for the system entropy, since $dS = dS^{\alpha} + dS^{\beta}$.

$$dS = (\frac{1}{T^{\alpha}} - \frac{1}{T^{\beta}}) dU^{\alpha} + (\frac{P^{\alpha}}{T^{\alpha}} - \frac{P^{\beta}}{T^{\beta}}) dV^{\alpha} + \sum_{j=1}^{Nc} (\frac{\mu_i^{\alpha}}{T^{\alpha}} - \frac{\mu_i^{\beta}}{T^{\beta}}) dN_i^{\alpha} \tag{2.6}$$

As stated by the Second Law, entropy always reaches a maximum at equilibrium.

When the system reaches this state of equilibrium, its first derivative must be zero. Therefore, the condition for equilibrium is given by Equation 2.7:

$$T^{\alpha} = T^{\beta} \quad , \quad P^{\alpha} = P^{\beta} \quad and \quad \mu_i^{\alpha} = \mu_i^{\beta} \tag{2.7}$$

The first equality on Equation 2.7 is known as the **thermal equilibrium condition**, which ensures that no heat is transferred between phases avoiding an increase in entropy by heat flux. The second is the **mechanical equilibrium condition** which ensures that mechanical energy is equally spread between phases and entropy will not increase by dissipating it. The third is the **chemical potential equilibrium condition**, which states that no net mass is transferred between phases, avoiding entropy by mixing and convection.

2.1.2 Properties of Mixture - Partial Molar Properties

Since a pure component is rarely the case for most of the process, an important topic of thermodynamics is the modeling of a mixture, which deals with many components interacting with each other. The main concept is the partial molar property and is defined for any property "M" by the variation of any thermodynamic property with the mole number of any component "i", keeping temperature, pressure, and other components mole number constant, as in Equation 2.10:

$$\overline{M_i} = (\frac{\delta n\overline{M}}{\delta N_m})_{P,T,N_{m\neq i}} \tag{2.8}$$

where $\overline{M_i}$ is the contribution of specie i on property $\overline{M}$ of the mixture.

The overline indicates that M is any molar property of mixture and its relationship with each partial molar property is given by Equation 2.9:

$$\overline{M} = \sum x_i \overline{M_i} \tag{2.9}$$

2.1.3 Chemical Potential and Fugacity

Chemical Potential

The most important partial property is the partial molar of Gibbs free energy, also known as chemical potential, defined in Equation 2.10:

$$\overline{G_i} \equiv \mu_i \equiv (\frac{\delta G}{\delta N_m})_{P,T,N_{m\neq i}} \tag{2.10}$$

The reason for the importance of partial molar properties relies on Equation 2.7. Even though a system has reached thermal and mechanical equilibrium, if it has a gradient in chemical potential, spontaneous mass transfer among phases will occur since Gibbs free energy decreases and entropy increases with this gradient until equilibrium (equality) is reached. Thus, like temperature and pressure, the chemical potential is a driving force for spontaneous changes in the system.

Chemical potential can be specified by other thermodynamic properties such as internal energy, enthalpy, or Helmholtz free energy, but these are not commonly used since they have the disadvantage of keeping entropy and/or volume constant instead of pressure and temperature.

Fugacity and Fugacity Coefficient

Fugacity was introduced by Lewis to provide a "*simpler, more general, and easier to manipulate*" (LEWIS, 1901) variable. Fugacity measures the deviation from the ideal, and was defined as:

$$\overline{\mu_i} - \overline{\mu_i^0} = RTln\Phi_i \tag{2.11}$$

where $\Phi_i = \frac{\widehat{f}_i}{y_i P}$, P is the system pressure, y_i is the mole fraction in the gas phase, and x_i when the phase is liquid. It is commonly used in simulators as x_{ij}, which is the mole fraction of component "i" in phase "j". The term $\widehat{f}_i$ represents the fugacity of component "i" in the mixture.

The Φ_{ij} is named the fugacity coefficient. With this definition, one can use fugacity instead of chemical potential and therefore, the equilibrium state can be rewritten from Eq. 2.7 to:

$$T^\alpha = T^\beta, \qquad P^\alpha = P^\beta, \qquad and \qquad \widehat{f}_i^\alpha = \widehat{f}_i^\beta \qquad \forall i = 1,2,... \tag{2.12}$$

2.1.4 Equation of State

The fluid behavior is driven by microscopic interactions between the atoms that form the molecules, and thus, the most advanced method for representing this phenomenon is molecular simulation. Although more rigorous, the molecular complexity

and unavailability of parameters for complex molecules and mixtures make molecular simulation less used than equations of state (EOS), especially cubic EOS, which is widely used in industries and commercial software.

The first EOS that could fit either the vapor or the liquid phase was proposed by van der Waals (vdW) in 1873.

$$P = \frac{RT}{\overline{V} - b} - \frac{a}{\overline{V}^2} \tag{2.13}$$

where **P** is the pressure, **R** is the universal gas constant, **T** is the system's temperature, $\overline{V}$ is the molar volume, **a** is the attraction term, and **b** is the repulsive term.

In Equation 2.13, **b** is the covolume representing the volume occupied by other molecules which reduces the volume available for molecules. The right-hand side term represents the attractive forces that reduce the collision of molecules on the walls, thus reducing the pressure. The vdW equation consists of two parts, one repulsive and the other attractive. The repulsive term is considered when molecules collide and are treated as hard spheres. In general, considering molecules as hard spheres is the main reason why cubic EOS has difficulty predicting liquid properties. Parameters **a** and **b** can be determined by experimental data for the pure substance or at a critical point, which has the first and second derivative of pressure with respect to volume CABRAL *et al.* (2019).

According to CABRAL *et al.* (2019), the modern development of cubic EOS began in 1949 with the modification of the vdW equation by introducing an explicit temperature on the attractive terms by Redlich-Kwong. In fact, the subsequent developments on cubic EOS were made by improving the attractive term, with the standard strategy of modifying the attractive term in REDLICH and KWONG (1949) by using the term at a critical point and a temperature-dependent multiplicative factor, as in SOAVE (1972), resulting in the Soave-Redlich-Kwong (SRK) Equation.

In an attempt to enhance the predictive accuracy of the SRK equation, PENG and ROBINSON (1976) proposed a model that preserved its simplicity and yet increased accuracy in the critical region and along the saturated liquid curve. According to ZABALOY and VERA (1998), the Peng-Robinson (PR) equation has been considered one of the best two-constant cubic EOS. In fact, over 40 years after its publication, the PR EOS has been successfully applied for thermodynamic predictions and the efforts to improve its forecast have demonstrated its acceptance by the industry and academic fields. This equation is so widely accepted and used that LOPEZ-ECHEVERRY *et al.* (2017) have enumerated over 300 modifications that were proposed to improve its prediction for pure substances and mixtures.

Peng and Robinson proposed a modification to their own EOS in 1978, resulting in

the following new model for EOS (PRIVAT and JAUBERT (2011)):

$$P = \frac{RT}{\overline{V}-b} - \frac{a(T)}{\overline{V}(\overline{V}+b)+b(\overline{V}-b)} \tag{2.14}$$

with:
$a(T) = ac.\alpha(T)$
$\alpha(T) = [1+m(1-T_r^{1/2})]^2$ with $T_r = \frac{T}{T_c}$
if $\omega \leq 0.491, m = 0.37464 + 1.54226\omega - 0.26992\omega^2$
if $\omega > 0.491, m = 0.379642 + 1.48503\omega - 0.164423\omega^2$
$ac = \omega_a \frac{R^2 T_c^2}{P_c} = 0.45724 \frac{R^2 T_c^2}{P_c}$
$b = \omega_b \frac{RT_c}{P_c} = 0.07780 \frac{RT_c}{P_c}$

To apply this EOS to mixtures, mixing rules are necessary to calculate **a** and **b**. In this work, and as in the majority of commercial reservoir simulators, a classical mixing rule proposed by vdW will be applied (PRIVAT and JAUBERT (2011)):

$$\begin{cases} a = \sum_{i=1}^{nc} \sum_{j=1}^{nc} x_i x_j (a_i a_j)^{\frac{1}{2}} (1-k_{ij})] \\ b = \sum_{i=1}^{nc} x_i b_i \end{cases} \tag{2.15}$$

Binary Interaction Coefficient

The k_{ij} in Equation 2.15 is the binary interaction coefficient (BIC), a parameter responds for the attraction energies (pairwise) between molecules i and j (ESPOSITO *et al.*, 2017). By definition, the $(k_{i=i})$ is zero and since hydrocarbons are essentially non-polar molecules their k_{ij} is typically set to zero (PEDERSEN *et al.*, 2006). However, nonzero binary coefficients are often adjustable parameters used to fit experimental data (PEDERSEN *et al.* (2006), ESPOSITO *et al.* (2017)).

2.1.5 Laboratory Data and EOS Tuning

As seen in the previous section, the PR EOS has many parameters, and these parameters hold physical meanings related to the fluid they represent. This section aims to mention the main aspects of matching the EOS to laboratory data (PVT data) to represent a fluid, without deeply discussing the aspect of tuning an EOS, which can be found in ESPOSITO *et al.* (2017) and PEDERSEN *et al.* (2006).

Composition

The essential information acquired from laboratory data is composition. This information is obtained through chromatography, which is similar to a distillation curve, separating each component. The aim is to obtain the amount of each component on a molar or mass basis. For the lightest component (up to $n-C_5$), the equipment is calibrated, and each component can be identified. From C_6 onwards, the amount of isomers increases significantly, and compositions are lumped into pseudo-components with the same number of carbon between the n-alkanes peaks (ESPOSITO *et al.*, 2017).

Besides the "pseudorization" of grouping compositions between the n-alkanes peaks at chromatography, another pseudorization is applied to heavy-end characterization. Since petroleum has thousands of components, and the equipment has a limit for detection, there is a single carbon number (SCN) that cuts-off characterization, and all carbons beyond this point are lumped into the "plus" fraction (THOMAS *et al.*, 2002), typically C20+ for oil and C7+ for gas. Despite a lower concentration of the plus fraction, it has a huge influence on fluid thermodynamic properties such as saturation pressure, phase density, and gas-oil ratio (GOR) (FOLSTA *et al.*, 2010).

PVT Analysis

The PVT analysis is a set of laboratory assays performed on a sample from a reservoir or a recombination of oil and gas at surface conditions to reproduce the reservoir fluid. The assays aim to estimate how volume (and other properties) may vary with pressure and temperature. The common assays are Constant Composition Expansion (CCE), Differential Liberation (Diflib), viscosity, and chromatography of dead oil and gas.

Typically, these assays measure and estimate some parameters of oil and gas at different pressures and temperatures to fit the EOS. The main properties are:

- Formation Volume Factor for oil and gas (Bo and Bg): the ratio of the volume at a given pressure and temperature over the volume in standard conditions (1 atm and 60^{o}F). For oil, since there might be some gas liberation (GOR) to reach standard conditions, the composition may change. For gas, the composition is the same.

- Gas Oil Ratio (GOR): the amount of gas still dissolved in oil at a given P and T, reported at standard conditions and divided by the oil volume at standard conditions.

- Density/Specific Gravity (ρ or SG): the ratio between mass and volume or its relative density (or specific gravity) related to a reference fluid, typically water at 4^{o}C for liquids and gas at 20^{o}C.

- Saturation Pressure: the pressure at which a monophasic fluid becomes two-phase. Also known as the dew point when the fluid is gas or the bubble point when the fluid is a liquid.
- Viscosity for oil and gas (μ_o and μ_g): the measurement of the resistance to deformation.
- Compressibility factor of gas (Z): gas deviation from ideality, directly proportional to **Bg**.

Laboratory Experiments to Evaluate Miscibility

A piece of important information about miscibility conditions can be acquired through some laboratory assays. To obtain this information, the three most important assays are the swelling test, the RBA (Rising Bubble Apparatus), and the Slim Tube Test.

A swelling test consists of a series of CCEs performed on an initial amount of oil, with increasing amounts of mixed gas. The assay records the new saturation pressure for each amount of gas added and the Swelling Factor, which is a ratio of the volume occupied by the oil at the new saturation pressure to the volume occupied at the original bubble point (ESPOSITO *et al.*, 2017). This is a static assay related to the equilibrium phase of gas and oil at different proportions.

The RBA (Rising Bubble Apparatus), however, is a dynamic assay that involves creating a bubble of gas at the bottom of the equipment, which rises in a tube containing oil. The test records the path, shape, and other movement information as this gas bubble rises through the apparatus. The Minimum Miscibility Pressure (MMP) is recorded as a function of the pressure of the experiment and the gas flowing in the oil characteristics.

A Slim Tube Test is also a dynamic test, acquired by filling live oil in a slim tube coil filled with a porous media and injecting gas, and measuring the recovery factor and the amount of gas injected. The report results are done by plotting the recovery factors for each of the pressures that the assay was performed. The limits vary, but one commonly used is plotting the recovery factor after injecting certain proportion of pore volume of gas versus pressure. The recovery factor increases as the pressure of the experiment increases until it reaches a plateau. The MMP is defined by connecting this linear trend with the trend line in which recovery surpasses 95% after cumulative injection of 120% of the pore volume (THOMAS *et al.*, 1994b) and (ZICK, 1986). The slim tube test is a dynamic test in a simplified porous media that considers gas-oil interaction in a porous media and focuses on what is important for project development, which is determining the conditions that maximize recovery.

EOS Tuning

The art of tuning an equation of state requires the selection and calibration of a mathematical model capable of precisely and successfully predicting the thermodynamic behavior of a mixture. The cubic equation is computationally efficient for EOS selection and can predict the phase behavior of petroleum fluids across a wide range of pressure and temperature (WANG and POPE, 2001).

Due to the fact that an EOS is a mathematical model that portrays the thermodynamic behavior of a fluid or mixture based on particular assumptions, approximations, and simplifications, tweaking an EOS involves a degree of empiricism (THOMAS *et al.*, 2002). The EOS parameters, which are coefficients used to adjust the EOS to fit experimental data, have a significant influence on the EOS's prediction accuracy and reliability. Consequently, the EOS tuning process may incorporate a constraint to maintain the changing parameters within acceptable physical limits.

According to THOMAS *et al.* (2002), the number of pseudo-components used to represent a real fluid or mixture in a simulation model depends on the phase behavior's complexity, the required accuracy and efficiency, and the chemical and physical characteristics of the fluid or mixture, as well as the simulation's objectives.

Frequently, the flexibility of representing the plus fraction as a single pseudo-component is insufficient for tweaking an EOS or representing the complexity and variation of a fluid in a reservoir. Therefore, SHIBATA *et al.* (1987) proposed a methodology to select and characterize the plus fraction in as many pseudo-components as needed to better represent fluid complexity. The concept uses the Gauss-Laguerre Quadrature to select a finite number of points to represent the integral of a weighted function. It is assumed that mole fraction has an exponential decay with the number of carbons in the pseudo-component, and by choosing an exponential as a weight function and assuming carbon number as a continuous variable, the points represent the integral. Applying a variable change, the pseudo-component can represent the plus fraction. A more in-depth discussion of the methodology and coding of SHIBATA *et al.* (1987)'s technique is presented in Appendix B.

2.1.6 Miscibility from Thermodynamic Perspective

By definition, an interface is a region where two phases separate from each other. It appears due to the preference of molecules from each phase to interact with ones from the same phase rather than mixing.

Miscibility occurs when the affinity between molecules from different phases is strong, and at equilibrium, there is no interface, resulting in a state with the minimum free energy level for the system, for any mixed proportion of oil and gas. Since the definition demands a monophasic system in all proportions, a critical point analy-

sis is required. Therefore, a thermodynamically rigorous concept of miscibility occurs when a system is above the critical point, which can be related to critical pressure and temperature or critical composition. A brief review of the interface (Section 2.2.1) and miscibility (Section 3.2.1) aspects of WAG will be discussed later in this work.

2.2 Fundamentals of Reservoir Engineering

In this section, a brief review of reservoir engineering concepts is done to support the understanding of secondary and enhanced recovery methods, providing basic concepts of reservoir engineering.

2.2.1 Basic Concepts

Porosity

Porosity is one of the most important parameters of reservoir rock, as it determines the amount of fluid storage. It is defined as the ratio of the void volume (V_p - porous volume) to the bulk volume (V_B - total bulk volume), as defined by Equation 2.16.

$$\phi = \frac{V_p}{V_B} \tag{2.16}$$

Saturation

Reservoir rocks are filled with fluids, and the volumetric proportion of each fluid determines its saturation. Neglecting the amount of hydrocarbon in the water, there are typically two liquid phases: water and oil, and a vapor phase that completes the three possible phases. As all porous media are filled with these fluids, Equation 2.17 introduces the volumetric constraint.

$$S_w + S_g + S_o = 1 \tag{2.17}$$

Permeability

Absolute permeability is another important reservoir rock parameter, represented by the letter **K**. It relates the ability of a fluid (saturation 100%) to flow through the porous rock and needs to be measured through a lab experiment, similar to Darcy's experiment (DARCY, 1856), or estimated through empirical formulas.

Despite no chemical reactions have been considered in this work, some interactions of fluid and rock are reviewed for a better understanding of recovery processes happening when WAG is applied as an EOR method.

Interface and Interfacial Tension

A boundary must exist when two phases are in contact, and for this boundary to be stable, it must have an interfacial free energy on which work has to be done to enlarge the interface area. If this is not the case, then no energy is required to increase the interfacial area and any forces, such as gravity or the natural movement of molecules, will twist the interface until phases become mixed.

Obeying the Second Law of thermodynamics, all systems tend to attain minimum free energy. So, when more than one phase is stable, the interface will spontaneously be reduced to a minimum energy level, reducing its area, and the two phases will tend to separate as much as possible, constrained by the mechanical movement, gravitational forces, and other factors, accordingly to MYERS *et al.* (1999), resulting in a region (interface) where intensive properties change from one phase to another.

SHAW (1980) explained the interfacial tension phenomena as a result of unbalanced attractive forces that molecules experience at the interface, resulting in an inward pull, as shown in Figure 2.1. These forces result from Van der Waals attractive forces.

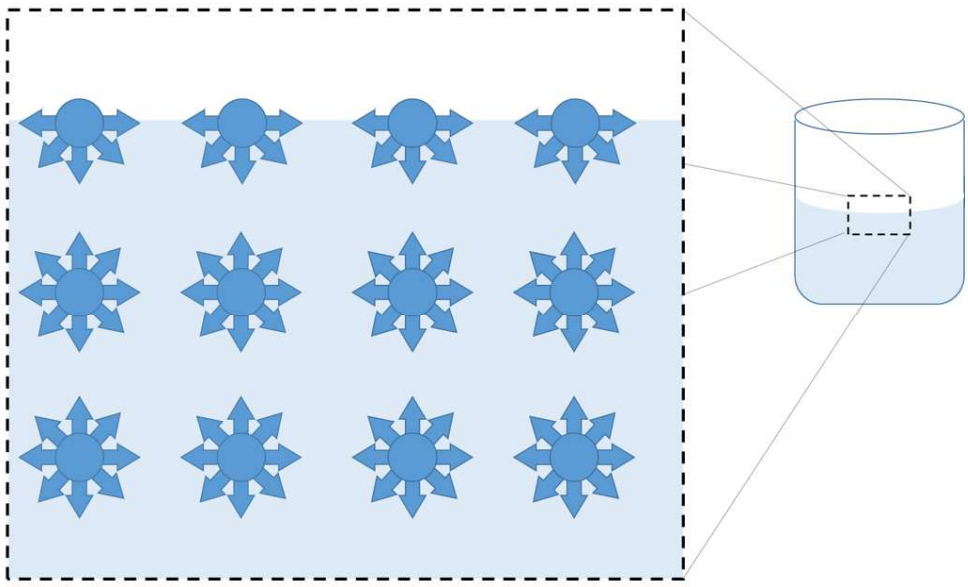

Figure 2.1: Forces balance at interface and bulk

Although the customary term used when one of the phases is gaseous is *surface*, this work will address it as *interface*, since there is no fundamental distinction between the terms (SHAW, 1980). The interfacial tension, represented by σ, has units of force

per length and is related to the amount of force needed to increase a unit of length or the work required to increase one unit of area (Equation 2.18).

$$\sigma = \frac{Force}{dx} = \frac{LForce}{Ldx} = \frac{Work}{dA} \tag{2.18}$$

It is important to note that interfacial tension can vary with changing conditions such as pressure, temperature, and composition (MYERS *et al.*, 1999). Therefore, during WAG cycles, when gas injection is performed, the overall composition changes, and the energetic situation at the interface may alter, even on immiscible injection, which can lower the interfacial tension at equilibrium.

Wettability and Contact Angle

Wettability is the tendency of one fluid to spread on a solid surface in the presence of another fluid. Therefore, the measurement requires a solid material and two immiscible fluids. For reservoir engineering purposes, the solid is the reservoir rock, and the immiscible fluid is either water-oil or gas-oil. The study of these sets aims to improve water or gas flooding recovery by promoting better conditions for oil sweep. Understanding the interfacial tension in injectant and displaced fluids is fundamental for designing methods such as injecting foam, surfactants, low salinity water, miscible and immiscible gas injections, WAG, and many others.

The contact angle is the most common feature used to measure the wetting characteristic (MYERS *et al.*, 1999). This angle (θ) is always measured from the liquid to the solid and varies between 0^o and 180^o. The lower the angle, the more wetting the fluid is for that surface. Angles above 90^o of the liquid are considered to be a non-wetting phase. This angle is dependent on the interaction between solid-liquid, solid-gas, and liquid-gas. As a result of each interfacial tension of those three groups, the angle is formed, as shown in Figure 2.2.

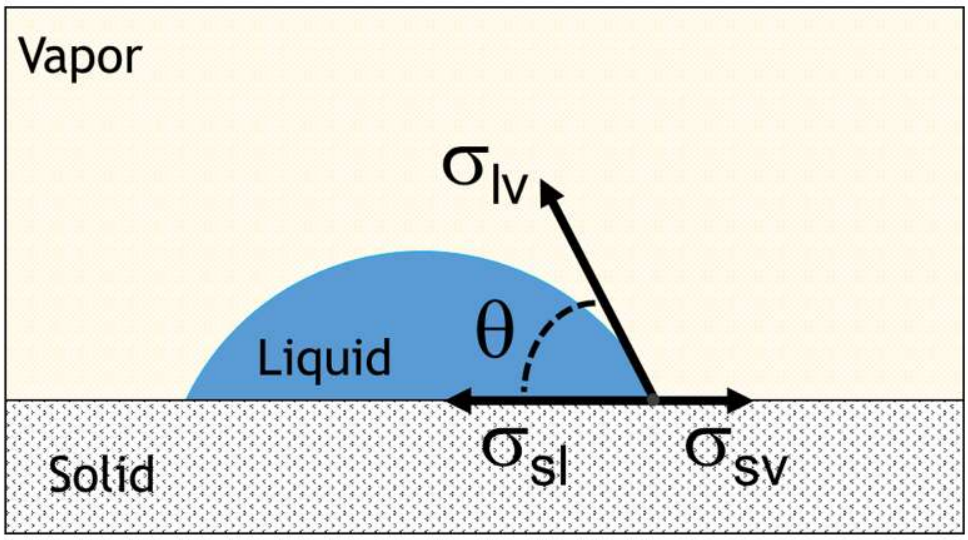

Figure 2.2: Interfacial tension causing contact angle

Capillary Pressure

According to AHMED (2010), capillary forces acting on petroleum reservoirs result from the combination of many factors, such as interfacial tensions, pore size and geometry, and wetting characteristics of rock and fluid.

The tension that exists at the interface that separates the liquid-fluid (gas or another liquid) might be curved. In such a case, there is a discontinuity in pressure, and there will be a difference in hydrostatic pressure across the interface (MYERS *et al.*, 1999). The Young-Laplace equation describes this phenomenon and relates the pressure difference between nonwetting and wetting phases. This difference is known as capillary pressure and is shown in Equation 2.19.

$$P_{nonwetting} - P_{wetting} = \sigma cos\theta \left(\frac{1}{R_1} + \frac{1}{R_2} \right) \tag{2.19}$$

The capillary rise experiment, shown in Figure 2.3, causes a wetting fluid to rise in a capillary glass tube due to the surface wettability and interfacial tension between phases. As the tube has a cylindrical shape, the curvature of the interface is spherical, and therefore, $R_1 = R_2 = r$. Equation 2.19 can be simplified to Equation 2.20a if the fluid that rises has perfect wettability (i.e., the contact angle is zero). A simpler Equation 2.20b can be used to model the phenomenon.

$$P_o - P_w = \frac{2\sigma cos\theta}{r} \tag{2.20a}$$

$$P_o - P_w = \frac{2\sigma}{r} \tag{2.20b}$$

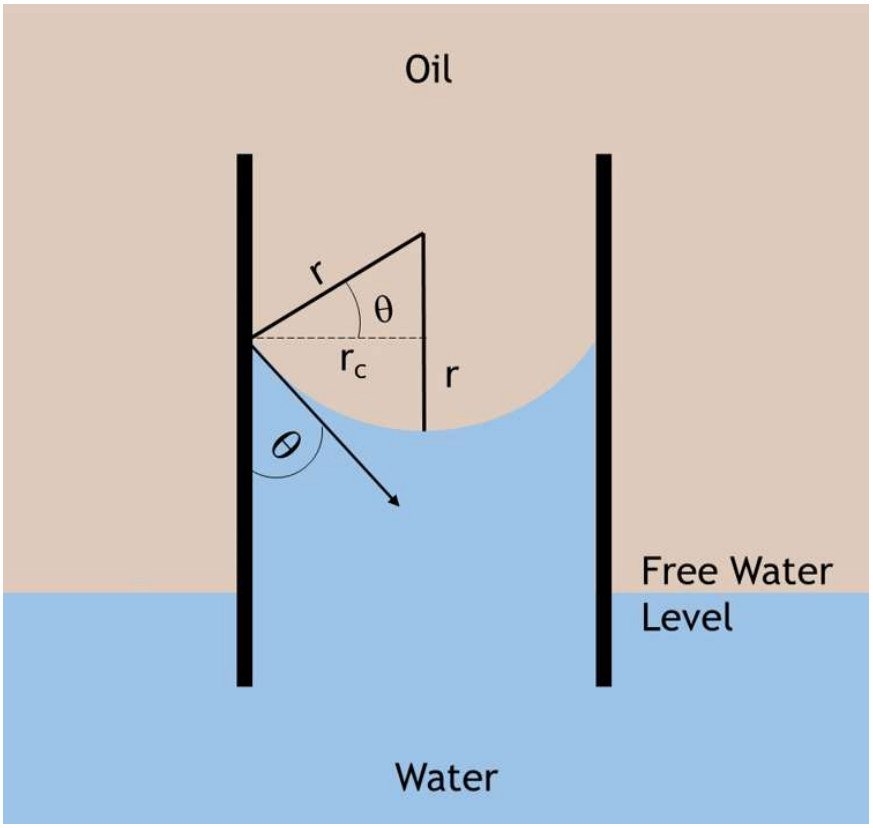

Figure 2.3: Capillary rise experiment

2.2.2 Relative Permeability

On multiphase flow, oil, water, and gas may compete for the ability to flow. Since each phase interacts differently with the other phases and with the rock, each phase has its own effective permeability. Several laboratory studies have concluded that effective permeability is a function of fluid saturation and the wetting characteristics of the formation (DAKE, 2001). The relative permeability of phase j (k_{rj}) is defined by the ratio of one phase's effective permeability (k_j) to the absolute permeability (K), shown by Equation 2.21.

$$k_{rj} = \frac{k_j}{K} \tag{2.21}$$

It has been observed that the simple presence of a different phase causes inhibition of the other to flow; thus, the sum of relative permeabilities is usually less than one. However, this is not uncommon for multiphase flow, especially for the pure water phase (100% saturation), in which the sum may reach unity, as shown in Equation 2.22.

$$0 < k_{ro} + k_{rw} + k_{rg} \leq 1 \tag{2.22}$$

Equation 2.22 is always greater than zero because it is a reasonable assumption that there is always at least one mobile phase. To facilitate the interpretation of fluid-rock flow properties, relative permeability is usually reported in two sets regarding phase interaction with the rock: wetting and nonwetting phases. In this regard, the three phases of interest are divided into two sets: oil and water, and liquid and gas. Relative permeabilities are commonly used in these two sets and are also proportional to water saturation, as shown in Figure 2.4 for oil-water. It is worth noting that relative permeability would have an X-shape if phases did not inhibit each other, been the phase's relative permeability linear with its saturation. Many studies on relative permeability are well documented in the literature, so this work will describe the main highlights of two-phase relative permeability. Although responsible for enhancing recovery on WAG, neither three-phase relative permeability nor hysteresis will be addressed in this work.

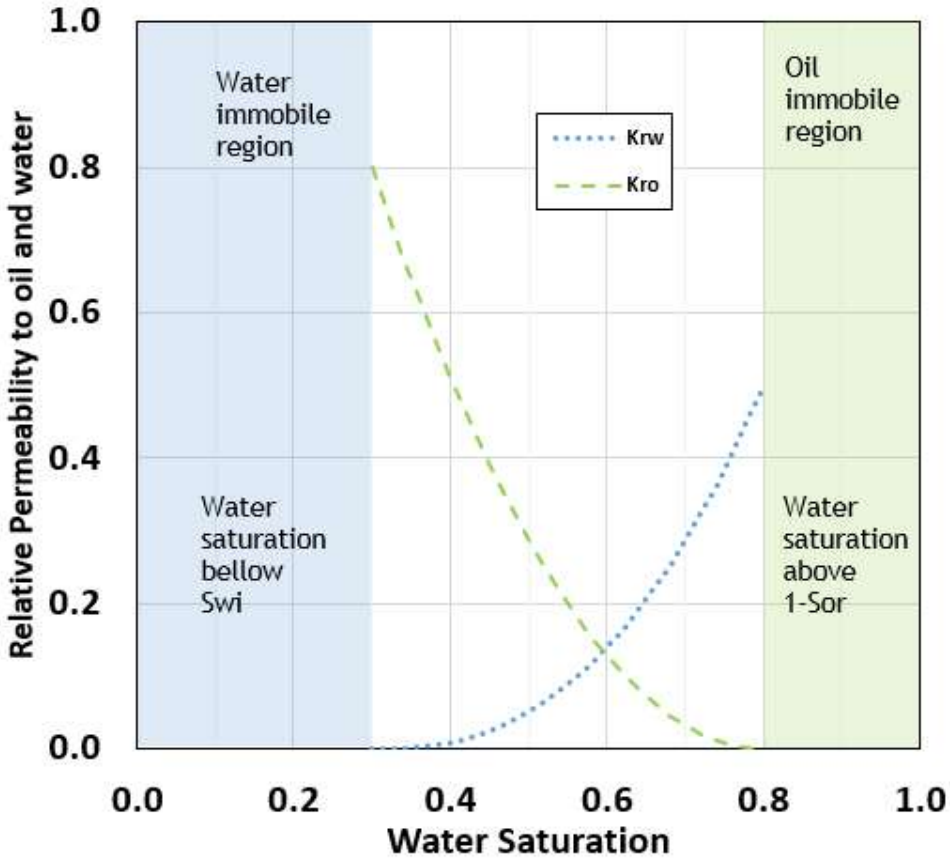

Figure 2.4: Relative Permeability for (- - - -) oil phase and (- - - -) water phase. Water and oil immobile regions are highlighted in blue and green, respectively.

Mobile Saturation

In an immiscible displacement, it is impossible to reduce the saturation of the displaced fluid to zero due to trapping caused by a balance between viscous and capillary

forces. At some low saturation, known as the residual saturation, the displaced phase becomes discontinuous and stops flowing. Similarly, a phase must accumulate a minimum saturation before it can begin to flow. This saturation is referred to as the critical saturation.

Water becomes mobile after the irreducible saturation (S_{wi}), which is the saturation trapped by capillary pressure due to interactions with the formation. Oil is mobile until the residual oil saturation (S_{or}), which is the minimum achievable oil saturation. These saturations are shown in Figure 2.4, the former in the blue area, and the latter in the green area.

Drainage and Imbibition Procedures

Residual saturation is measured by reducing the saturation, while critical saturation is measured by increasing the saturation. Although theoretically the saturations should be the same, they are not due to irreversibilities on increasing and decreasing saturation, a phenomenon called hysteresis. Therefore, the saturation history matters.

When the process to obtain data is performed by increasing the wetting saturation, it is called imbibition. When the data is acquired by reducing the wetting phase saturation, the process is classified as drainage (AHMED, 2010).

It is generally agreed that in a water-wet oil reservoir, the pore volume was filled with water, and later the oil was moved into pore spaces, displacing the water and reducing its saturation until reaching its irreducible saturation, in a drainage process since the nonwetting phase increases saturation. When discovered, reservoirs are filled with connate (assumed to be irreducible) water saturation and oil. If water flooding is applied, the water saturation will increase in the porous media to displace oil, increasing the wetting saturation in an imbibition process.

Besides what was discussed in Section 2.2.1 regarding wettability, there are several differences in the relative permeability of oil-wet and water-wet rocks (AHMED, 2010), such as:

- **Equal relative permeability:** The intersection point for the relative permeability of water and oil will be greater than 50% for the water-wet system.
- **Irreducible water saturation:** Since in a water-wet system, the water will preferentially adhere to the pore surface, the S_{wi} will be greater than 25%, while in an oil-wet system, it would be less than 15%.
- **Maximum water relative permeability:** For a water-wet system, it should be less than 0.3, and for an oil-wet system, greater than 0.5.

The work of AHMED (2010) provides valuable insights into rock/fluid wettability through graphical analysis, despite the general separation of water-wet and oil-wet ex-

posure. However, it is important to note that real data is not always so clear-cut, and the industry recognizes a third option of mixed-wet as a result of the heterogeneity of grains in the reservoir rock.

Relative Permeability Model

The most used model for describing the behavior of relative permeability is Corey's, which is popular for its simplicity and effectiveness. In this model, each relative permeability phase is a function of its own normalized saturation (COREY, 1954). The equations used to describe this behavior are shown in Equations 2.23 and 2.24.

$$k_{rw} = (k_{rw} \quad at \quad S_{or}) \times \left(\frac{S_w - S_{wi}}{1 - S_{or} - S_{wi}} \right)^{n_w} \tag{2.23}$$

$$k_{ro} = (k_{ro} \quad at \quad S_{wi}) \times \left(\frac{1 - S_{or} - S_w}{1 - S_{or} - S_{wi}} \right)^{n_o} \tag{2.24}$$

where:

S_w is the water saturation at a given moment.
n_o and n_w are the exponent of a power law model for oil and water, respectively.
k_{ro} is the oil relative permeability for a S_w or S_o.
k_{rw} is the oil relative permeability for a S_w or S_o.
S_{wi} is the water irreducible saturation.
S_{or} is the oil residual saturation.

2.2.3 Mobility Ratio

With the previous definition, it is possible to define mobility, which is the ratio of the effective permeability (k_j) of phase j to its viscosity (μ_j). Mobility describes how easily a phase flows in porous media. The mobility ratio (M), which is the ratio of the mobility of one phase to the mobility of another phase, is commonly used to compare the flow of two phases in a reservoir. This ratio is often used to compare water or gas to oil, and it is given by Equation 2.25.

$$M = \frac{(k_w/\mu_w)}{(k_o/\mu_o)} \text{ or } M = \frac{(k_g/\mu_g)}{(k_o/\mu_o)} \tag{2.25}$$

A mobility ratio greater than one (M>1) is disadvantageous for drainage because viscous fingering may occur (LIMA, 2016). It causes instability at the displacement

front, leading to early breakthrough and leaving most of the reservoir unswept. Two approaches are used to avoid this undesirable situation:

- **Altering relative permeability ratio:** using methods to improve the interaction between the fluid and formation. This is typically used for water-oil displacements, such as low salinity injection, chemicals for wettability change, and many others.
- **Altering viscosity ratio:** this is one of the advantages of WAG. As long as some oil swelling is expected, even on immiscible gas injection, a reduction in viscosity is also awaited, reaching a more favorable mobility ratio for oil drainage.

2.2.4 Recovery Efficiency

The recovery efficiency of water flooding is measured by the product of the estimates of three different efficiencies, as shown in Equation 2.26 (DE FARIAS, 2013).

$$E_R = E_A.E_H.E_D \tag{2.26}$$

E_A is the areal sweep efficiency of the analyzed method, which is measured through the ratio of the sweep area over the total area between the producer and injector wells, and is a function of horizontal heterogeneity and mobility ratio. E_H is the vertical sweep efficiency, calculated through the ratio of the effective sweep of the vertical section over the total vertical length. It depends on vertical heterogeneity, formation orientation, the ratio between horizontal and vertical permeability, the mobility ratio, and the difference in fluid density. The product of these is the volumetric sweep efficiency (E_V), which is related to the amount of oil that a method can sweep. The measure for some flaws in the displacement of swept regions is considered in E_D, the displacement efficiency, which is related to the microscopic capability of moving oil towards the producer wells.

2.3 Fundamentals of Reservoir Simulation

In this section, some equations and assumptions commonly used in reservoir simulation are reviewed to support an understanding of computational modeling, which provides the majority of WAG evaluation.

The so-called black-oil formulation assumes constant composition in each phase, although it allows for gas condensation and oil vaporization. Due to its simplicity and efficiency (DOS SANTOS, 2017), it is used in several reservoir cases, except for two,

which require a compositional approach (COATS, 1980): depletion on volatile oil and gas condensate or miscible flooding.

Accordingly, COATS (1980) stated that black-oil simulators are not suitable for miscible flooding, which is the purpose of this work. However, to follow the evolution of reservoir simulators and due to its importance, the black-oil formulation is presented.

The black-oil formulation has n_c=3 components (oil, water, and gas) and n_p=3 phases (oil, water, and gas). Gas is the only component allowed in more than one phase (oil and gas). The other two components are only present in the phase with the same name. This formulation has 6 unknowns (pressure and saturation for each phase). On the other hand, the compositional formulation has the same n_p=3 phases (some compositional formulations allow a second non-aqueous phase, reaching n_p=4 phases (CHANG, 1990), but this is used for very specific cases only) with n_c components and has $2n_c$+6 unknowns (the 6 of black-oil plus n_c mole fraction for each component on the oil phase $(x_1, x_2, ..., x_{nc})$ and n_c mole fraction for each component on the gas phase $(y_1, y_2, ..., y_{nc})$). The equations needed to solve each formulation are reviewed in this chapter.

2.3.1 Material Balance Equation

The continuity equation, one of the fundamental equations of fluid mechanics, states that in the absence of consumption or generation (no chemical reaction), any conservative quantity (such as mass or moles) accumulating inside a given volume is equal to the net sum of its fluxes plus a source term that might add or subtract this quantity. Therefore, the mass conservation (or material balance) for one phase in porous media is given by Equation 2.27.

$$\frac{\partial(\phi\rho)}{\partial t} + \nabla(\rho u) = q_m \tag{2.27}$$

The first term accounts for the accumulation of fluid (porosity (ϕ) multiplied by fluid density (ρ)) over time, and the second accounts for the net fluxes resulting from flows in and out (fluid density (ρ) multiplied by superficial fluid velocity (u)), and the third, which follows the equal sign, is the source term (external mass flow rate (q_m)) where mass can be added or taken from reservoir, for example by a well.

For the multiphasic case, the material balance for each phase is given by Equation 2.28, where the subscript indicates phase "j".

$$\frac{\partial(\phi\rho_j S_j)}{\partial t} + \nabla(\rho_j u_j) = q_{jm} \tag{2.28}$$

The Equation 2.28 is used for black-oil simulators. For compositional simulators, a material balance for each component is required. The description of each term (accumulation, flux, and source term) on the material balance is well described by CHANG (1990), resulting in Equation 2.29.

$$\frac{\partial\left(\phi \sum_{j=1}^{np} \xi_j S_j x_{ij}\right)}{\partial t} + \nabla\left(\sum_{j=1}^{np} \xi_j x_{ij} u_j - \phi \xi_j S_j \overline{\overline{\kappa_{ij}}} \nabla x_{ij}\right) = \frac{q_i}{V_b} \tag{2.29}$$

Where ϕ is the porosity of the control volume, ξ_j is the molar density of phase j (number of moles in the phase over the phase volume), S_j is the saturation of phase j, x_{ij} is the mole fraction of component i in phase j (usually written in the literature as x for the liquid phase and y for the gas phase), u_j is the superficial velocity (flux) of phase j, $\overline{\overline{\kappa_{ij}}}$ is the full dispersion tensor for component i in phase j, q_j is the molar flow rate of component i on well production or injection, and V_b is the bulk volume of the referred control volume.

The first term of Equation 2.29 represents the accumulation term, and inside the sum, the terms combine resulting in the number of moles of component i per pore volume, given by $\xi_j S_j x_{ij} = N_i$ (SANTOS, 2013). The second term, inside the parenthesis, accounts for fluxes and considers the convective flux and the dispersive flux. The convective part is governed by the superficial velocity of the phase, modeled by Darcy's law (Equation 2.33). The dispersive part considers the transport of mass due to molecular diffusion and mechanical dispersion, which is modeled and incorporated into the dispersion tensor $\overline{\overline{\kappa_{ij}}}$. This dispersive term is often neglected because the numerical dispersion on simulators causes a mixing zone length due to the grid cell size used (CAVALCANTE FILHO and PIZARRO, 2019). It is possible to adapt the grid cell size to meet dispersion phenomena at the field scale and neglect dispersion modeling. The last term is responsible for the source term caused by wells injecting or producing molar flow rates.

Using both substitutions on the accumulation term and the absence of dispersive terms, Equation 2.29 is reduced to Equation 2.30.

$$\frac{\partial\left(\phi N_i\right)}{\partial t} + \nabla\left(\sum_{j=1}^{np} \xi_j x_{ij} u_j\right) = \frac{q_i}{V_b} \tag{2.30}$$

2.3.2 Darcy's Law

The physical representation of porous media flow is governed by Darcy's law (DARCY, 1856), which empirically describes water flow through sand beds. Darcy observed the linear relationship between apparent velocity and potential in his experiment. The proportionality constant was divided into two parts, representing rock and fluid properties, as shown in Equation 2.31. Darcy's law is valid for laminar flow, as the dimensions of interstices in porous media formed by fine-grained sediments are small, and therefore the flow is laminar.

$$u_a = -\frac{K}{\mu}\left(\nabla P + \gamma \nabla Z\right) \tag{2.31}$$

The apparent velocity can be related to the fluid interstitial velocity by $u_a = \phi u$, where it describes the average velocity through a section in porous media (volumetric flow rate over area Q/A). The term ∇P represents the pressure gradient, and $\gamma \nabla Z$ represents the specific weight times the elevation. Both of these terms are potential causes of flow. The proportional constant K/μ takes into consideration the rock properties in the numerator and the fluid properties in the denominator. When gravitational forces can be neglected, Equation 2.31 becomes Equation 2.32. This law is analogous to many linear laws that relate flux to its potential, such as Fourier's law in heat conduction flux, Ohm's law in electrical flux, or Fick's law in diffusion mass flux.

$$u = \frac{Q}{A_t} = -\frac{\mathbf{K}}{\mu}\nabla P \tag{2.32}$$

MUSKAT and MERES (1936) adapted Darcy's Law to make it suitable for the oil and gas industry by extending its usage for multiphase flow in porous media (Equation 2.33). The ratio $\lambda_j = k_{rj}/\mu_j$ in the proportional constant for multiphase flow is also known as the mobility of phase "j".

$$u_j = -\frac{\mathbf{K}k_{rj}}{\mu_j}\left(\nabla P_j + \gamma_j \nabla Z\right) \tag{2.33}$$

2.3.3 Coupled Equation

As Darcy's law (Equation 2.33) is explicit in velocity, one can substitute the velocity in the material balance equation (Equations 2.28 for black-oil or Equation 2.30 for com-

positional simulation). To use this equation numerically, one needs to discretize the material balance equations and use a numerical approximation for the derivatives. One can use the concept of compressibility, defined as in Equation 2.34, and assume that the mass of each phase (m_j) remains constant, i.e., there are no chemical reactions.

$$c = -\frac{1}{V}\frac{\partial V}{\partial P} \tag{2.34a}$$

$$c_{formation} = -\frac{1}{V_p}\frac{\partial V_p}{\partial P} = -\frac{1}{V_b\phi}\frac{\partial\left(V_b\phi\right)}{\partial P} = -\frac{1}{\phi}\frac{\partial\phi}{\partial P} \tag{2.34b}$$

$$c_{phase} = -\frac{1}{V_j}\frac{\partial V_j}{\partial P} = -\frac{m_j}{m_j V_j}\frac{\partial V_j}{\partial P} = -\frac{1}{\rho_j}\frac{\partial\rho_j}{\partial P} \tag{2.34c}$$

At this point, the black-oil formulation is complete, since enough equations have been presented to solve for the six unknowns in this formulation, which are the pressure and saturation for oil, gas, and water. The six equations are:

- **3 equations:** from the material balance for oil, water and gas (Equation 2.28).
- **2 equations:** from the capillary pressure (Equation 2.19 for oil/gas and water/oil)
- **1 equation:** from volumetric (or saturation) restriction (Equation 2.17)

It is important to note that molecular interactions are not considered in this formulation, and all fluid information is obtained by correlating variables with pressure. For a compositional simulator with $j = n_p = 3$ phases and $i = n_c$ components, at this point, we lack n_c equations to solve the $2n_c + 6$ variables (2 n_c mole fractions for gas and oil phases plus pressure and saturation for the three phases - water, oil, and gas), since we have so far introduced $n_c + 4$ equations with 2 more restrictions below, for a total of $n_c + 6$ equations:

- $\boldsymbol{n_c + 1}$ **equations:** n_c from the material balance for each component and for water (Equation 2.29).
- **2 equations:** from the capillary pressure (Equation 2.19 **a** and **b**)
- **1 equation:** from volumetric (or saturation) restriction (Equation 2.17)
- **2 equations:** for the mole fraction restriction. Not yet presented for simplicity, and analogy with volumetric restriction (Equation 2.35 **a** and **b**). The second sum uses the definition introduced in Equation 2.29, x_{ij}, with the phase definitions $j = 1$ for the aqueous phase, $j = 2$ for the oil phase, and $j = 3$ for the gas phase.

$$\sum_{i=1}^{n_c} x_i = \sum_{i=1}^{n_c} x_{i2} = 1 \tag{2.35a}$$

$$\sum_{i=1}^{n_c} y_i = \sum_{i=1}^{n_c} x_{i3} = 1 \tag{2.35b}$$

To reduce the degrees of freedom of this system, the remaining n_c equations will come from the phase equilibria restriction.

2.3.4 Phase Equilibria

Although no reservoir could be considered at equilibrium since its entropy is always increasing as a result of heat flow from Earth's geothermal gradient, a steady state will most likely be reached within a geological timescale from the time oil migrated until discovery (ESPOSITO *et al.*, 2017). To avoid the use of the complex equation of irreversible (or non-equilibrium) thermodynamics, reservoir flow simulators consider local equilibrium and equality in fugacities.

Therefore, the remaining equation comes from fugacity equilibrium (Equation 2.12), introduced by Lewis, for each component in all phases. The n_c equations are shown in Equation 2.36, already with phase numbering presented in the previous equation.

$$\widehat{f}_i^{j=2} = \widehat{f}_i^{j=3}; \text{for i=1 to } n_c \tag{2.36}$$

Chapter 3

Literature Review

The main focus of this work relates to gas injection and its mechanism, since WAG is a widely applied large-scale EOR method worldwide that combines water flood and gas injection. The water flood aims to divert gas injection into a new pathway in porous media, accessing oil that would be bypassed in a pure gas injection scheme. As water flood acts as a gas mobility control in the process, a literature review was performed on WAG.

Despite WAG's simple concept of alternating fluids, it involves complex thermodynamic effects and rock-fluid interactions that make it difficult to predict its behavior and evaluate its effectiveness. This section conducts a literature review aiming to deepen knowledge of the physical phenomenon, working mechanism, and other main factors for implementing a successful WAG project, especially since the gas injection characteristics are a key factor for this method.

3.1 WAG Process

3.1.1 History

Regarding immiscible displacement, such as water flooding, the ability to reduce residual oil saturation is limited due to capillary forces formed as a result of interfacial tensions, resulting in a significant amount of oil left behind in the swept zone. Eliminating interfacial tension could reduce S_{or} to almost zero (HOLM, 1976).

To ensure a reduction, or even elimination, in interfacial tension at equilibrium, as discussed in Chapter 2.1.6, miscibility needs to develop at reservoir conditions between the injected gas and original oil in-place. Initially, the idea was to inject less valuable liquid solvents to promote more efficient oil displacement. Although successful in laboratory experiments requiring small quantities of solvent, larger quantities of solvent were required at a field scale, making it economically unattractive, as stated by KOCH and SLOBOD (1957).

CAUDLE and DYES (1958) proposed a new technique to reduce mobility in the swept region to increase sweep efficiency. They suggested simultaneous injection of water and gas behind the miscible displacement to reduce permeability and increase viscosity in the swept regions. The reduction in permeability was expected by reducing overall mobility since gas and water were proposed to be injected, and, as discussed in Section 2.2.2, both fluids inhibit each other's flows. Since water is more viscous than the gas it replaced, the viscosity in the swept region should increase. Although the gas-to-water ratio was difficult to determine, simultaneous water/gas injection was considered low-risk because if too much gas was injected, flooding would approach gas-driven displacement. If less gas was injected, the reservoir would perform like water flooding.

BLACKWELL *et al.* (1960) confirmed the theory postulated by CAUDLE and DYES (1958) through a sand-pack model scaled to represent some reservoirs and noticed that, although the water-solvent mixture does not flow together, water flows preferentially along lower parts of the reservoir since it has higher density, while the solvent had the tendency to flow through upper parts of the reservoir. In all the experiments, the water-solvent mixture resulted in higher recovery than water flooding or solvent injection.

Later on, the technique considered to be more practical to enhance recovery efficiency was alternate gas-water injection (HOLM, 1976). The water alternating gas (WAG) technique reduces the mobility ratio by increasing viscosity and reducing overall mobility in the flushed region. This increase in mobility ratio would make the next gas displacement contact another region (increase volumetric sweep efficiency, E_V) and block high permeability layers mitigating the viscous fingering (increase microscopic displacement efficiency, E_D in equation 2.26).

The approach of promoting a miscible displacement evolved to the use of natural gas at high pressure, which acts like a solvent to promote a vaporizing drive mechanism through multiple contact miscibility (MCM - which will be addressed further in Section 3.2.1). The light end of the oil (C_2 to C_6) vaporizes from the oil and moves to the oil/gas front, resulting in a higher concentration of these intermediates and enhancing recovery. Furthermore, HOLM (1976) noticed that CO2 might promote MCM due to the fact that it does not depend on the light end and is able to extract heavier components (between C_5 to C_{30} at an appropriate pressure), requiring lower injection pressure than natural gas to perform as described.

Therefore, the WAG technique benefits from coupling improved displacement of gas flooding with higher macroscopic sweep efficiency of water injection (CHRISTENSEN *et al.*, 2001).

3.2 Improvement Expected on Displacement

Many factors influence a gas injection project, as referred by THOMAS *et al.* (1994a), who discussed the effects on geology at two scales: macro and micro. Macro heterogeneity can impact flow and can negatively affect even well-designed gas injection schemes. On the micro scale, pore size distribution is the main factor affected by two other factors: interfacial tension (IFT) and viscosity ratio. As previously stated, gas injection is the focus of this work, as it is responsible for most of the improvement in displacement.

3.2.1 Miscibility from Reservoir Perspective

Miscibility is dependent on pressure, temperature, and the composition of both phases. Since reservoirs are considered isothermal, at least locally, the petroleum industry's interest is to maximize the region where the drainage occurs to a single phase, referred to as "miscible", despite not being miscible in any proportion, but in the range of proportions applied in the field. Furthermore, a mixing of oil and gas might result in a monophasic fluid or it might experience a condensing/vaporizing process that, onwards on drainage, results in a miscible condition. The miscibility process is classified considering the manner in which miscibility is developed: first-contact miscibility (FCM) and multiple-contact miscibility (MCM).

First Contact Miscibility and Critical Point Analysis

In FCM, as the name implies, the injected fluid is miscible with crude oil on first contact. In other words, the mixture forms a single phase at reservoir conditions (reservoir pressure and temperature) at all proportions. For FCM miscibility to occur, there is a minimum miscibility pressure (MMP) required for the injected fluid and crude oil to become monophasic at any proportion.

If the reservoir temperature is below the critical temperature of the primary slug, then the MMP is the pressure that ensures the first slug of gas injected will liquefy. In this situation, the MMP has a maximum at the cricondenbar since the composition injected is liquid above this pressure. Depending on the reservoir temperature, the MMP may be less than cricondenbar (GREEN and WILLHITE, 1998).

If the reservoir temperature is above the critical temperature of the primary slug, the required pressure for complete miscibility becomes very hard to estimate. In this situation, it is not possible to liquefy the solvent, and the MMP must be above the cricondenbar, which depends on reservoir temperature and crude oil composition (GREEN and WILLHITE, 1998).

Multiple Contact Miscibility and Expected Mechanism

In MCM, the miscible condition develops due to a composition change during flow through the reservoir. This process is classified regarding the mechanism of displacement to achieve miscibility: vaporizing gas and condensing (enriched gas) (PEDERSEN *et al.*, 2006).

Vaporizing gas displacement usually uses low molecular-weight hydrocarbons or inert gas (such as nitrogen). Some intermediate components are vaporized to inject gas through multiple contacts with oil, enriching the gas. This alters the composition of the injected front, which could be miscible with the original oil beyond in the flow (GREEN and WILLHITE, 1998).

In condensing, or enriched gas, some medium-weight hydrocarbon is injected, and the reservoir oil is enriched by the condensation of those components. As the oil is contacted several times by the injected gas, after a while, it is expected that the oil will be enriched until miscibility with the injected fluid happens (GREEN and WILLHITE, 1998).

ZICK (1986) states that the condensing approach is more likely to be a combined mechanism of condensation and vaporization processes. The condensing mechanism, as described in the last paragraph, does not occur alone because the middle intermediates might be stripped out from the oil into the gas. After some contact between the oil and injected gas, the oil receives light intermediates from the gas but loses middle intermediates to the gas. As a net result, the oil becomes heavier. This prevents the development of miscibility by the newly injected gas and heavier oil. Ultimately, when all the middle intermediates are removed, the heaviest nonvolatile components are left behind.

The equilibrium gas, a very lean gas since it lost its intermediates, moves ahead and contacts more fresh oil performing a vaporizing mechanism, with the peculiar difference that the gas is enriched until it can perform condensing mechanism ahead when it contacts more fresh oil. Authors affirm that miscibility is "nearly" achieved before the condensation process reverts to the vaporization process again. Even though miscibility is never completely achieved (two phases are not miscible at all proportions), this mechanism results in a very efficient displacement.

3.2.2 Viscosity Reduction

When differential pressure is applied, gas tends to preferentially flow (THOMAS *et al.*, 1994a), causing viscous fingering. This happens because the tendency to flow is inversely proportional to viscosity, and oil viscosity is 5 to 10,000 times higher than gas viscosity. The authors suggest that in large pore throats reservoirs, viscosity reduction is the crucial factor and often dominates in a system with a larger pore size range.

DEHYADEGARI and RABBANI (2014) attribute the good performance of CO2 injection to the increase in reservoir pressure and the significant reduction of oil viscosity, which unclogs the movement of oil to producer wells.

3.2.3 IFT Reduction

On the microscale perspective, THOMAS *et al.* (1994a) associated reduction in IFT with a significant decrease in residual oil saturation since gas can access smaller pore throats that were isolated at higher interfacial tension levels. This expected mechanism drives the interest in gas injection projects by the oil and gas industry. Depending on the micro and macro scale geological characteristics, the IFT or mobility influences will dominate controlled by viscous ratio. Authors suggest that on smaller pore throats reservoirs, the IFT optimization is more crucial.

3.3 Main Project Parameters

3.3.1 WAG Ratio

The WAG ratio is the ratio between the injected volumes of water and gas, at reservoir conditions, over a period of time. This variable will define the balance between volumetric and displacement efficiency (LAFORCE and ORR, 2008).

If the WAG ratio is too low, the gas will reach the gas/oil front earlier due to its greater mobility and will tend to form fingerings on more permeable intervals. If the ratio is too high, the water front will perform as water flooding, not taking advantage of the microscopic improved sweep.

The volume of gas injected should be sufficient to increase gas saturation in the front and promote efficient displacement. This way, when the fluid is switched, water traps pathways that were already swept by the injected gas (LAFORCE and ORR, 2008).

The most commonly used WAG ratio is 1 (CHRISTENSEN *et al.*, 2001), but it can vary in a range of 0.5 to 4 (GREEN and WILLHITE, 1998). However, optimizing the WAG ratio can be challenging due to limited resources, and smaller WAG ratios may not be feasible for some projects.

CHRISTENSEN *et al.* (2001) introduced the tapering technique, which involves altering the WAG ratio throughout the flooding process. Typically, this change is not planned but rather a result of changes in recycling rates. Tapering is used in the late stages of injection to increase the WAG ratio and control channeling and gas breakthrough.

3.3.2 WAG Cycles

A cycle is defined as the pattern of alternating gas and water injections. By fixing the WAG ratio and gas rate, the water rate and total cycle time can be calculated.

GHARBI (2003) concluded that smaller cycles result in better efficiency for both miscible and immiscible injection. Smaller cycles increase breakthrough fluid alternation, making the primary process on FPSO easier, but they also make the injection operation more challenging due to the frequency of fluid changes.

According to DYER and FAROUQ ALI (1994), the optimal number of slugs is 10, with the first slug being the most important in terms of recovery.

3.3.3 Injected Volumes

There are several reports of field experiences that estimate injected volumes varying between 10% to 50% of hydrocarbon pore volume (HCPV) on average, such as (GREEN and WILLHITE (1998), STALKUP (1983), and BROCK and BRYAN (1989)).

STALKUP (1983) reported that for FCM, the injected slug volume varies from 1-12% of HCPV. For MCM, the condensing gas drive injected volumes vary between 2% up to 50% HCPV, with most of them greater than 10% HCPV. Field experiences for CO2 displacement report a recovery of 3.5% up to 18% of original oil in place (OOIP) with 10% to 50% HCPV slug injections.

3.3.4 Reservoir Pressure

The factors that affect miscibility are composition, temperature, and pressure. The variable to design a proper WAG method is related to composition alteration since the objective is to mix the highest possible amount of oil with the injected gas. Since it is difficult, nearly impossible, to alter the reservoir temperature, the reservoir pressure is another crucial parameter. Although not easily altered, the depletion rate might be arranged to optimize recovery and, if necessary, restrained, considering that not all reservoir regions are at the same pressure, and some regions might be below the minimum miscibility pressure levels.

3.4 Field Experience

CHRISTENSEN *et al.* (2001) reviewed 59 cases of WAG injection in the literature. The increase in recovery factor varied from 5% to 10%, with few unsuccessful field trials reported, although some operational problems were reported, such as scale, corrosion, loss of injectivity, and formation of asphaltene and hydrates.

MANRIQUE *et al.* (2007) compiled EOR methods used in carbonate reservoirs within the United States (US) by going through databases such as TORIS and Journals. The paper analyzed gas, chemical, and thermal methods. Focusing on gas injection, as it has been the most used enhanced oil recovery method for crude-oil reservoirs, the author highlighted some aspects of CO_2, nitrogen, and hydrocarbon injections:

- **CO2 Injection:** It has been the principal EOR process in carbonates in the US, either continuously or in the WAG method. 67% of active CO_2 projects are in carbonate reservoirs. The popularity of this contaminant injection is related to the abundant natural sources of CO_2 and CO_2 pipelines close to oil fields.
- **Nitrogen injection:** More than 30 nitrogen injection projects had been developed in the US until 2007. Nitrogen injection can achieve miscibility in the flood in deep, high-pressure, and light-oil reservoirs. However, immiscible nitrogen injection has been performed for pressure maintenance, condensate cycling, and as gas for miscible slugs.
- **Hydrocarbon injection:** Very few hydrocarbon gas injection projects have been reported. The shortage of projects is related to the high gas price.

BERGE *et al.* (2002) reported a SWAG (simultaneous WAG) for Siri Field in the North Sea. Since gas exportation was economically unattractive, the SWAG method was implemented and is performing according to the author's expectations, and it might increase recovery up to 6% in comparison to water flooding.

NING and MCGUIRE (2004) reported an immiscible WAG design for the Milne Point Kuparuk reservoir in Alaska. Through numerical simulation, the authors evaluated a possible increase of 6% up to 9% of additional recovery over a water flooding scheme.

WAG is the most used EOR method, significantly increasing recovery, with the average increase in the range of 5% to 15%. Most evaluations were performed through phenomenological numerical simulation on a reservoir model.

3.5 WAG Surveillance

In the literature review, some parameters were monitored for specific alterations caused by the WAG method, being classified by, first, its objective and, second, the parameter monitored in the surveillance.

3.5.1 Asphaltic Precipitation

Through Oil Composition

HWANG and ORTIZ (1998) monitored changes in oil composition aiming to evaluate asphaltene precipitation, which was confirmed by field-scale and core analysis observation of injectivity loss and reduction in asphaltene composition.

Through Geochemical Biomarkers

DEHYADEGARI and RABBANI (2014) evaluated some biomarkers from geochemical analysis and concluded that, rather than removing light ends from crude oil, WAG was improving recovery by removing the heavy ends through asphaltic precipitation.

3.5.2 WAG Performance

Through Logging and/or Chemical Tracers

CROGH *et al.* (2002) reported on a WAG project, from its pilot up to a 5-year experience, on the Statfjord Field (in Brent reservoirs). To estimate incremental production and optimize injection on the WAG method, an extensive WAG surveillance program was planned and carried out. The surveillance included:

- *Saturation and production logging:* those logs on producer wells serve to estimate the degree of water flooding and gas flooding as the areas are swept and unswept.
- *Pressure data:* for estimating the degree of connectivity and support between regions.
- *Chemical Tracers:* Chemical tracers were used extensively on WAG injection. This was important information to provide a better understanding of the structure and flow paths.

Authors reported that until May 2002, 55% of injected gas was retained in the reservoir, and the water cut could be reduced from 90% to 20% in some wells, causing the oil rate to double or even triple. The incremental oil could be estimated through decline since the field was producing in the early 1990s.

In HERNANDEZ *et al.* (2002), a surveillance using a chemical tracer in the Lagocinco field in Venezuela was reported. With the tracer information, the authors were able to:

- *History match:* Information on communication along the flow pathway was used to calibrate the reservoir model and simulations.

- *Decision support:* Initially, the strategy could be adapted and contribute to better management of production decisions.

Oil Composition

PANDA *et al.* (2011) used a ratio between C_1 (methane) and C_3 (propane) to evaluate WAG flood performance. Since the reservoir oil has a larger ratio (C_1/ C_3=25) than the miscible injectant (C_1/ C_3=1.5), a reduction of this ratio was expected after the injectant breakthrough. Although the authors were able to identify gas breakthroughs, the question of whether a miscible displacement took place or not remains unanswered.

In THOMAS *et al.* (1994a), three major factors for gas injection design were considered: geology, interfacial tension, and viscosity ratio. The authors evaluated miscible and near-miscible gas injection by comparing the evolution of bottom-hole samples in a P-x diagram. They confirmed monophasic flow at the producer well, although the gas-oil ratio (GOR) increased from 370 m^3/m^3 to 900 m^3/m^3 (2.5 times the initial value). The doubt of whether it was a miscible displacement or a condensing/vaporizing mechanism was indirectly answered. Although the composition at the bottom-hole sample was a dewpoint (suggesting an MCM process), because the crude oil was very light (> 50ºAPI), an FCM process was expected rather than an MCM process. By analyzing the composition alteration in the heavier ends (C_6^+) and the expectation that it should reduce in an MCM process, the authors attributed an FCM process, assuming preferential flow through larger pore throats, similar to channeling, to explain the high GOR.

The work of THOMAS *et al.* (1994a), through a thorough literature review, was the primary work in which oil composition alteration was used to estimate information on phase behavior (FCM or MCM) in fluid flow dynamics in the reservoir.

Chapter 4

Methodology

WAG and/or gas injection surveillance is a multi-million dollar endeavor. Cheaper sources of information, such as those collected by FPSOs, may replace expensive ones like well logging, thereby enabling marginal projects and/or increasing their economic value.

The main hypothesis is that miscible and immiscible gas displacement may cause different alterations in the composition of produced oil. If so, this can be used to infer the mechanism of displacement under reservoir conditions. This hypothesis was formulated based on observations of alterations in the proportion of some components over time in producers located closer to WAG injectors at the pre-salt fields.

The methodology to investigate this hypothesis is divided into two parts. The first part is related to the reservoir fluid: selecting a reservoir fluid and PVT data to calculate the MMP for a chosen gas injection composition to define the pressure for scenarios of miscible and immiscible gas injection on 1D numerical simulations. The second part is simulating the selected miscibility condition in a 1D reservoir model, with a gas injector at the beginning and a producer at the end, to scrutinize composition and phase behavior and test the hypothesis on produced composition over time.

4.1 Fluid Selection

4.1.1 Reservoir Fluid

For the reservoir fluid, the composition and data described in MOORTGAT *et al.* (2013) were used and are reported in this work as **ResFluid1**. The composition and the PVT data used reported by the authors are in Tables 4.1 and 4.2.

Table 4.1: Composition for ResFluid1 (MOORTGAT *et al.*, 2013)

Component	**Mole Fraction (%)**	**Component**	**Mole Fraction (%)**
CO_2	8.24	C_9	1.69
N_2	0.37	C_{10}	1.55
C_1	51.29	C_{11}	1.26
C_2	7.07	C_{12}	1.15
C_3	4.87	C_{13}	1.19
iC_4	0.9	C_{14}	0.98
nC_4	1.79	C_{15}	0.96
iC_5	0.59	C_{16}	0.75
nC_5	0.86	C_{17}	0.68
C_6	1.13	C_{18}	0.69
C_7	1.64	C_{19}	0.63
C_8	2.1	C_{20+}	7.62
SG C_{20+}	0.9594	MW C_{20+}	536 g/mol

Table 4.2: PVT Data for ResFluid1 (MOORTGAT *et al.*, 2013)

Pressure (kgf/cm²)	ρ_{oil} **(g/cm³)**	μ_{oil} **(cP)**	**GOR (m³/m³)**	**Bo (1)**	**Bg (1)**
550	726	1.30	235	1.552	-
530	724	1.27	235	1.556	-
510	722	1.24	235	1.560	-
490	720	1.22	235	1.564	-
470	718	1.19	235	1.568	-
450	716	1.17	235	1.573	-
430	714	1.16	235	1.578	-
415	712	1.16	235	1.581	-
400	711	1.17	235	1.585	-
392.5	710	1.14	235	1.587	-
350	726	1.28	203	1.509	0.0033
310	739	1.38	178	1.448	0.0034
270	750	1.50	155	1.396	0.0036
230	762	1.62	134	1.348	0.0040
190	773	1.78	113	1.303	0.0048
150	785	1.89	92	1.260	0.0061
110	798	2.35	72	1.216	0.0087
70	812	2.99	51	1.170	0.0145
35	825	4.03	31	1.127	0.0306
0	855	8.54	0	1.033	

To assess the impact of fluid properties on the results, a second fluid from an oil

field (used with permission from Petrobras S.A.), referred to as **ResFluid2**, was also evaluated. The composition and PVT data for ResFluid2 can be found in Tables 4.3 and 4.4, respectively.

Table 4.3: Composition for ResFluid2.

Component	**Mole Fraction (%)**	**Component**	**Mole Fraction (%)**
CO_2	0.87	C_9	1.37
N_2	0.40	C_{10}	1.28
C_1	62.01	C_{11}	1.02
C_2	7.42	C_{12}	0.94
C_3	5.16	C_{13}	0.91
iC_4	1.00	C_{14}	0.77
nC_4	1.94	C_{15}	0.73
iC_5	0.61	C_{16}	0.56
nC_5	0.87	C_{17}	0.51
C_6	1.14	C_{18}	0.51
C_7	1.16	C_{19}	0.49
C_8	1.67	C_{20+}	6.66
SG C_{20+}	0.9380	MW C_{20+}	481 g/mol

Overall, it would be interesting to investigate if the type of fluid used has a significant effect on the performance of miscibility markers. The second fluid, ResFluid2, differs from the first one in terms of having a very low concentration of CO_2 and a different PVT data set. In addition to the effect of composition/PVT data, the initial parameters of the equation of state (EOS) used to model thermodynamic behavior are also important to differ from ResFluid1. As discussed in section 4.2.4, a different set of initial parameters, especially the binary interaction coefficients, was selected to tune ResFluid2 to become a different thermodynamic representation of the fluid from the first one.

4.1.2 Gas Injection Composition

The initialization of the reservoir fluid is the same in both simulations to evaluate the miscibility condition scenario, and it is assumed that the temperature will remain constant (and equal in both scenarios). As previously stated, the Minimum Miscibility Pressure is dependent on temperature and composition. Therefore, it is impossible to analyze circumstances above and below the MMP when the pressure, temperature, and composition of the original oil and injected gas are the same.

We simulate different alternative sets of miscibility scenarios, each with a single

Table 4.4: PVT Data for ResFluid2.

Pressure (kgf/cm²)	ρ_{oil} **(g/cm³)**	μ_{oil} **(cP)**	**GOR (m³/m³)**	**Bo (1)**	**Bg (1)**
600	634	1.33	364	1.886	-
580	632	1.30	364	1.891	-
560	630	1.23	364	1.898	-
540	628	1.16	364	1.904	-
520	626	1.09	364	1.911	-
510	625	1.06	364	1.914	-
500	624	1.00	364	1.918	-
492.2	623	0.96	364	1.921	-
450	657	1.28	290	1.726	0.0030
400	679	1.32	245	1.613	0.00305
350	699	1.38	205	1.519	0.0032
300	716	1.43	173	1.446	0.0034
250	731	1.51	145	1.384	0.0038
200	746	1.64	118	1.326	0.0045
150	763	1.76	93	1.271	0.0060
100	780	2.06	67	1.216	0.0098
50	799	2.34	41	1.159	0.0206
0	847	5.46	0	1.035	-

variable that is altered to provide a distinct miscibility condition yet a similar case. The first set of scenarios consists of the same gas injection content but at different pressures, whereas the second set consists of the same pressure but different gas injection compositions.

The two gas injection composition utilized in each reservoir fluid consists mostly of carbon dioxide and/or methane, selected arbitrarily. For the same composition set, a CO_2-containing mixture was chosen. For ResFluid1, the amount of CO_2 in the injected fluid was 50% CO_2 (and 50% C_1). For the same pressure set, a composition consisting entirely of C_1 was chosen for the second set. For ResFluid2, the objectives were different, and a composition of 10% CO_2 (and 90% C_1) was chosen for the first group, while 100% C_1 was chosen for the second group.

4.2 Thermodynamic Fluid Model

Winprop, a commercial program included in the CMG package, was used to estimate the EOS properties and match laboratory data using version 2020.10. Properties from Winprop's library were utilized up to C_{19}.

In addition to the molecular weight and specific gravity measured from laboratory assays, an estimate of the boiling temperature was used to complete the initial calculation of the plus fraction's properties, including critical information. However, due to

the inherent uncertainty in the molecular weight of the plus fraction (THOMAS *et al.*, 2002), it was subject to regression in parameter estimation.

4.2.1 Plus Fraction Analysis

Four thermodynamic EOS models were fit to lab data to evaluate the influence of a plus fraction on ResFluid1. A Shibata routine (SHIBATA *et al.* (1987) and ESPOSITO *et al.* (2017)) was performed for 1 to 4 quadrature point estimation (results in Figure 4.1. Details, for repeatability of results, on Table 4.5 with Δ, η and Φ).

Table 4.5: Quadrature Points for Reservoir Fluid 1

Quadrature Points	Carbon (SCN)	z (%mol)	MW (g/mol)	wi(Shibata)	zi(Shibata)
1	38.6	7.62	536.00	1.0000	0.7713
2	28.3	5.27	392.86	0.6916	0.3578
	61.5	2.35	857.04	0.3084	1.6987
3	24.6	3.54	340.50	0.4652	0.2065
	44.7	3.15	622.24	0.4128	1.0204
	71.0	0.93	989.58	0.1220	2.0816
4	22.8	2.49	315.51	0.3261	0.1344
	36.2	3.04	502.94	0.3994	0.6758
	56.4	1.61	786.23	0.2112	1.4942
	75.0	0.48	1045.49	0.0633	2.2431
Δ	2.4670	η	19.5	Φ	80.5

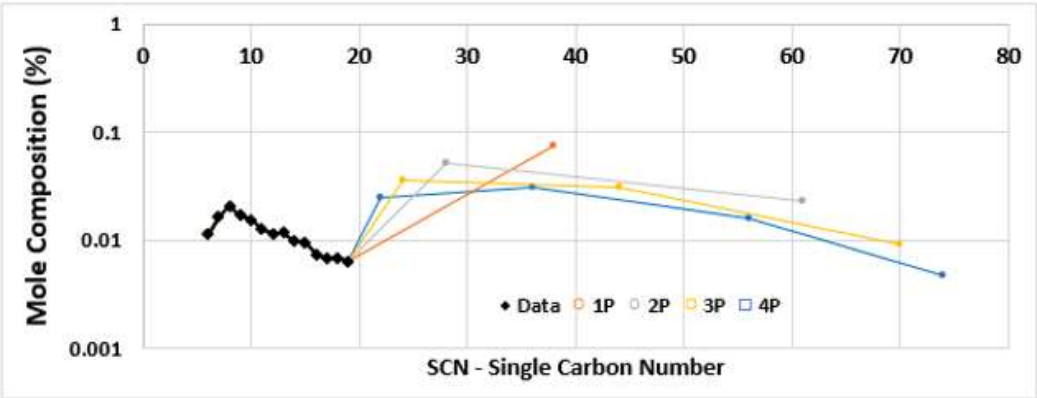

Figure 4.1: Mole Composition for 1-4 Quadrature Points

Each model contained several variables that required parameter estimation in order to match laboratory results. For the plus fraction, these values included P_c, T_c, V_{shift}, MW, $BIC_{CO_2-C_n}$, and $BIC_{C_1-C_n}$, in addition to the viscosity parameters. As seen in Figure 4.2, these parameters retained the same degree of physical coherence upon regression.

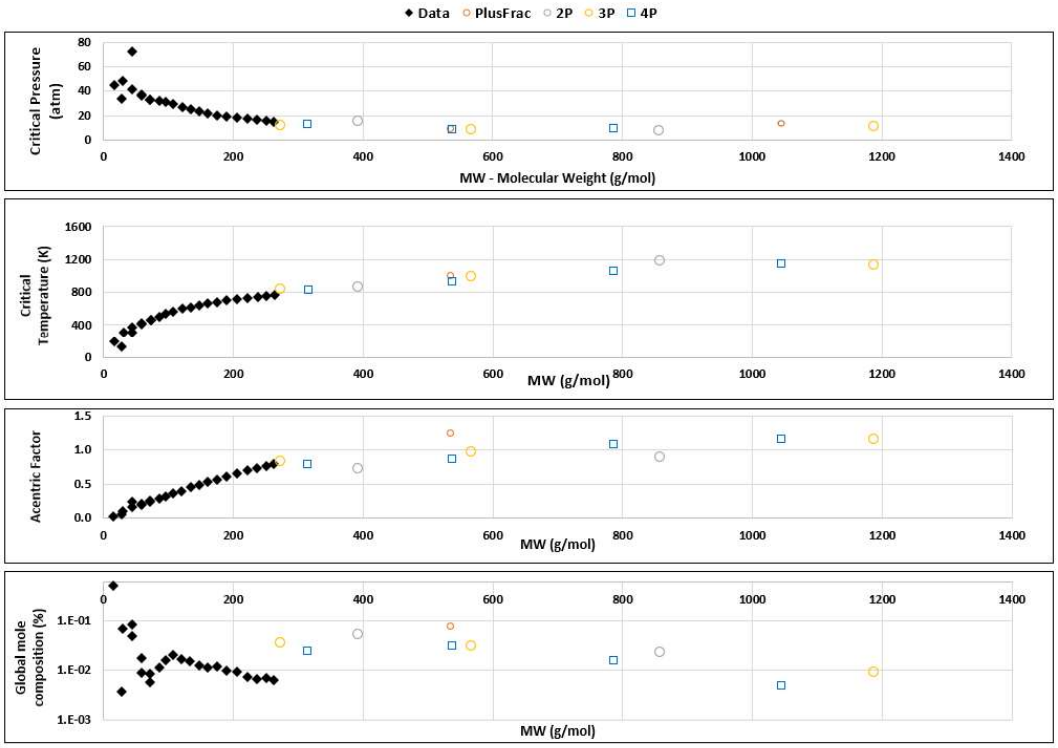

Figure 4.2: Parameters for 1-4 Quadrature Points after tuning

The results of simulations of data that were subjected to tuning using four alternative thermodynamic models for ResFluid1 are displayed in Figure 4.3. Bg and μ_{oil} (MuL) have a significant inaccuracy in the low-pressure zone; nevertheless, the monophasic region is a meaningful location to discuss miscibility, and therefore, this region has a lower importance for the analysis. However, even in the sub-saturation interval at pressures greater than 200 kgf/cm^2, for example, the absolute error is less than 3% for both Bo and densities (DL), and less than 10% for viscosity, GOR, and Bg.

Figure 4.4 displays a two-phase envelope for the four thermodynamic models. It illustrates that one pseudo-component has a distinctive form, which results in an expansion of the two-phase region. Although the two-pseudo-component model had a greater cricondentherm, the 2-4 pseudo-component has a similar outcome, while the three-pseudo-component model and the four-pseudo-component model are almost indistinguishable from each other.

Although the low-pressure range is not critical for miscibility, it can still affect the overall accuracy of the thermodynamic models under investigation. It is worth noting that the aim was to determine the optimal number of pseudo-components and EOS for the simulation, which will undergo lumping and further tuning.

A three-pseudo-component model was chosen for ResFluid1, while a two-pseudo-component model was chosen for ResFluid2 to increase the thermodynamic dissimilarity between the fluids.

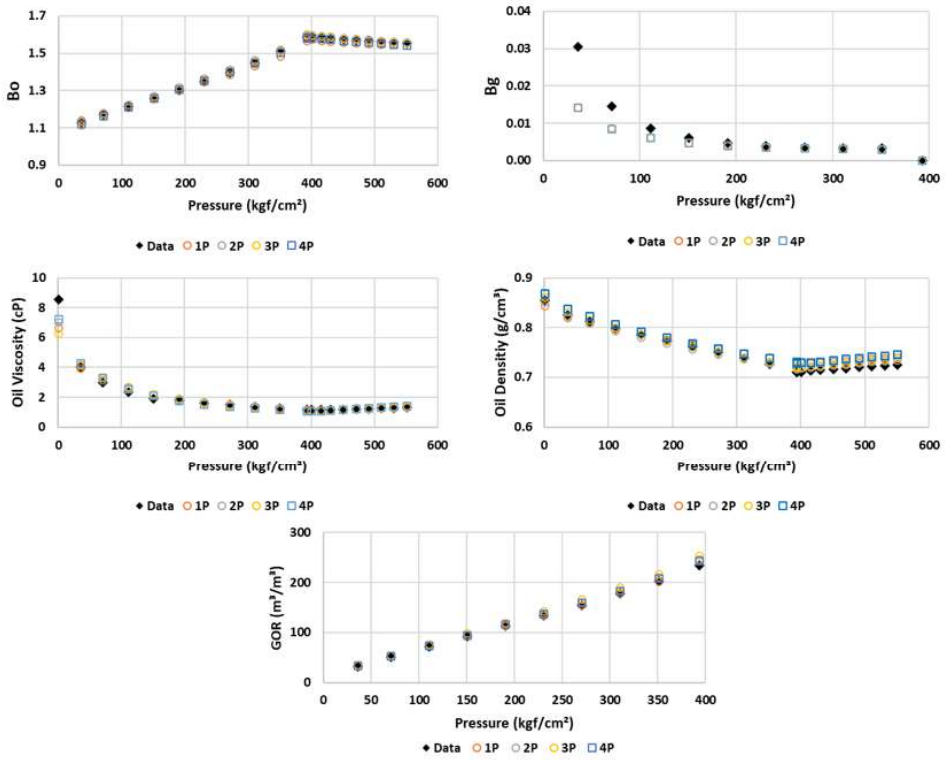

Figure 4.3: PVT Data Simulated - Small error in focus of interest region (above saturation point)

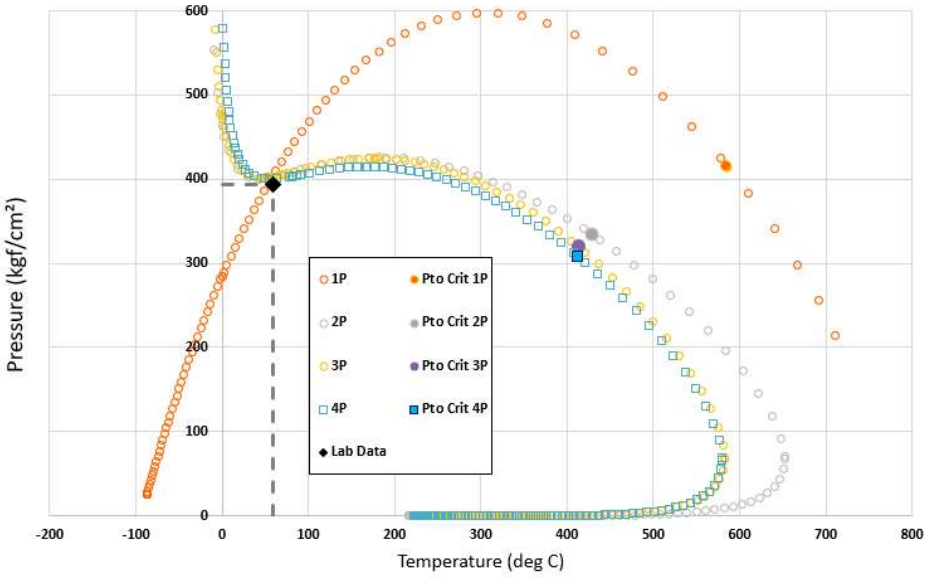

Figure 4.4: Two-phase Envelop for 1 to 4 Quadrature Point

4.2.2 EOS Tuning

As described in Section 2.1.5, simulating petroleum accurately is impossible due to the presence of several hundred to thousands of unique components (WANG and POPE, 2001). Tuning an EOS is therefore considered an art because a large number of esti-

mated parameters must be selected as adjustable variables throughout regression optimization. As the degree of freedom is high, the procedure must take into account the physical and chemical properties of the components and mixtures to avoid overfitting the model and making it incapable of predicting phases and composition. Therefore, a good initial estimation of component parameters is required, and guidance was sought from Winprop's library and some correlations in ESPOSITO *et al.* (2017), particularly for Binary Interaction Coefficient.

To make reservoir simulation viable, a small number of pseudo-components are required, limiting the degree of freedom. Consequently, a lumping procedure is necessary, often resulting in between 6 and 15 pseudo-components (WANG and POPE (2001) and AGUILAR and MCCAIN (2002)). The lumping procedure involves aggregating a number of Single Carbon Numbers into a single Multiple Carbon Number component. The selection of components that should be grouped and the number of pseudo-components after grouping is highly subjective, and the scheme proposed by ESPOSITO *et al.* (2017) was employed as a guide.

Due to the relevance of CO_2 to EOR as well as in miscibility, it remains a single element. Since $N2$ has a molar composition of less than 0.5% and is not the primary focus of this study, it has been grouped with C_1. From SCN C_2 through all isomers of C_5 were combined to form the third lumped pseudo-component, which consists of the vaporizable lights. Additionally, their tabulated properties facilitate the calculation of critical properties using a mixing rule. Noteworthy alternatives grouping include treating C_2 as a single component since it is non-condensable at standard conditions and/or grouping only C_3+C_4 because C_5 could form the liquid intermediate end. From C_6 to C_{19}, two lumpings with 7 SCN per lumped pseudo-component were conducted, grouping the intermediates (C_6 to C_{12}) and heavier ends (C_{13} to C_{19}). As previously stated, the plus fraction contains three pseudo-components for ResFluid1 (QC_{24}, QC_{44}, and QC_{70}) and two pseudo-component for ResFluid2 (PC_{27} and PC_{60}). The notation "P" on the pseudo-component indicates the origin of the plus fraction or "QC" to indicate quadrature. There is some difference in the number of carbon atoms from SHIBATA *et al.* (1987), but since the parameter is sensitive to regression/optimization, it served as an initial guess.

To tune the EOS, the next step is to select suitable data for fitting, broken down into parts, as well as the adjustable parameters of the EOS, followed by the application of a fitting/optimization technique. According to WANG and POPE (2001), "selecting relevant data" means combining similar data, such as data regarding phase-equilibrium (such as saturation pressure), molar and volumetric (molar/volume fraction), MW (mass densities), and viscosity. It is essential to tune the EOS step by step to monitor changes to the EOS, check for errors in all accessible data, and ensure coherence in parameter changes.

Due to the simplicity of having just one set of PVT data, the procedure was partially applied to fitting PVT data. Instead of working on each group of data and parameters separately, a set of data was selected to impact the specified adjustable variable. First, saturation pressure and liquid properties (such as Bo and densities) were fitted for all available pressures, followed by gas properties (such as Bg, GOR). If available, the strategy would include miscibility data, such as slim tube or swelling tests.

All of the data was adjusted using the same set of variables, with an alteration of how the variable is allowed to change (by the group with the same ratio, individually, etc.) to capture the subsequent batch of data if necessary. However, this alteration was not incorporated into the original EOS until PVT data are tuned. Each step of regression/optimization must include a consistency check to preserve chemical and physical properties coherence. As the number of carbon atoms increases, T_c, ω, $BIC_{C_1-C_n}$, and MW also increase, however, P_c and $BIC_{CO_2-C_n}$ decrease.

Only when a suitable match was found, component attributes were modified. The error must be as small as possible, with phase-equilibrium and miscibility data being considered more important in tuning, so there is a small tolerance for error in those data. The final set of information to be modified is the viscosity (for both phases, if available). Appendix A contains the procedure applied to tuning ResFluid1 and ResFluid2.

4.2.3 EOS for ResFluid1

Following the proposed step-wise tuning process, the PVT data for ResFluid1 were fitted to a thermodynamic model for this fluid. The initial parameters followed as suggested in the list.

The selected data to fit reached all available data, and the EOS-adjusted parameters were done by altering groups of variables by equal ratios each for 7 parameters. The group was: P_c, T_c, ω, and MW from $C_6 - C_{12}$, V_{shift} from $N_2 - C_1$ and the BIC_{CO_2} and $BIC_{N_2-C_1}$ from $C_2 - C_5$. Those variables susceptible to variation are shown in Table 4.6. It is worth mentioning that BIC_{i-i} is set to zero, and $BIC_{N_2-C_1-CO_2}$ is the same as $BIC_{CO_2-N_2-C_1}$ and was not altered for this modeling.

The results of tuning EOS parameters are in Table 4.7. All others missing BIC were set to zero and not subject to alteration. The comparison and absolute errors with PVT data are displayed in Figure 4.5.

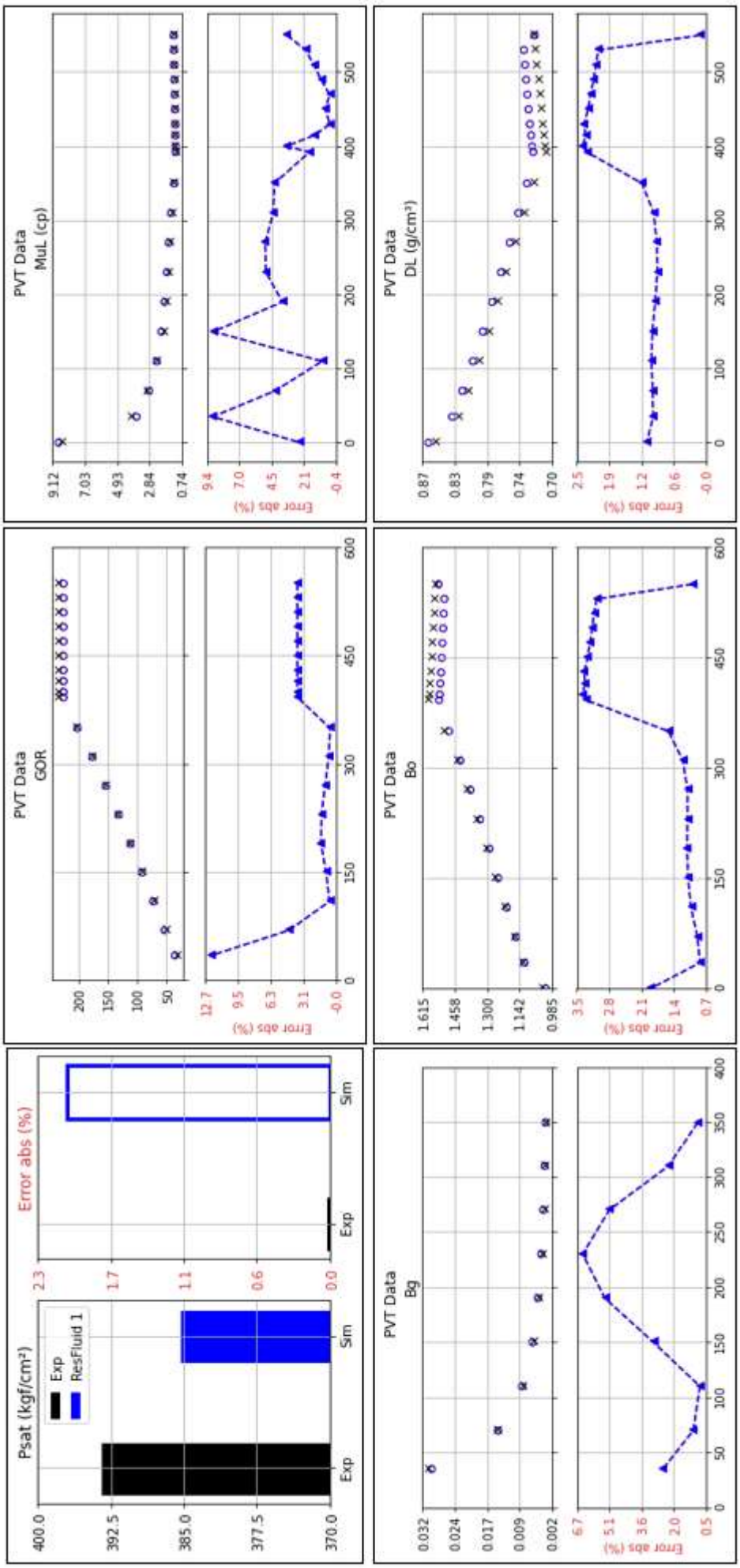

Figure 4.5: Simulated PVT Data *versus* Pressure, after tuning process for ResFluid1 EOS

Table 4.6: EOS's adjustable variables for ResFluid1 in tuning process

Comp	**Pc**	**Tc**	ω	**MW**	V_{shift}	BIC_{CO_2}	$BIC_{N_2-C_1}$
CO_2	-	-	-	-	-	-	-
N_2-C_1	-	-	-	-	Group 5	-	-
$C2_C5$	-	-	-	-	Group 5	Group 6	Group 7
C_6-C_{12}	Group 1	Group 2	Group 3	Group 4	Group 5	Group 6	Group 7
$C_{13}-C_{19}$	Group 1	Group 2	Group 3	Group 4	Group 5	Group 6	Group 7
$QC24$	Group 1	Group 2	Group 3	Group 4	Group 5	Group 6	Group 7
$QC44$	Group 1	Group 2	Group 3	Group 4	Group 5	Group 6	Group 7
$QC70$	Group 1	Group 2	Group 3	Group 4	Group 5	Group 6	Group 7

Table 4.7: Pseudo-Component's properties for ResFluid1 after tuning process

Comp	**Pc (atm)**	**Tc (K)**	ω	**MW (g/mol)**	V_{shift}	BIC_{CO_2}	$BIC_{N_2-C_1}$
CO_2	73.0291	304.2000	0.2250	44.01	-0.07180	0	0.15000
N_2-C_1	45.3189	190.1163	0.0082	16.13	-0.15317	0.15000	0
C_2-C_5	42.8819	363.4256	0.1422	42.81	-0.09294	0.14700	0.01000
C_6-C_{12}	28.6266	711.4190	0.3918	143.52	-0.02957	0.13113	0.01318
$C_{13}-C_{19}$	20.2931	823.4548	0.7041	217.08	0.00644	0.11177	0.01705
QC_{24}	14.1621	946.3550	0.8851	345.29	0.03530	0.08577	0.02226
QC_{44}	10.7077	1106.3214	1.0489	630.99	0.07278	0.02782	0.03386
QC_{70}	7.5246	1241.9333	1.2596	1003.49	0.10162	0.00103	0.04899

4.2.4 EOS for ResFluid2

Similar to the procedure for ResFluid1, the PVT data for ResFluid2 was fitted to the thermodynamic model, but some initial parameters differed from those proposed in the list.

Using PEDERSEN *et al.* (2006) as a guideline, the BIC_{CO_2} was set to 0.11 for all components, including the two from the plus fraction's quadrature points. The exception was the $BIC_{CO_2-C_1}$ which was kept at the suggested value of 0.15. The initial values for BIC_{C_1} followed the correlation of ARBABI and FIROOZABADI (1995), $BIC_{C_1-C_n} = 0.289 + 0.0001633 * SCN_n$. This was a small change compared to the suggestion in Appendix A. Another difference was the small value set for initial $BIC_{C_2-C_5}$, which was 0.02. All these dissimilarities aimed to produce a different thermodynamic model to validate the results found with ResFluid1.

All available data was sufficient for fitting the EOS since the first group of data from STEP3 (Saturation Pressure plus Liquid properties) in Appendix A was enough for tuning. The EOS adjusted parameters were also done by altering groups of variables by

equal ratios but also relied on some individual alterations as follows: P_c was a group from $C_6 - C_{12}$ to PC_{27} and an individual variable for $Pc_{PC_{60}}$. Three other groups were for T_c, ω, and MW from $C_6 - C_{12}$, 3 variables for V_{shift}, a group from $N_2 - C_1$ to $C_2 - C_5$, a group from $C_6 - C_{12}$ to PC_{27}, and an individual for PC_{60}. And two groups for BIC, BIC_{C_1} and $BIC_{C_2-C_5}$ from $C_2 - C_5$. These variables, susceptible to variation, are shown in Table 4.8.

Table 4.8: EOS's adjustable variables for ResFluid2 in the tuning process

Comp	**Pc**	**Tc**	ω	**MW**	V_{shift}	BIC_{CO_2}	$BIC_{N_2C_1}$	$BIC_{C_2C_5}$
CO_2	-	-	-	-	-	-	-	-
$N_2 - C_1$	-	-	-	-	Group 5	-	-	-
$C2_C5$	-	-	-	-	Group 5	-	Group 7	-
$C_6 - C_{12}$	Group 1	Group 2	Group 3	Group 4	Group 6	-	Group 7	Group 8
$C_{13} - C_{19}$	Group 1	Group 2	Group 3	Group 4	Group 6	-	Group 7	Group 8
$PC27$	Group 1	Group 2	Group 3	Group 4	Group 6	-	Group 7	Group 8
$PC60$	X	Group 2	Group 3	Group 4	X	-	Group 7	Group 8

Table 4.9: Pseudo-Component's properties for ResFluid2 after tuning process

Comp	**Pc (atm)**	**Tc (K)**	ω	**MW (g/mol)**	V_{shift}	BIC_{CO_2}	$BIC_{N_2C_1}$	$BIC_{C_2C_5}$
CO_2	72.8000	304.2000	0.2250	44.01	-0.07180	0	0.15000	0.11000
$N_2 - C_1$	45.3275	190.1672	0.0082	16.12	-0.23010	0.15000	0	0.01795
$C2 - C5$	42.8585	363.5518	0.1423	42.84	-0.13950	0.11000	0.01795	0
$C_6 - C_{12}$	26.4635	580.8096	0.4017	101.18	-0.05864	0.11000	0.02265	0.03000
$C_{13} - C_{19}$	17.3743	710.6802	0.7002	179.06	-0.00729	0.11000	0.02895	0.03000
$PC27$	14.0211	901.2980	0.8820	424.08	0.07009	0.11000	0.04885	0.03000
$PC60$	7.1413	1079.7841	1.6460	928.53	0.11952	0.11000	0.05500	0.03000

The result of tuning EOS parameters is in Table 4.9 and all others missing BIC were set to zero and not subject to alteration. The comparison and absolute errors with PVT data are displayed in Figure 4.6.

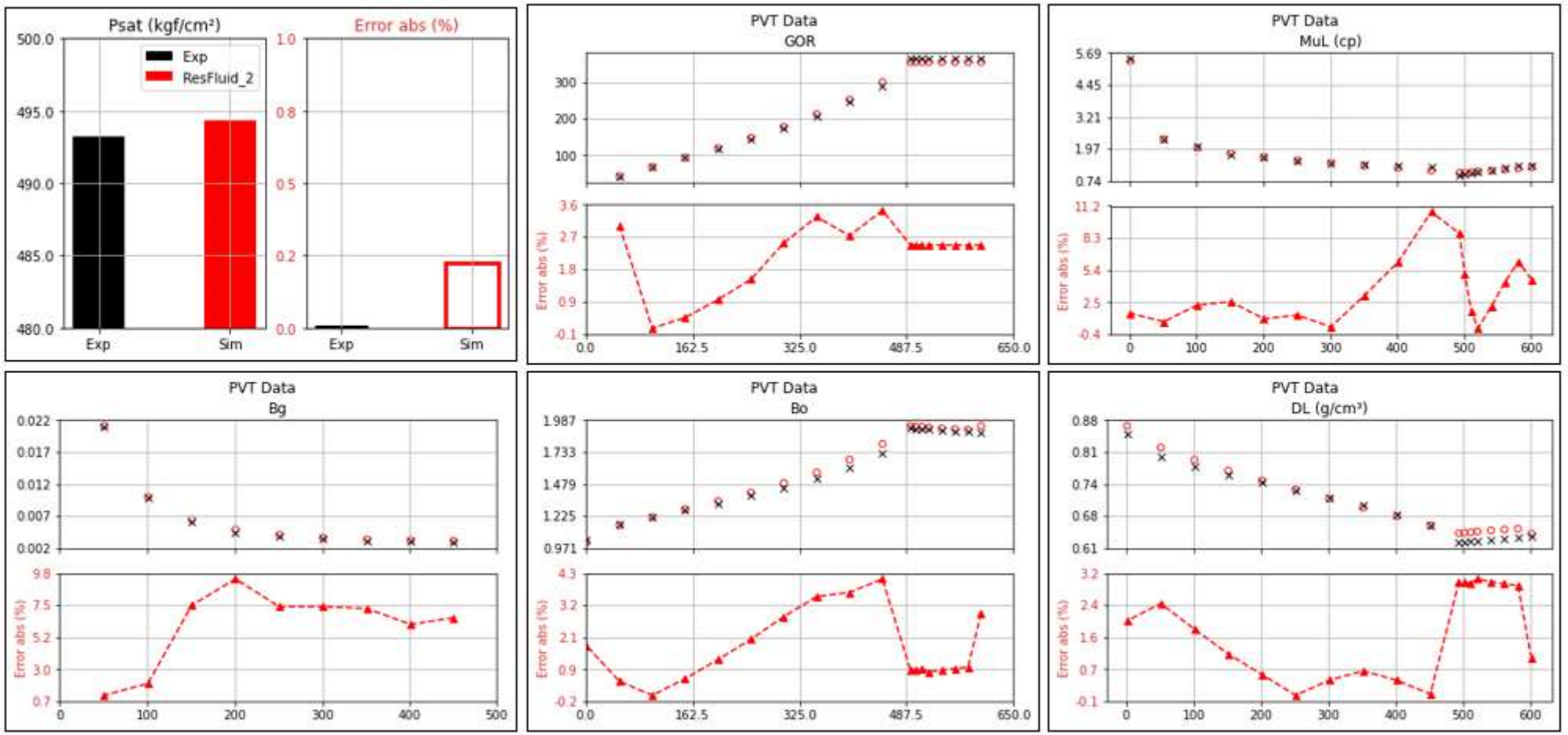

;

Figure 4.6: Simulated PVT Data *versus* Pressure, after tuning process for ResFluid2 EOS

4.2.5 MMP Calculation

Once the two thermodynamic models for ResFluid1 and ResFluid2 were developed, the estimation of MMP was performed numerically using a 1D model, which is further described in Section 4.3. The concept was to simulate a slim tube test, and the MMP was defined as the pressure at which the recovery factor (the percentage of oil recovery from porous media) reaches at least 95% after injecting 120% of the pore volume, as discussed in Laboratory Experiment to Evaluate Miscibility in Section 2.1.5.

To conduct the test, the original reservoir oil was inputted into a simulator for ResFluid1 and ResFluid2 (as described in Table 4.1 and 4.3), along with the two compositions of injected gas described in Section 4.1.2, above the saturation pressure. After plotting the recovery factor against pressure, the MMP was determined as the pressure at which the recovery loses its linear trend and reaches the high recovery factor plateau.

Res Fluid 1

For ResFluid1, two different gas injection compositions, referred to as "Mix," were evaluated with differing concentrations of CO_2. Mix1 consists of 50% CO_2 and 50% $N_2 - C_1$ (mainly methane since this pseudo-component has no significant contribution of N_2), while Mix2 is purely methane (100% $N_2 - C_1$). The simulation results, including the linear extrapolation of ResFluid1 behavior and the MMP, are shown in Figure 4.7.

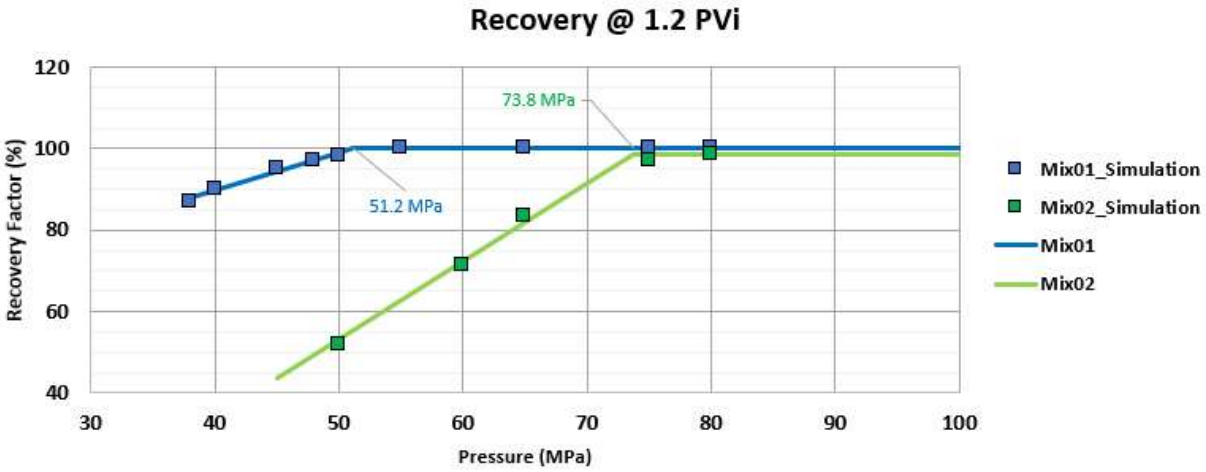

Figure 4.7: MMP for ResFluid1 - Recovery Factor at 1.2 Injected Pore Volume versus Pressure

Res Fluid 2

For ResFluid2, a new gas mixture had to be simulated since Mix1 maintained a high recovery factor of over 95% at all pressure ranges, despite showing a linear decay in recovery factor with smaller pressure. As a result, the proportion of CO_2 was changed,

and Mix3 was defined to contain 10% CO_2 and 90% $N_2 - C_1$. The results for ResFluid2, including those for Mix1, are displayed in Figure 4.8.

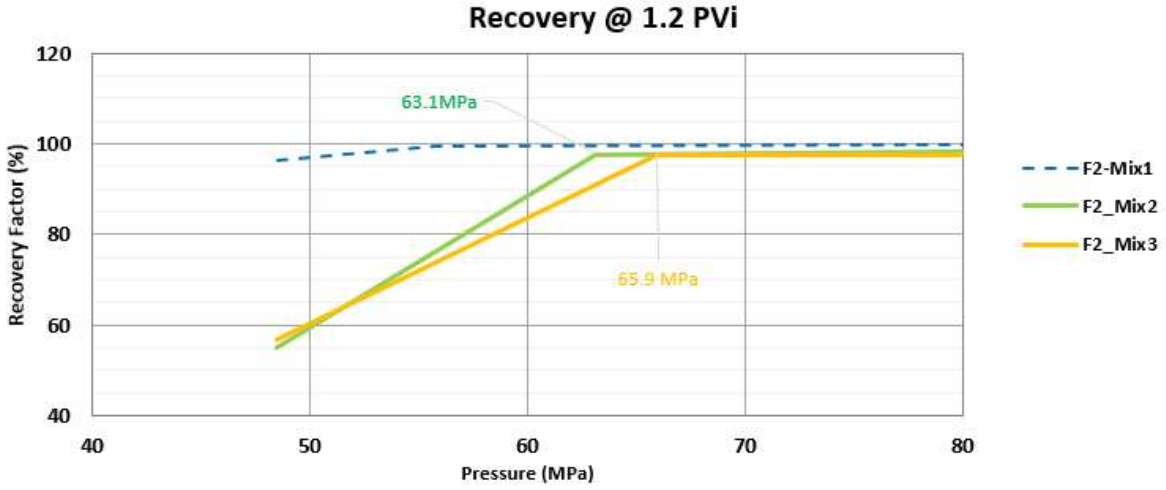

Figure 4.8: MMP for ResFluid2 - Recovery Factor at 1.2 Injected Pore Volume versus Pressure

4.3 Reservoir Model

To perform the numerical simulation of the slim tube test and the reservoir, a 1D model was utilized. The reservoir dimensions, displayed in Figure 4.9, were divided into 400 cells in the I direction to minimize numerical effects. The porosity (Φ = 25.7%) and permeability (K=2000 mD) were constant throughout the reservoir.

The relative permeability was assumed to be the same as WANG *et al.* (2020), and the initial water saturation was set to a very low value ($S_w = 1E-8$) as the focus was on the gas and oil interaction.

A gas injector with a constant composition (Mix 1, 2, or 3) was placed at the beginning of the grid, with a constant rate of almost 17% of pore volume per day at reservoir conditions, and a producer was placed at the end of the grid operating at a bottom-hole pressure equal to the reservoir's pressure.

For the numerical simulation, the GEM software from CMG's package was used. To achieve accuracy, a fully-implicit formulation was chosen. Unlike explicit solvers that use only the past time step while updating the solution, implicit solutions derive the solution at the subsequent time step by solving a set of equations involving subsequent time steps. Therefore, implicit solvers are generally more stable and error-tolerant than explicit solvers. Additionally, a TVD (Total Variation Diminishing) flux limiter was activated to ensure numerical stability and eliminate under and over-shoot in the calculation. Furthermore, the flash routine was set to be solved at every Newtonian iteration rather than only at the same level as the flow equation.

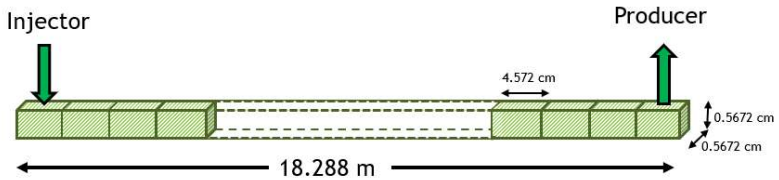

Figure 4.9: Numerical Model - Reservoir Dimensions

4.4 Case Studies

As presented in section 4.1.2, two different scenarios for investigating miscibility were established to minimize the differences between the cases. The first case was simulated with the same temperature, initial oil composition, and gas injection composition but at a different pressure to yield two scenarios of miscibility: above and below MMP. The second case was simulated with the same temperature, initial oil composition, and pressure but at a different gas injection composition, also resulting in two scenarios of miscibility: above and below MMP. For ResFluid2, two sets of miscibility scenarios, for validation purposes, were simulated with and without CO_2. The scenarios and their respective cases are presented in Table 4.10.

Table 4.10: Cases Evaluated for Different Scenarios

Scenarios	**Oil Composition**	**Gas Composition**	**MMP (MPa)**	**Pressure (MPa)**	**Miscibility Condition**
Same Gas Injection	ResFluid1	Mix 1	51.2	40	Immiscible
	ResFluid1	Mix 1	51.2	60	Miscible
Same Pressure	ResFluid1	Mix 2	73.8	60	Immiscible
	ResFluid1	Mix 1	51.2	60	Miscible
Validation without CO2 injection	ResFluid2	Mix 2	63.1	50	Immiscible
	ResFluid2	Mix 2	63.1	70	Miscible
Validation with CO2 injection	ResFluid2	Mix 3	65.9	50	Immiscible
	ResFluid2	Mix 3	65.9	70	Miscible

Chapter 5

Results and Discussion

In this chapter, we discuss the outcomes of a series of numerical simulations performed with ResFluid 1 oil and two different gas compositions. As stated in the previous chapter and displayed in Table 4.10, numerical experiments were also conducted with ResFluid 2 oil to validate results using a different thermodynamic model.

The results were analyzed and compared to assess the impact of miscibility on oil composition and to determine if it is possible to construct a chemical alteration indicator to indirectly estimate miscibility under reservoir conditions.

5.1 Same Gas Composition and Different Pressure

The first simulation to evaluate the alteration in producer composition depending on the miscibility scenario was conducted by keeping the gas composition constant (Mix1 - 50% CO_2 and 50% C_1) and varying the pressure (40 MPa and 60 MPa) to obtain distinct miscibility conditions. The simulation conditions are displayed in the MMP diagnostic curve for Mix1 in Figure 5.1.

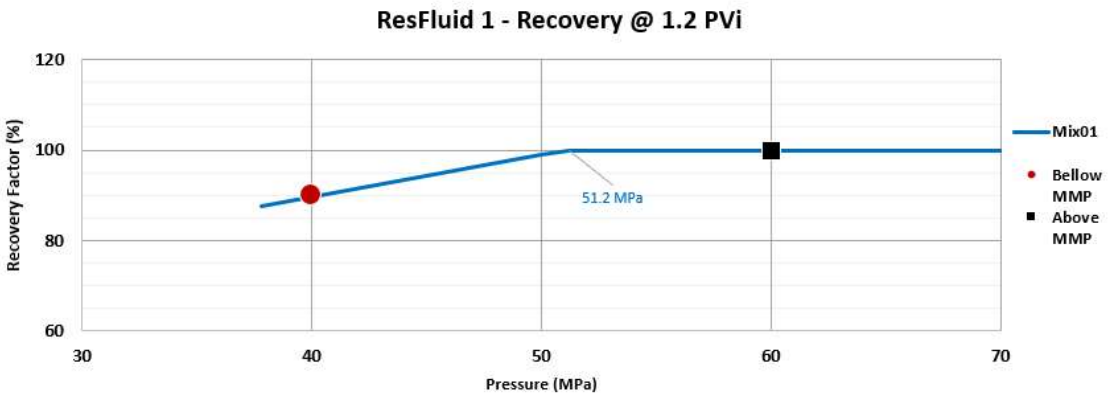

Figure 5.1: Different Pressure Cases for Mix1

To present results independent of the characteristics of the reservoir model and

wells, such as permeabilities, rates, and well spacing, the results are plotted as a function of the amount of injected pore volume (IPV or iPV), which is a function of the constant gas rate injection at reservoir condition, and is a function of time. By changing the x-axis, the results can be compared with other examples.

In the first set of cases, the case below MMP has a lower recovery factor (RF), under 80%, and its behavior changes at two different moments (at IPV 45% and 85%), as seen in Figure 5.2a. These derivative alterations in RF are associated with gas breakthrough on the producer, as seen in the vapor fraction and GOR (Figure 5.2b and c/d, respectively).

It is also noteworthy that GOR only increases in the case above MMP after IPV=100%, when the recovery reaches its maximum, i.e., the gas-injected mixture with oil was able to mobilize the oil after a shock wave of gas promoting a very efficient sweep, as expected. The graph and these three IPV moments are highlighted in Figure 5.2.

One may notice that the simulator has some difficulty in phase identification in Figure 5.2b, in the case above MMP over IPV 100% (changing the phase identification from gas to liquid), but since the phase is monophasic, recovery has already reached its maximum, and liquid production is virtually zero, this is not an issue.

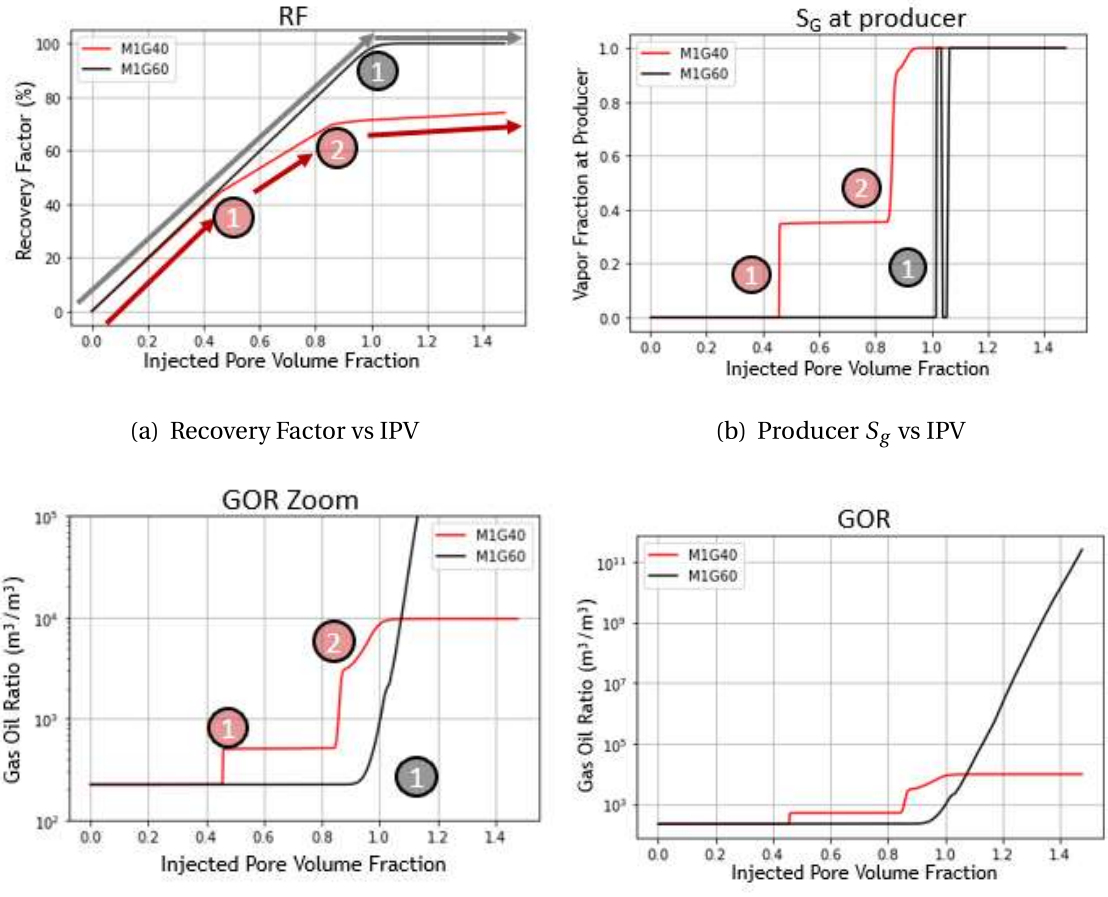

(a) Recovery Factor vs IPV

(b) Producer S_g vs IPV

(c) Zoom in GOR vs IPV

(d) GOR vs IPV

Figure 5.2: Different Pressure Cases. RF, GOR and, S_g on producer. (——) Above MMP1 - ResFluid 1 + Mix1 and (——) Below MMP1 - ResFluid 1 + Mix 1.

As for the stock-tank oil (or dead oil), Figure 5.3 shows the first six graphs of each pseudo-component, and the last graph shows the sum of all quadrature compositions, since the objective is to mimic laboratory data. The first three graphs represent the lightest pseudo-components, which tend to be in the vapor phase (as seen by their small amounts in the liquid composition), and the three in the middle row represent the main constituents of the liquid phase. In the beginning, the light-ends (C_6-C_{12}) are shown, followed by the intermediates ($C_{13}-C_{19}$) in the middle, and finally, the heavier-ends (plus fraction: $QC_{24}+QC_{44}+QC_{70}$) of the liquid phase. The bottom three graphs represent GOR, RF, and the molecular weight of the liquid, allowing for a comparison of the alteration in oil composition with those variables.

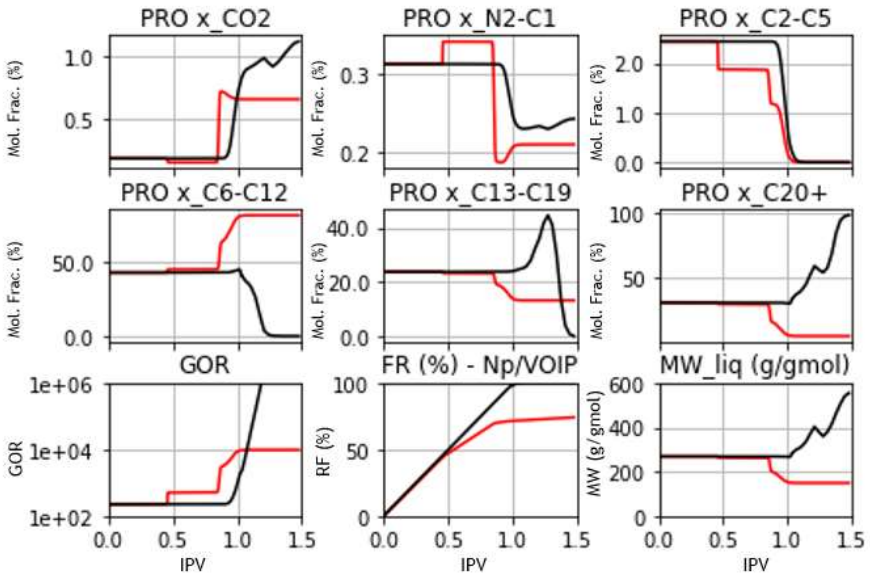

Figure 5.3: Results for Different Pressure Cases. Producer liquid composition, GOR, RF and Molecular weight of stock-tank oil. (——) Above MMP1 and (——) Below MMP1.

For these results, a chemical marker might be present indicating the condition of gas displacement in the reservoir since the cases below and above MMP have different behavior. Liquid's light-ends ($C_6 - C_{12}$) tend to increase below MMP and decrease above MMP. Intermediates ($C_{13} - C_{19}$) and heavier (plus fraction) components decrease below MMP while they increase above MMP, and intermediates also decrease just above MMP after a while. As a tendency to produce heavier components, the molecular weight may also be a marker of miscibility. Possible markers are indicated in Figure 5.4, showing how the composition of each component changes over the IPV, with arrows pointing out the variable tendency. The IPV composition up to 80% is the same for both cases. At 90% IPV, the below MMP case increases in light-ends and decreases in intermediate and heavier components, while the above MMP case reduces light-ends and increases intermediate and heavier components. At 110% IPV, above MMP reduce lights and increase intermediate and heavier components. At 140% there is a more expressive increase in plus fraction components noticeable above MMP.

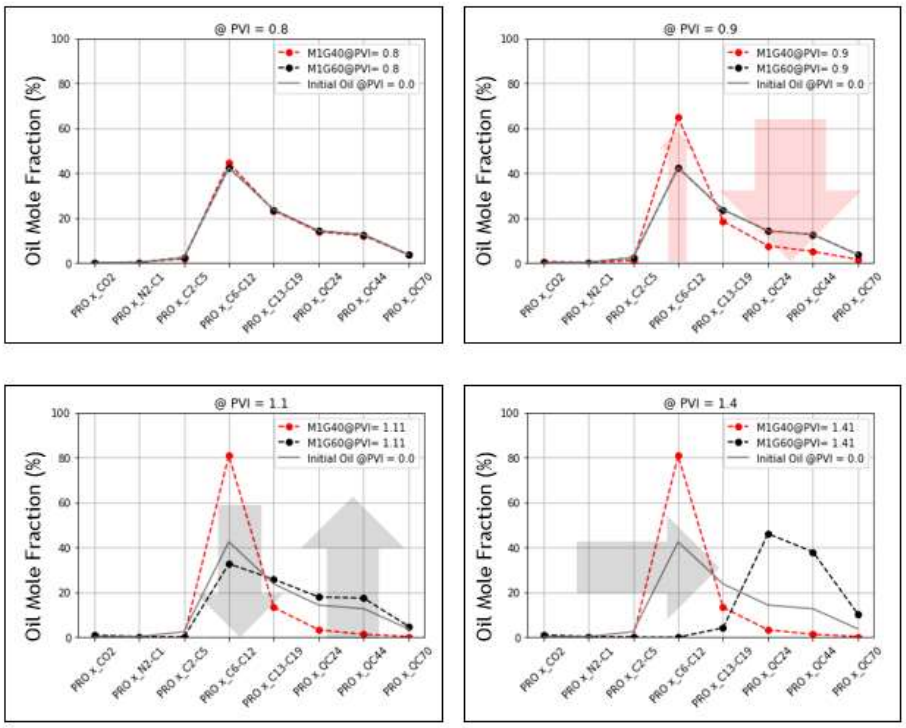

Figure 5.4: Composition at 80%, 90%, 110%, and 140% IPV for Different Pressure Cases. (——) ResFluid 1 initial composition, (- - - -) Above MMP1, and (- - - -) Below MMP1.

5.2 Same Pressure and Different Gas Composition

The first experiment revealed the presence of certain promising chemical markers. However, since the cases operated at different pressures, it was unclear whether these markers were connected with miscibility at reservoir conditions or if the pressure difference was the primary cause. To remove any trace of uncertainty, the investigation was expanded to include a series of cases that had the same pressure but a different gas injection composition to promote different scenario of miscibility.

The findings of the simulation with a different injection composition (Mix2 - 100% C_1) were examined and combined with the results from the earlier study for the second analysis, using ResFluid 1. The comparison was made between the case that is above MMP with Mix 1 and the case that is below MMP with Mix 2 (Below MMP2), and both of these cases had the same reservoir pressure of 60 MPa, as shown in Figure 5.5.

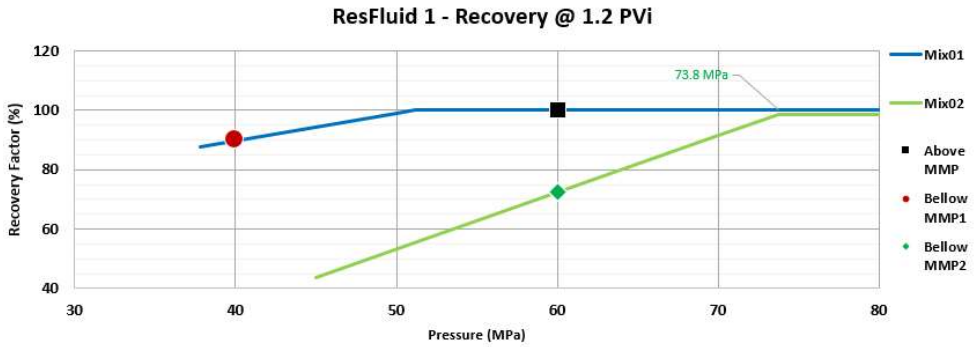

Figure 5.5: Different Composition and Different Pressure Cases

Figure 5.6 illustrates an analogous graph for Recovery Factor (Figure 5.6a), gas saturation or vapor fraction at producer (Figure 5.6b), and GOR (Figure 5.6c and d). The GOR behavior is comparable to the preceding Below MMP1 instance but occurs a little later at 60% IPV (instead of 45% and 60%) and more aggressively, nearly in a single step, reaching close to 2000 m^3/m^3. As seen in Figure 5.6b, this increases the saturation near the producer, which reaches near 90% of S_g. At 80% IPV, a second breakthrough occurs, which decreases the RF derivative and raises the GOR above 10,000 m^3/m^3. Additionally, the recovery factor is considerably lower, showing that CO_2 has the ability to extract more oil even below MMP.

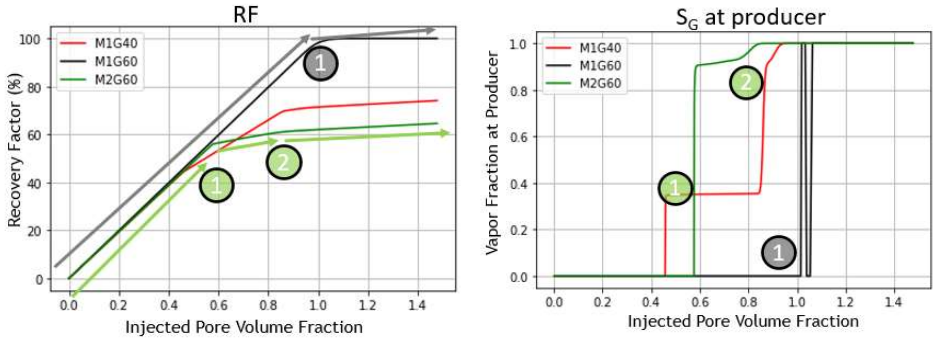

(a) Recovery Factor vs IPV

(b) Producer S_g vs IPV

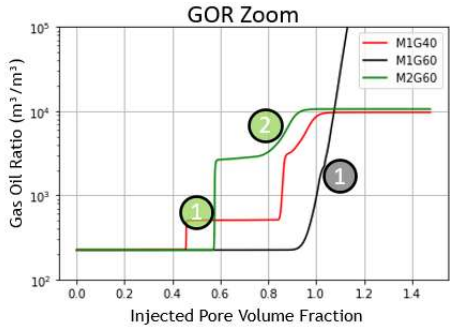

(c) Zoom in GOR vs IPV

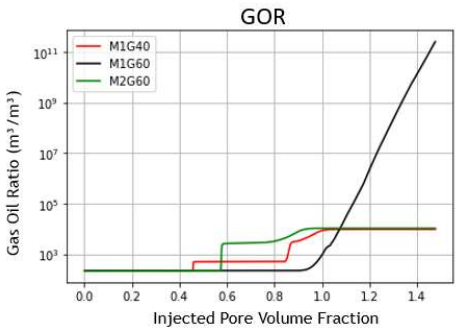

(d) GOR vs IPV

Figure 5.6: Different Pressure Cases. RF, GOR and, S_g on producer. (——) Above MMP1, (——) Below MMP1, and (——) Below MMP2 - ResFluid 1 + Mix 2.

As shown in Figure 5.7, Below MMP2 exhibited a similar response regarding the earlier candidates for miscibility indicators as Below MMP1. The concentration of light ends tended to rise below the MMP threshold and fall above it. Below MMP, intermediates and heavy components decreased while those above MMP increased. After some additional IPV, intermediates decreased solely above MMP. With these findings, the theory that the pressure difference was the primary reason for marker differences was refuted, promoting good sweep and obtaining high recovery as a result of miscibility is the cause of marker differences.

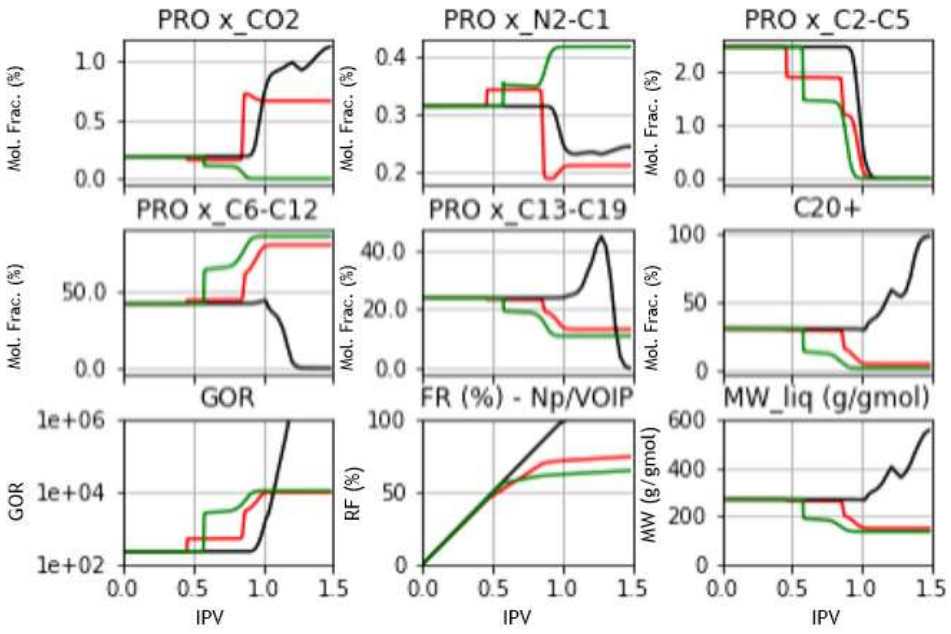

Figure 5.7: Same Pressure and Different Gas Composition Cases. Producer liquid composition, GOR, RF and Molecular weight of stock tank oil. (——) Above MMP1, (——) Below MMP1, and (——) Below MMP2.

Changes in the molar composition fraction of each component over the IPVs are shown in Figure 5.8 for Above MMP1, Below MMP1, and Below MMP2. Up to 50% IPV, the compositions are the same for all cases. From 60% to 100% IPV, the cases below MMP (Below MMP1 and Below MMP2) exhibit an increase in lights and a decrease in intermediate and heavier components. At 120% IPV, Above MMP1 shows a decrease in lights and an increase in intermediate and heavier components, while the below MMP cases show a further reduction in heavier components.

Through these experiments, we have identified certain chemical markers that can predict whether the recovery factor will be high or low based on the miscibility condition of the injected gas with the reservoir oil. This suggests that the presence of a marker may serve as a valid predictor of miscibility in gas injection. Additionally, the results obtained from Below MMP2 are similar to those obtained from Below MMP1, indicating that the behavior is reproducible and not specific to a particular gas injec-

tion composition or pressure.

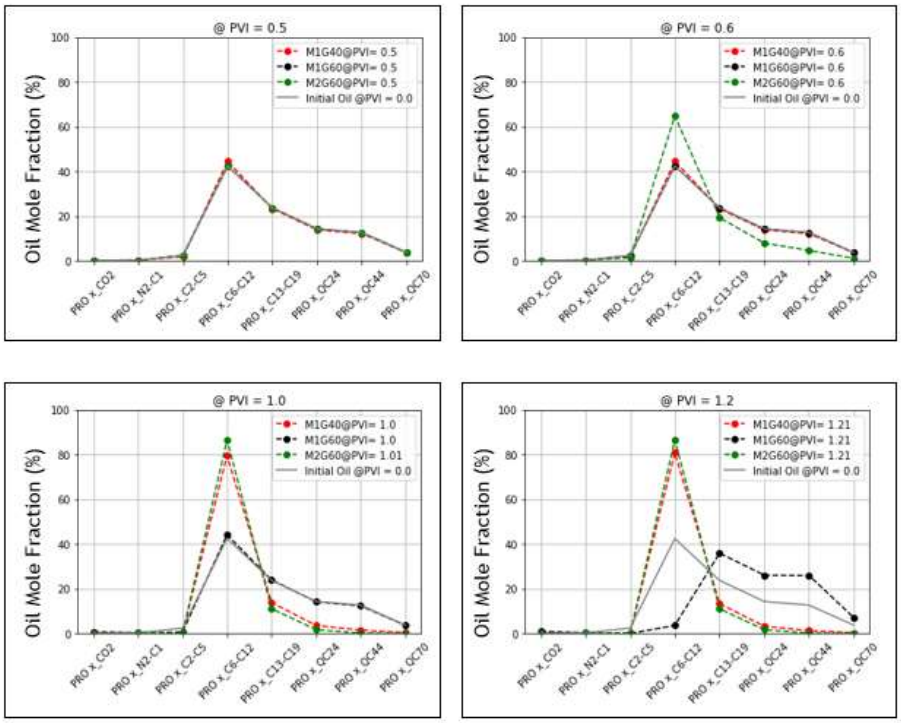

Figure 5.8: Composition Mole Fraction in Different IPV's.
(——) ResFluid 1 initial composition, (- - - -) Above MMP, (- - - -) Below MMP1, and (- - - -) Below MMP2.

Table 5.1 presents the results of three simulations using ResFluid 1 for the two evaluated scenarios, while Figure 5.9 shows the trends in the miscibility indicator identified by changes in a specific variable.

Table 5.1: Cases Evaluated for Different Scenarios with ResFluid 1

Scenarios	**Oil Composition**	**Gas Composition**	**MMP (MPa)**	**Pressure (MPa)**	**Miscibility Condition**
Same Gas Injection	ResFluid1	Mix 1	51.2	40	Immiscible
	ResFluid1	Mix 1	51.2	60	Miscible
Same Pressure	ResFluid1	Mix 2	73.8	60	Immiscible
	ResFluid1	Mix 1	51.2	60	Miscible

The chemical indicator of miscibility occurs when the contribution of the liquid's light ends decreases and the contribution of the liquid's intermediate and heavy components increases, causing the liquid's molecular weight to increase (Figure 5.9). When miscibility is not present at reservoir conditions, the liquid phase loses contributions of intermediates and heavier ends, and the proportion of liquid light ends increases.

For an immiscible situation, it is assumed that heavier components will be lost since phase-equilibrium results in a two-phase fluid, and gas with better mobility

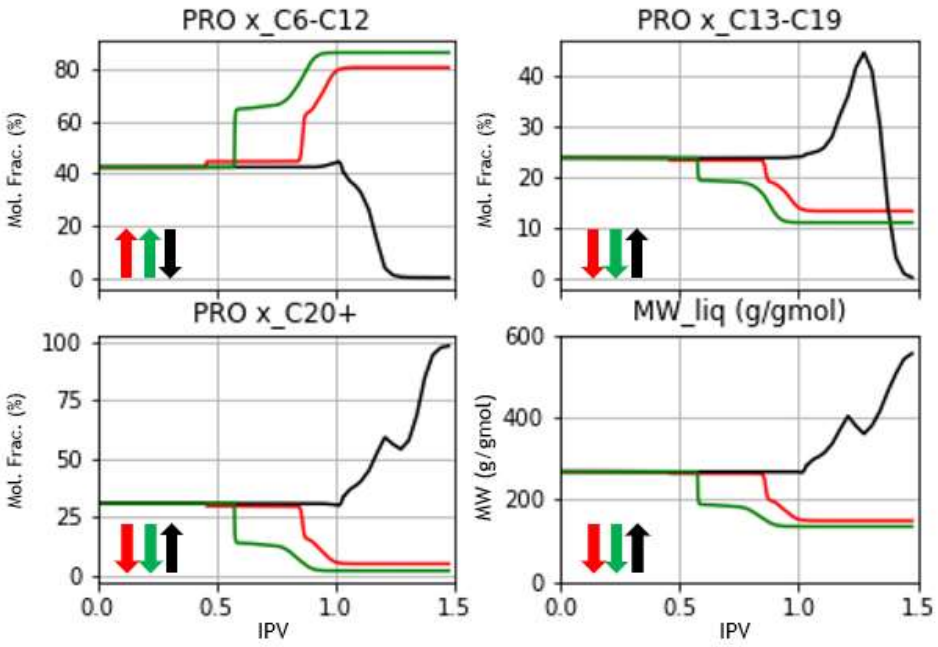

Figure 5.9: Variables and Tendencies for an Indicator of Miscibility. (——) Above MMP, (——) Below MMP1, (——) Below MMP2.

might extract the lighter component from oil, leaving behind the heavier components in the liquid phase. However, in a miscible state, enriching the liquid phase with the heaviest component is counterintuitive, as one would anticipate the composition to remain constant or become lighter, or, if the intermediate/heavy component becomes more concentrated, to undergo a reversal at some point (as the intermediate did in the above MMP case).

Therefore, the indicator behavior must be explained by a mechanism incorporating both the thermodynamics of molecule interaction and the flow dynamics as components are swept in the reservoir.

5.3 Relative Permeability Influence

In this study, variations in relative permeability shape will be investigated to analyze their impact on miscibility indicators. As explained in Chapter 2, Section 2.2, relative permeability reflects the relationship between fluid flow and the characteristics of the reservoir rock.

The wetting phase, which has a stronger affinity for the reservoir rock, adheres to and flows closer to the grains, while the non-wetting phase tends to flow towards the center of the pore throat. Due to the interaction of these two phases, they disturb each other's flow, resulting in a unique relative permeability shape based on the saturation levels of each phase and their interaction. One approach to minimize this disturbance

between phases is to model relative permeability using an X-shaped curve, which is only dependent on the saturation of each phase.

Mobile oil is defined as oil that is able to flow in its liquid phase and is calculated between the critical saturation, which is the saturation phase required for flow to begin, and the residual oil saturation, a saturation that cannot flow and is adhered to the rock after a drainage process. It is an important parameter from relative permeability that affects recovery. It is important to note that a phase can reduce below its saturation point, despite the fact that it cannot flow. Molecular interactions can extract components to another phase, hence reducing the volume and lowering the saturation. The influence of mobile oil must also be evaluated.

In the previous situations (Above MMP, Below MMP1, and Below MMP2), two new relative permeabilities were added to be analyzed to determine the influence of relative permeability. The first alteration involves preserving the relative permeability of mobile oil and changing its shape into an X. The second step is to transform the shape into an X and allow all oil to be mobile, i.e., to reduce the residual saturation of oil to zero. Figure 5.10 depicts the change in Gas-Liquid relative permeability. Since the water saturation is essentially zero, the water-oil relative permeability is superfluous, and the liquid phase consists of only oil.

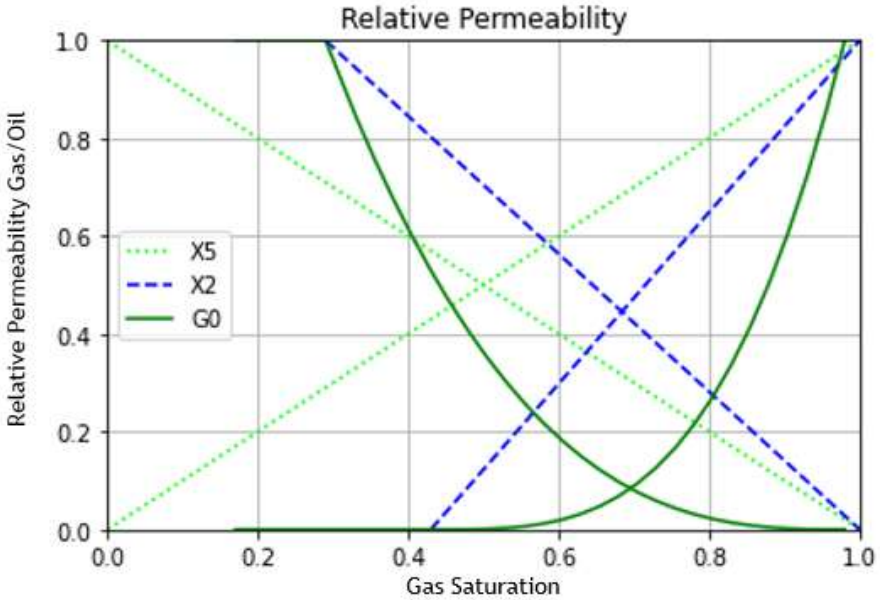

Figure 5.10: Variation in Gas-Liquid Relative Permeability. (——) G0 - Relative Permeability (Original), (- - - -) X2 - Relative Permeability in X-shape with same mobile oil, (·····) X5 - Relative Permeability in X-shape with all oil mobile ($S_{or} = 0$).

The results are shown in Figures 5.11, 5.12, and 5.13 for the Above MMP, Below MMP1, and Below MMP2 cases, respectively. As expected, the variation of relative permeability has a significant impact on the recovery factor for both cases below MMP,

since a different saturation profile is imposed by relative permeability, particularly the one containing all mobile oil, which is predicted to have a high level of phase disturbance and interfacial tension. As anticipated, the shape of relative permeability had no effect on recovery above MMP due to the absence of a significant interfacial tension effect. The composition varies slightly, but the behavior did not vary in any of the three instances. Therefore, the conclusion of this subsection is that relative permeability is not the primary factor, at least not by itself.

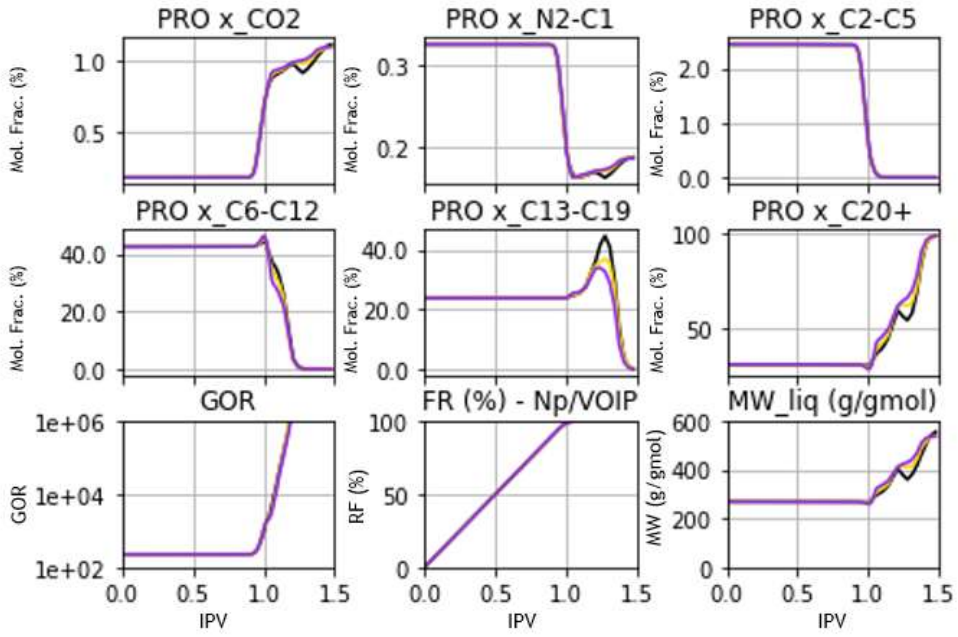

Figure 5.11: Results forAbove MMP differing: (——) Relative Permeability (Original), (——) X-shape with same mobile oil, (——) X-shape with all oil mobile.

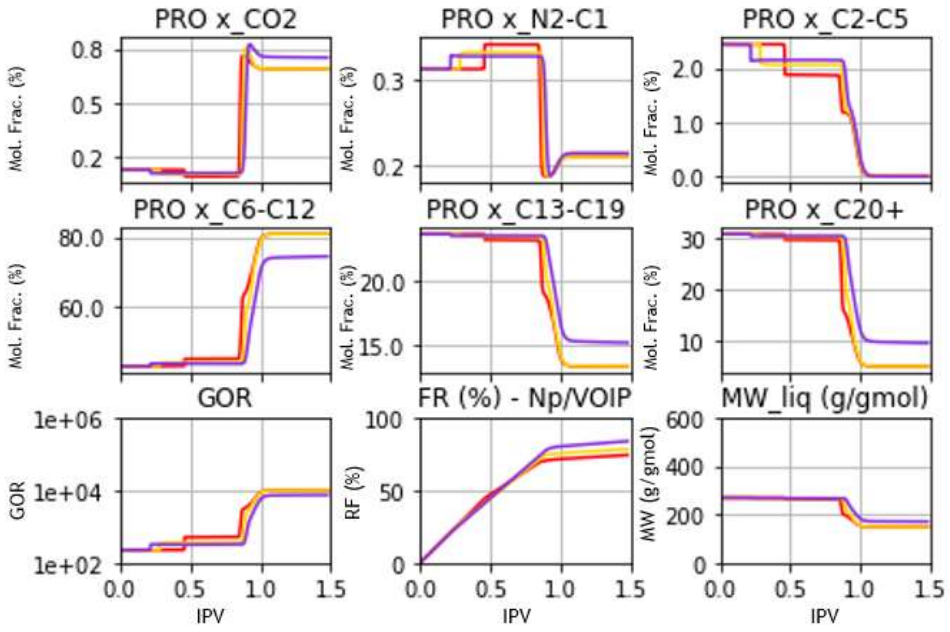

Figure 5.12: Results for Below MMP1 differing: (——) Relative Permeability (Original), (——) *X*-shape with same mobile oil, (——) *X*-shape with all oil mobile.

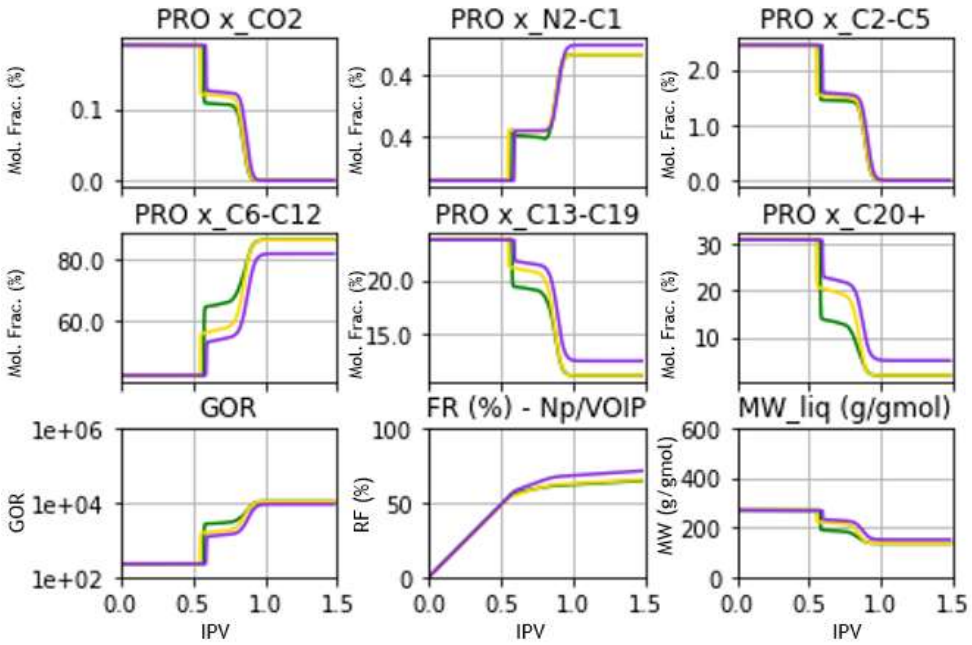

Figure 5.13: Results for Below MMP2 differing: (——) Relative Permeability (Original), (——) *X*-shape with same mobile oil, (——) *X*-shape with all oil mobile.

5.4 Viscosity Influence

Since relative permeability was not the main parameter influencing the behavior of indicators, the next evaluation focused on the gas injection's ability to cause oil swelling

and lower its viscosity. The displacing fluid, gas in this case, which has a lower viscosity than oil, improves its ability to sweep oil since the mobility ratio is reduced, favoring oil flow conditions and improving hydrocarbon recovery.

To analyze the viscosity alteration without tuning another model, the corresponding state for viscosity (PEDERSEN and FREDENSLUND, 1987) was disabled, and a constant viscosity for all pseudo-components was defined. With this alteration, the phases, oil and gas, have a fixed viscosity of 1 centipoise. This alteration is for investigation purposes only since there is no mechanism to fix the viscosity of a component or even phases. However, it is an interesting line of investigation since the swelling effect and gas/oil interaction can be evaluated without corresponding alterations in viscosity.

The results for cases above MMP, below MMP1, and below MMP2, and the respective cases with fixed viscosity, are shown in Figure 5.14. There were slight changes in the producer oil composition, GOR, RF, and MW_{liq}, but the overall behavior did not change, especially in the miscibility indicator, as seen in Figure 5.15.

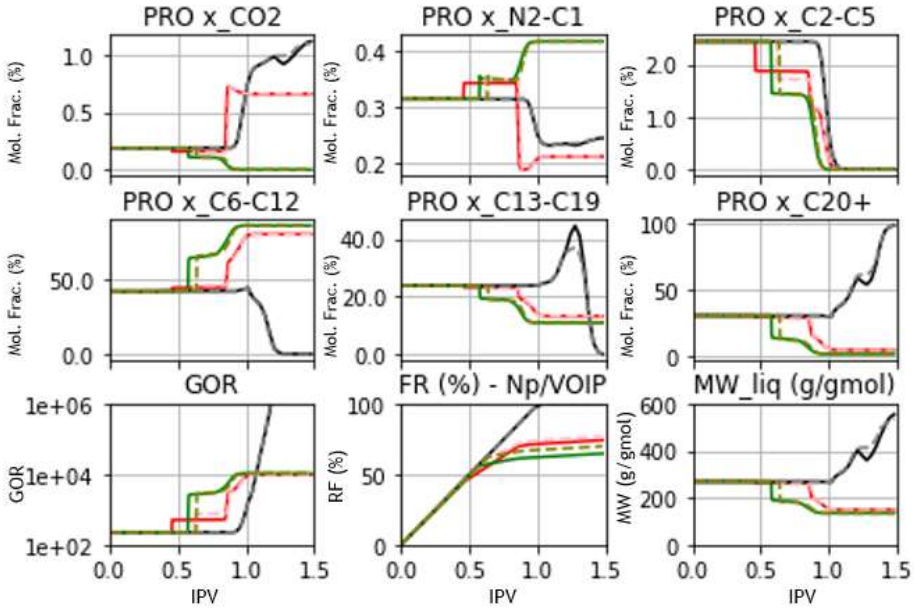

Figure 5.14: Viscosity alteration: (——) Above MMP, (- - - -) Above MMP fixed viscosity, (——) Below MMP1, (- - - -) Below MMP1 fixed viscosity, (——) Below MMP2, (- - - -) Below MMP2 fixed viscosity.

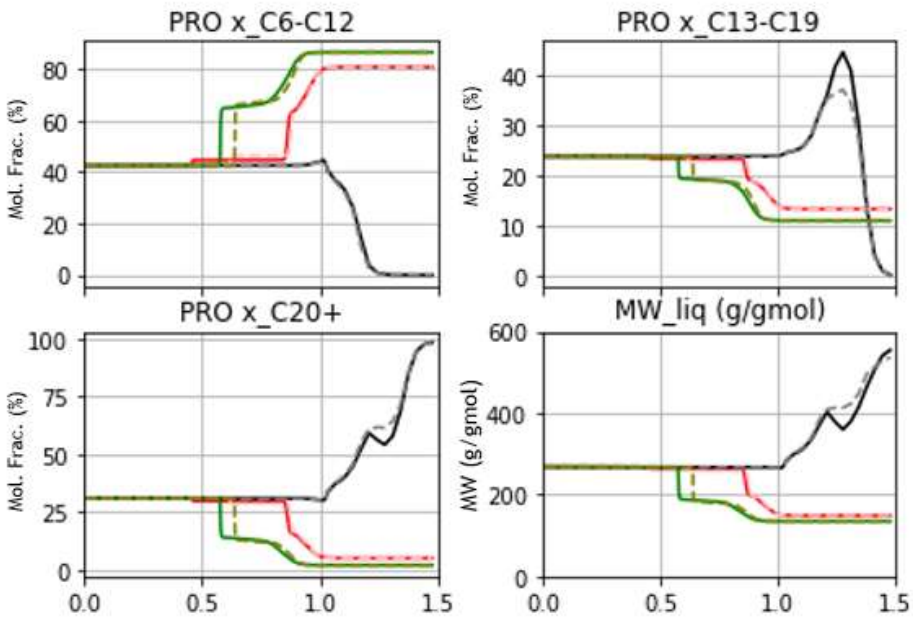

Figure 5.15: Miscibility Indicator with and without Fixed Viscosity: (——) Above MMP, (- - - -) Above MMP fixed viscosity, (——) Below MMP1, (- - - -) Below MMP1 fixed viscosity, (——) Below MMP2, (- - - -) Below MMP2 fixed viscosity.

5.5 Combined Effect: Relative Permeability and Viscosity Influence

As seen in the preceding subsections, the relative permeability instances were assembled using three cases, whereas the viscosity instances were assembled using two cases. Prior to this point, the analysis was conducted individually for each change. The outcomes of combining an X-shape, maintaining and increasing mobile oil, and keeping the viscosity of all phases constant are demonstrated for each example. Above the MMP, below the MMP1, and below the MMP2 are shown in Figure 5.16, 5.17, and 5.18, respectively.

There is no noticeable or meaningful change above the MMP. The behavior of each indicator is the same, with only minor variations depending on the simulations evaluated. In both the Below MMP1 and Below MMP2 scenarios, the same phenomenon occurs, with the exception of one simulation that performs differently from the others. The light components of the liquid decrease, the intermediate composition rises and declines, and the heavier components increase. Additionally, the liquid's molecular weight increases.

This is the same behavior, with minor changes, as exhibited by the miscibility indicator above the MMP, except it occurs below the MMP with fixed viscosity and an "X-shaped" relative permeability with all oil mobile. Through a detailed analysis of these graphs, one might notice that having a fixed viscosity and an X-shaped relative

permeability with the same amount of mobile oil was not enough to produce a change in the miscibility indicator tendency. Only when all the oil was susceptible to flow did this behavior change.

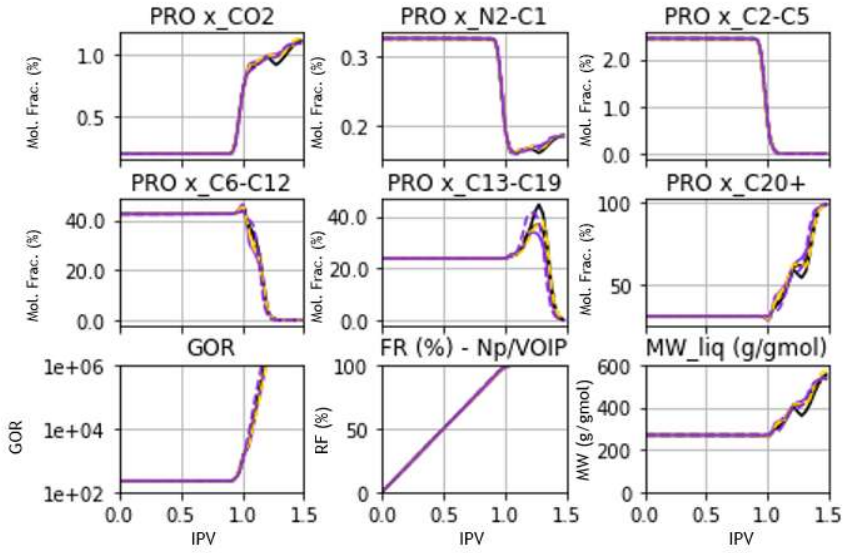

Figure 5.16: Results for Above MMP differing: (——) Relative Permeability (Original), (- - - -) Original + Fixed Viscosity, (——) *X*-shape with same mobile oil, (- - - -) *X*-shape with same mobile oil + Fixed Viscosity, (——) *X*-shape with all oil mobile, (- - - -) *X*-shape with all oil mobile + Fixed Viscosity.

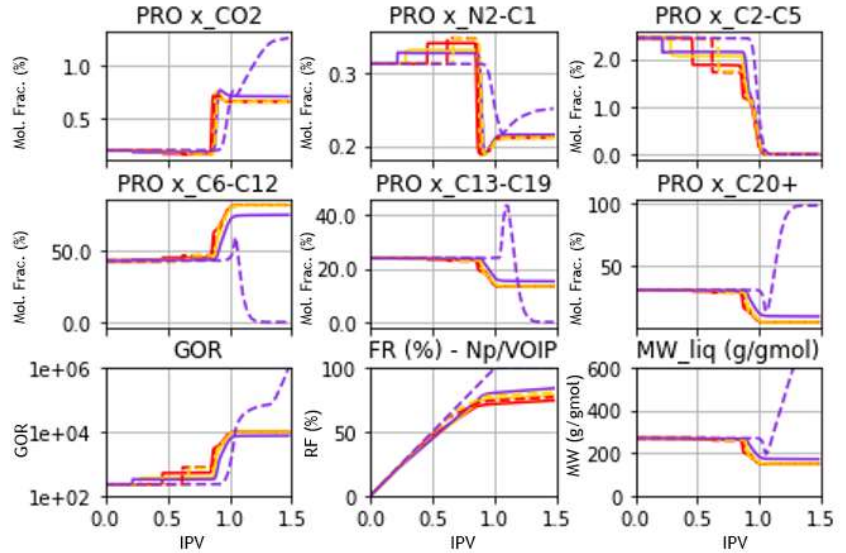

Figure 5.17: Results for Below MMP1 differing: (——) Relative Permeability (Original), (- - - -) Original + Fixed Viscosity, (——) *X*-shape with same mobile oil, (- - - -) *X*-shape with same mobile oil + Fixed Viscosity, (——) *X*-shape with all oil mobile, (- - - -) *X*-shape with all oil mobile + Fixed Viscosity.

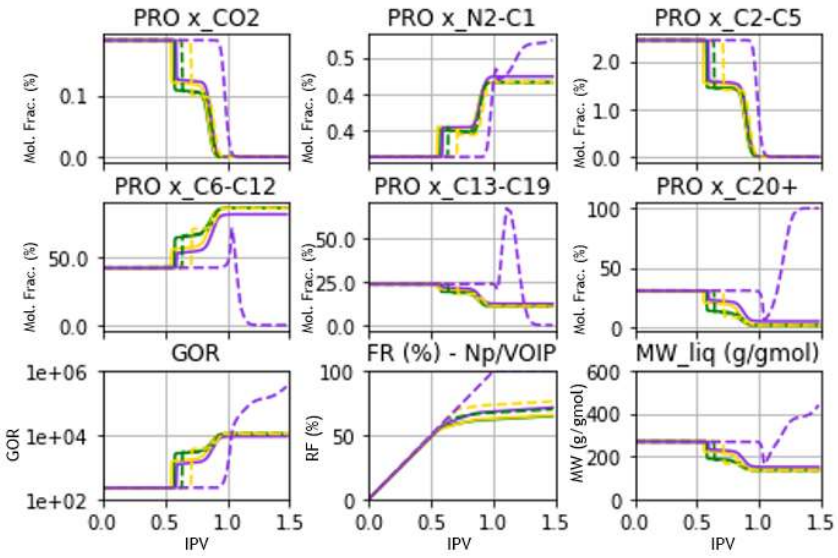

Figure 5.18: Results for Below MMP2 differing: (——) Relative Permeability (Original), (- - - -) Original + Fixed Viscosity, (——) X-shape with same mobile oil, (- - - -) X-shape with same mobile oil + Fixed Viscosity, (——) X-shape with all oil mobile, (- - - -) X-shape with all oil mobile + Fixed Viscosity.

For comparison of results, Figure 5.19 shows the miscibility indicator for the original cases Above MMP, Below MMP1, and Below MMP2, along with the case with X-shaped relative permeability with all oil mobile and fixed viscosity. There are some small differences in the behavior of the liquid phases. For example, the light component of the liquid phases ($C_6 - C_{12}$) has a small peak before dropping in molar composition, while the plus fraction composition has a small drop before starting to increase. The intermediates behave similarly to the Above MMP case. Additionally, there are some differences in when the indicator occurs, but these are minor changes and if surveillance were performed in a project with such characteristics as simulated, the indicators would be triggered.

There may be other factors at play that influence whether or not the fluids are miscible, since in this particular case that triggered the indicators, they were not miscible. For example, the mechanism of how sweep is carried out, the flow dynamics of phases, and many others in this complex system. It is therefore important to consider all relevant factors when attempting to determine what indicators are indirectly measuring.

Despite these potential limitations, a careful analysis of the recovery factor in these cases concluded that all the cases that triggered the indicators reached full recovery, just as the Above MMP case did. This suggests that the miscibility indicator may be a useful predictor of high recovery when gas flooding is applied on the drainage strategy.

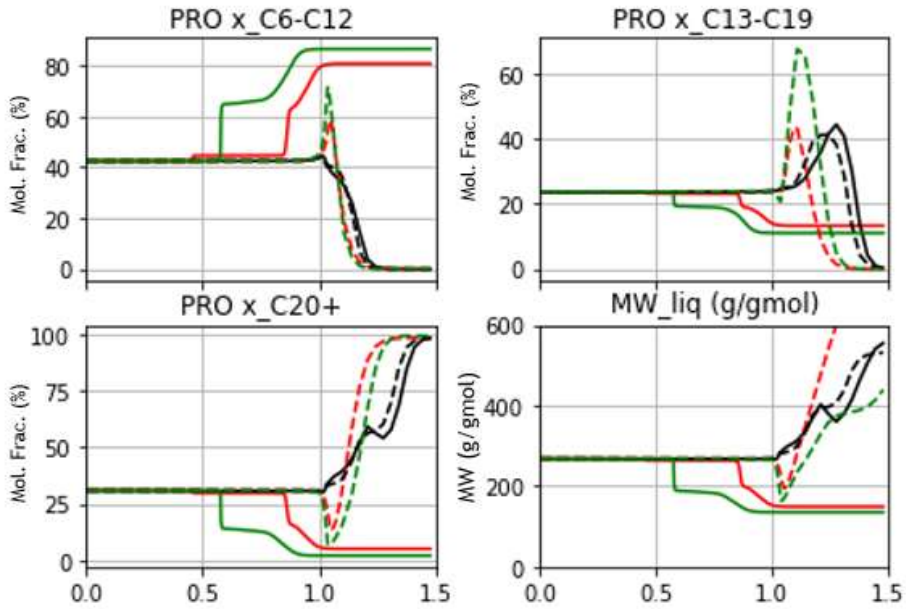

Figure 5.19: Indicators for: (——) Above MMP, (- - - -) Above MMP with *X*-shape real. perm. and fixed viscosity, (——) Below MMP1, (- - - -) Below MMP1 with *X*-shape real. perm. and fixed viscosity, (——) Below MMP2, (- - - -) Below MMP2 with *X*-shape real. perm. and fixed viscosity.

It is worth noticing that any immiscible case was able to trigger the indicators, except this one with all oil mobile, X-shape relative permeability, and a fixed viscosity. This scenario is an abstraction, especially regarding the last consideration of the same viscosity for both gas and oil phases, assembled to prove that in any practical scenario in which gas and reservoir fluid are immiscible, the indicator would not be triggered. In other words, despite the absurdity (*reductio ad absurdum*), indicators are indeed a miscibility indicator capable of predicting high recovery regarding the miscibility condition of injected gas with original oil in place.

5.6 Mobile Oil Influence

In the previous section, we observed that the indicators were able to related to high recovery and miscibility despite they exhibited the same behavior as above the MMP when fixed viscosity was applied and the relative permeability was in an X-shape with all oil mobile, but not when a small amount of mobile oil was present.

To evaluate the behavior of recovery regarding the amount of mobile oil, several new X-shape relative permeabilities were evaluated to determine if the behavior is continuous, as expected, or if there is a discontinuity after a certain amount of mobile oil, especially to replicate the miscibility's indicator. The variation in relative permeability is shown in Figure 5.20, which includes the original relative permeability in a dashed line for comparison and the previously evaluated X5 and X2.

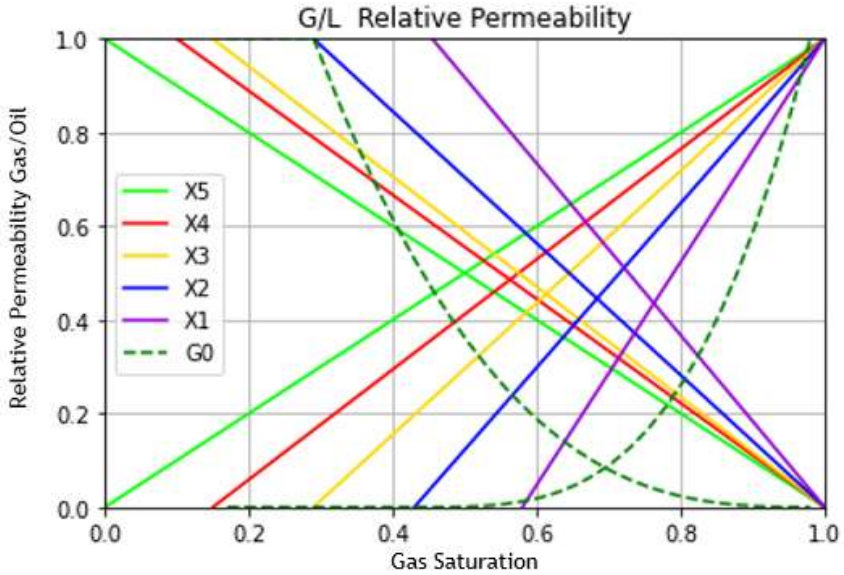

Figure 5.20: Variation in mobile oil in different X-shape relative permeabilities for Gas-Liquid.

Figure 5.21 presents results for RF in each relative permeability with and without a fixed viscosity in Below MMP2 (ResFluid1, Mix 2, and pressure below MMP2) case and Figure 5.22 presents the Indicators for Figure 5.21 simulations.

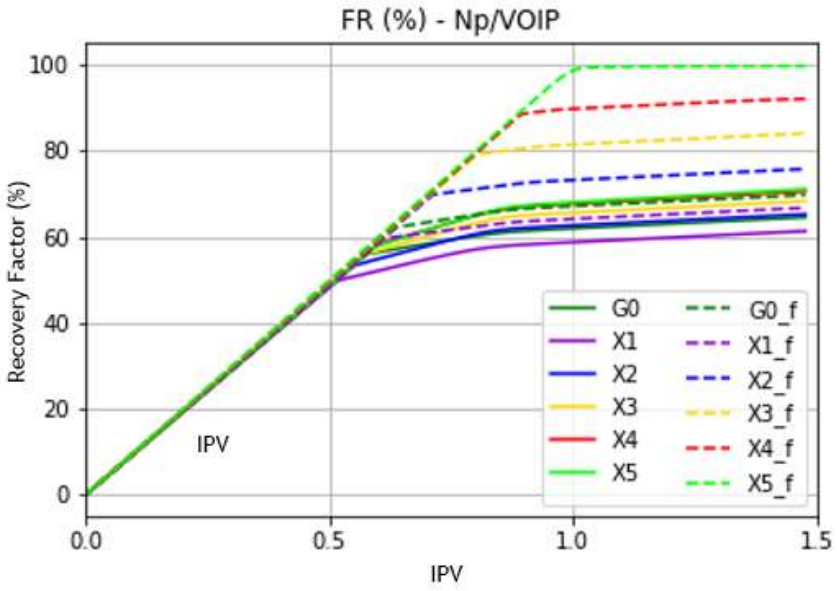

Figure 5.21: Recovery Factor for Below MMP2 with Different X-shape Relative Permeability in Figure 5.20 with (——) unfixed viscosity and (- - - -) fixed viscosity.

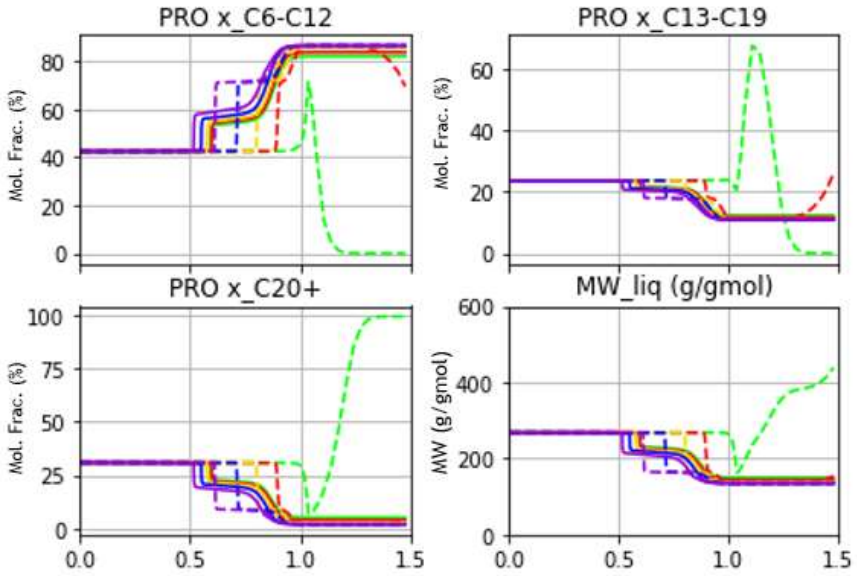

Figure 5.22: Indicators for Figure 5.21's simulations.

Recovery factors behave continuously as mobile oil is increasing in relative permeability, as expected, and also Indicators only are triggered when a very efficient sweep has been promoted. So indicators found are still valuable and important for designing surveillance in an EOR project and also to infer its condition in the reservoir.

5.7 Main Mechanism: Convective Displacement or Molecular Interaction?

We observed that the indicators might be used for monitoring a drainage strategy to identify a high rate of recovery. However, based on Figure 5.15, the primary mechanism causing below MMP cases to switch between leaving some oil unswept, achieving low/moderate recovery, to promote a very efficient sweep capable of triggering indicators only when miscibility conditions were imposed has yet to be identified. Are the convective and viscous forces in a fixed viscosity displacement the dominant mechanisms for achieving high recovery, or is it merely a means to promote molecular interaction resulting in a mixture of hydrocarbons that can be swept into the producer, extracting the intermediate and heavy components after the gas shock wave has passed?

To investigate the mechanism, a black oil simulator was employed using IMEX from the CMG 2020.10 package. This formulation lacks molecular interaction (by definition), and since water is not a component of our evaluation, the formulation consists of two components and two phases (gas and oil). Gas can exist in both phases, but oil can only exist in the oil phase. If significant recovery is still shown in black oil simulations, the primary cause may be convective displacement forces, given the absence of

molecular interaction.

To perform the modeling with the black oil approach, one set of fluid and gas injections was selected. Both gas injection compositions could have been selected, but Mix 2 was chosen due to the absence of CO_2 in the injected fluid, as molecular interactions are not considered, and methane has much less polarity than carbon dioxide, resulting in less error in swelling. For this analysis, only ResFluid 1 and Mix 2 (100% C_1) were considered.

5.7.1 Black Oil Fluid Model

For a Black Oil simulator, each cell can be in two states in an oil-gas system: saturated or undersaturated. In a saturated state, there is free gas, and the cell pressure is at the oil's bubble point. A pressure drop will cause a reduction in the bubble point, and the gas component will move from the oil to the gas phase. The undersaturated state is when there is no free gas in the reservoir cell, and its pressure is greater than the oil's bubble point. Using the GOR and cell pressure, a simulator can calculate the bubble point. Once the bubble point and the system pressure are known, the simulator can access information on the relationship between the variables and the pressure, such as Bo and oil viscosity.

To build the black oil fluid model and provide the gas-oil variables' relationship with pressure, the thermodynamic model for ResFluid 1 (described in Section 4.2.3) was updated considering the injected composition from Mix 2. The results of the black oil fluid model and the laboratory data from Table 4.2 are presented in Figure 5.23. The multiple lines in Bo and μ_{oil} represent the variables' relationship with pressure at different bubble pressures.

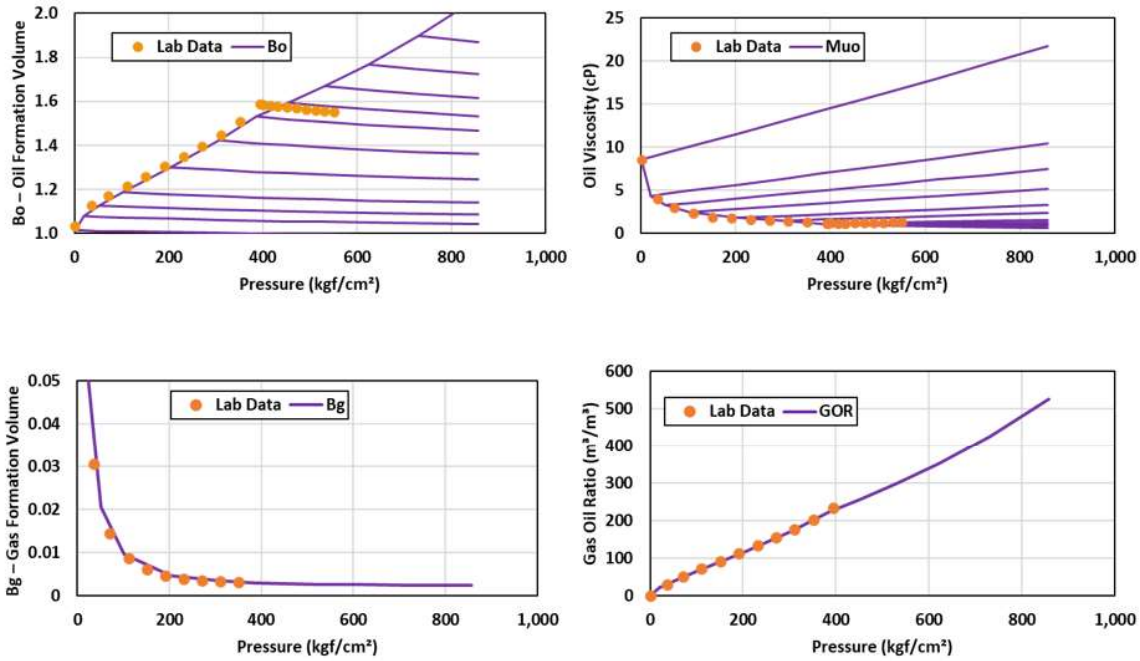

Figure 5.23: Black Oil Model Fluid Relationship: for ResFluid 1 and Mix 2

Figure 5.24 shows the results for the compositional and black oil recovery factor of the below MMP2 case (ResFluid 1 and Mix 2 at 40 MPa). The compositional results were already presented in Figure 5.21. As a comparison, it can be observed that a part of the recovery is associated with molecular interaction since it improves when changing the formulation from black oil to compositional, which models the fluid interaction.

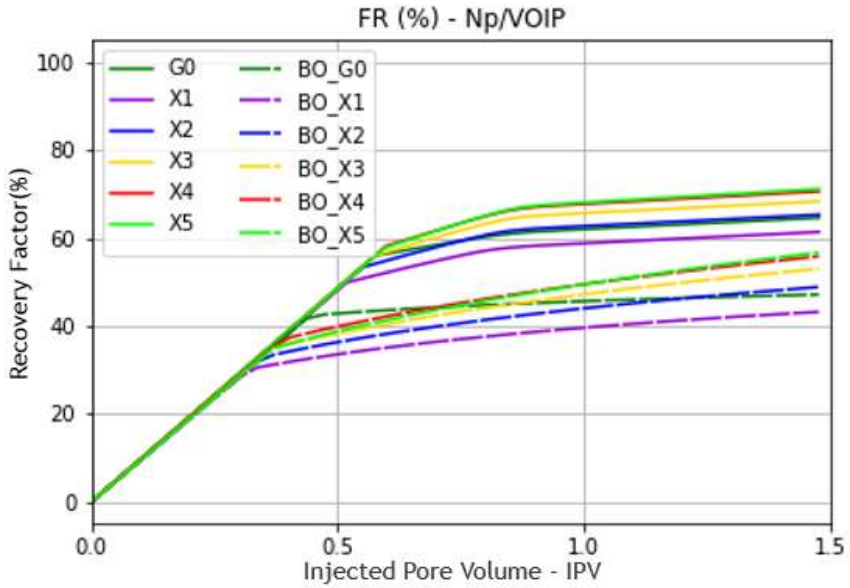

Figure 5.24: Comparison (- - - -) Black Oil versus (——) Compositional Simulator for each Relative Permeability (Figure 5.20).

As for the comparison of the fixed viscosity cases, the results are presented in Figure

5.25. The recovery factor was always greater in the compositional formulation, except for the case where all the oil is mobile in the X5 relative permeability. These cases behave exactly the same, and are almost indistinguishable from each other.

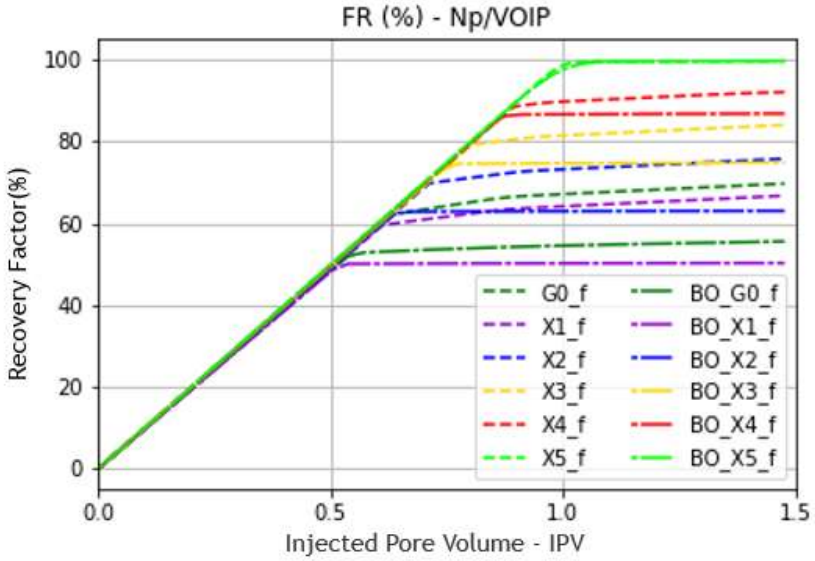

Figure 5.25: Comparison (-—-) Black Oil fixed viscosity versus (- - - -) Compositional Simulator fixed viscosity for each Relative Permeability (Figure 5.20).

To better analyze the X5 relative permeability case, Figure 5.26 focuses only on this specific case. In this figure, one can better estimate the influence of the simulator formulation for the fluid. It is observed that the black oil formulation resulted in a smaller recovery factor due to the negligence of molecular interaction. Additionally, it is observed that cases with fixed composition are equal regarding the fluid's modeling.

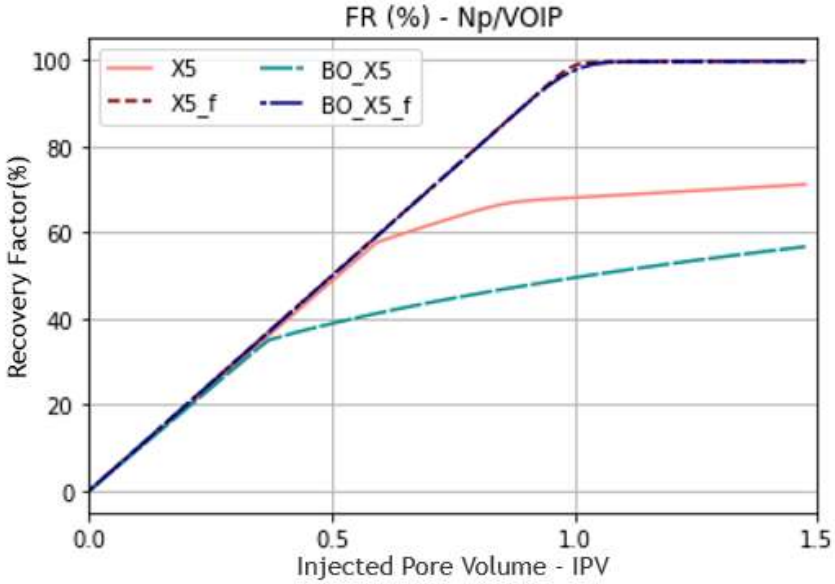

Figure 5.26: Comparison Black Oil versus Compositional Simulator for Relative Permeability X5: (——) Black Oil, (-·—·-) Black Oil fixed viscosity, (——) Compositional, and (- - - -) Compositional fixed viscosity.

To eliminate doubts about the main mechanism of recovery, oil swelling was prevented by fixing the Bo at every pressure in the fluid relationship. Another case with no swelling and fixed viscosity was built, and the results are presented in Figure 5.27. The impact of swelling can be seen in the two results for Black Oil with unfixed viscosity, but both results, with or without swelling, reached high recovery. This demonstrates that the mechanism to obtain high recovery when all oil is mobile is independent of molecular interaction or oil swelling.

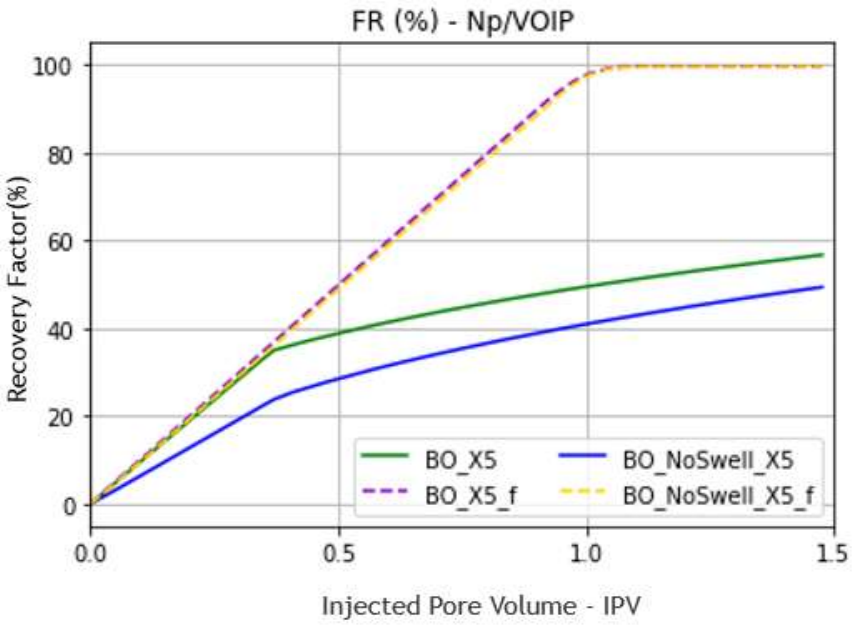

Figure 5.27: Impact of Swelling and Viscosity in Black Oil formulation for X5 Relative Permeability. (——) Original (Unfixed viscosity with swelling), (——) Unfixed viscosity without swelling, (- - - -) Fixed viscosity with swelling, (- - - -) Fixed viscosity without swelling.

5.8 Compositional Evaluation of Results

To evaluate the effects of changing in the overall composition due to gas injection, a middle position in the reservoir, shown in Figure 5.28, was selected to observe phase-equilibrium alteration as a gas shock wave progresses and hydrocarbon is drained.

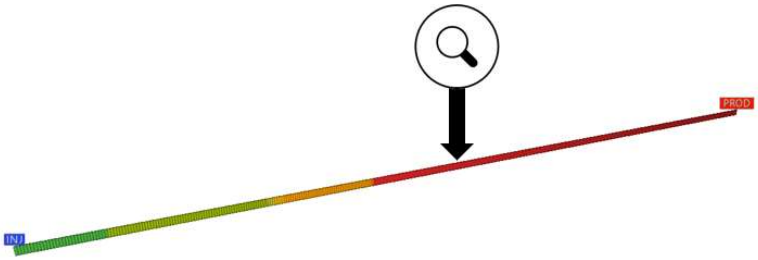

Figure 5.28: Reservoir Cell Monitored Composition

Three sets of cases were assembled to track alterations in the composition and their effects on the two-phase envelope. The first set consisted of the original cases: Above MMP, Below MMP1, and Below MMP2, which were evaluated in Sections 5.1 and 5.2. The other two groups were selected based on cases that mimic the situation above MMP, even though they are below MMP. These other two sets of cases, for Mix1 and Mix 2, were simulated with the X5 relative permeability, which has all oil mobile, in

three different situations: above MMP (increasing the pressure), one below the MMP (reducing the pressure), and one case below MMP that can reproduce the indicator (reducing the pressure and fixing the viscosity).

5.8.1 Case 1: Above MMP, Below MMP1 and Below MMP2

The outcomes of Case 1 are illustrated in Figure 5.28. Plots have been made of the two-phase envelopes for the composition in each of the different IPVs (injected pore volumes). These envelope compositions were selected based on the relevant changes in the composition monitoring. The cricontherm has a downward trend, as seen in the Above MMP plot (Figure 5.28a), accompanied by some variance in the cricondenbar. The cricondenbar behavior is noteworthy: after an initial increase, it reaches a maximum and starts decreasing, resulting in an oscillating trend of the saturation pressure at reservoir temperature (in vertical gray dashed line). As the cricondenbar and saturation line increase, the simulation pressure slightly reaches the saturation line.

A slight decline in cricontherm and an oscillating trend in cricondenbar can be seen in the Below MMP1 plot (Figure 5.28b). Due to the simulated pressure in this scenario being 40 MPa (equivalent to about 407 kgf/cm² - horizontal gray dashed line), it has altered its initial condition, exiting the monophasic region and entering the biphasic region. The cricontherm and cricondenbar for the Below MMP2 plot (Figure 5.28c) share some parallels with the previous case below MMP; however, this example has the predisposition to enlarge the biphasic region, as a result of the injected gas having less affinity with other components due to the lack of CO_2 in its content.

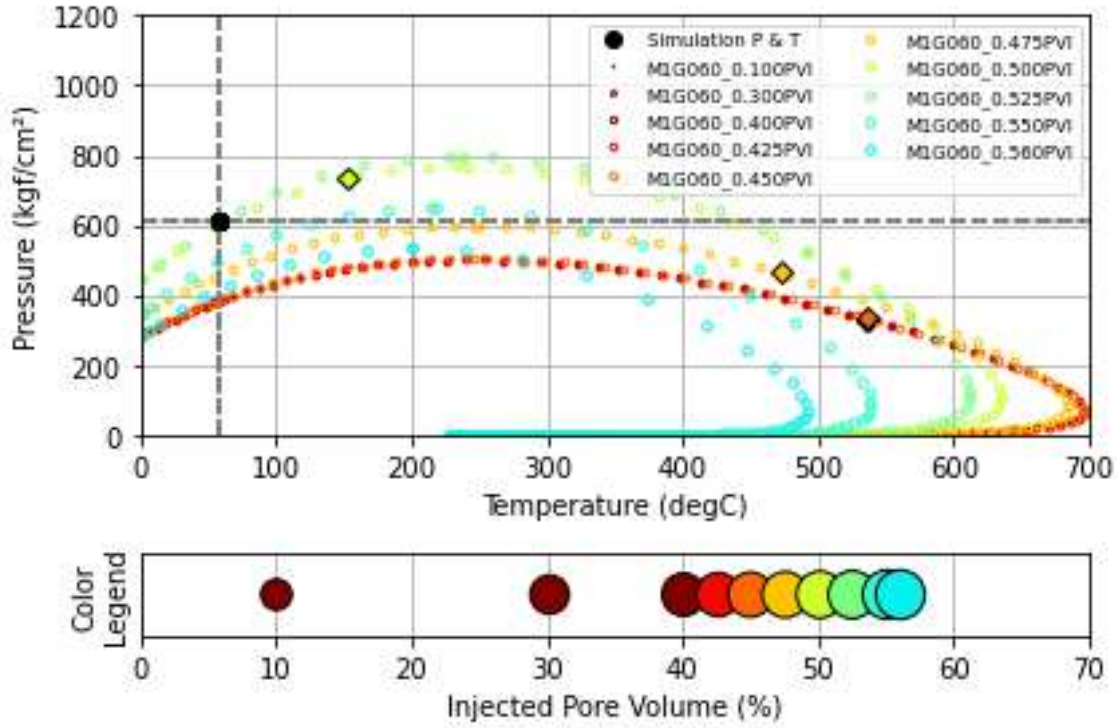

(a) Two-phase envelopes at different IPV for Above MMP1 conditions

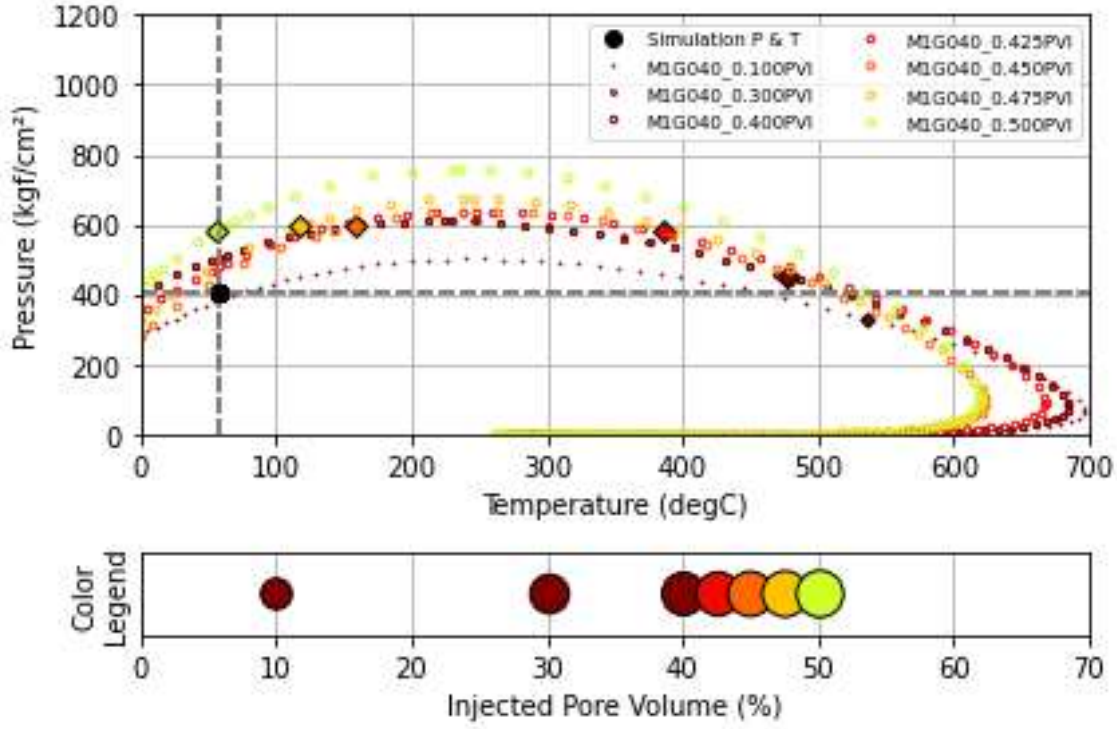

(b) Two-phase envelopes at different IPV for Below MMP1 conditions

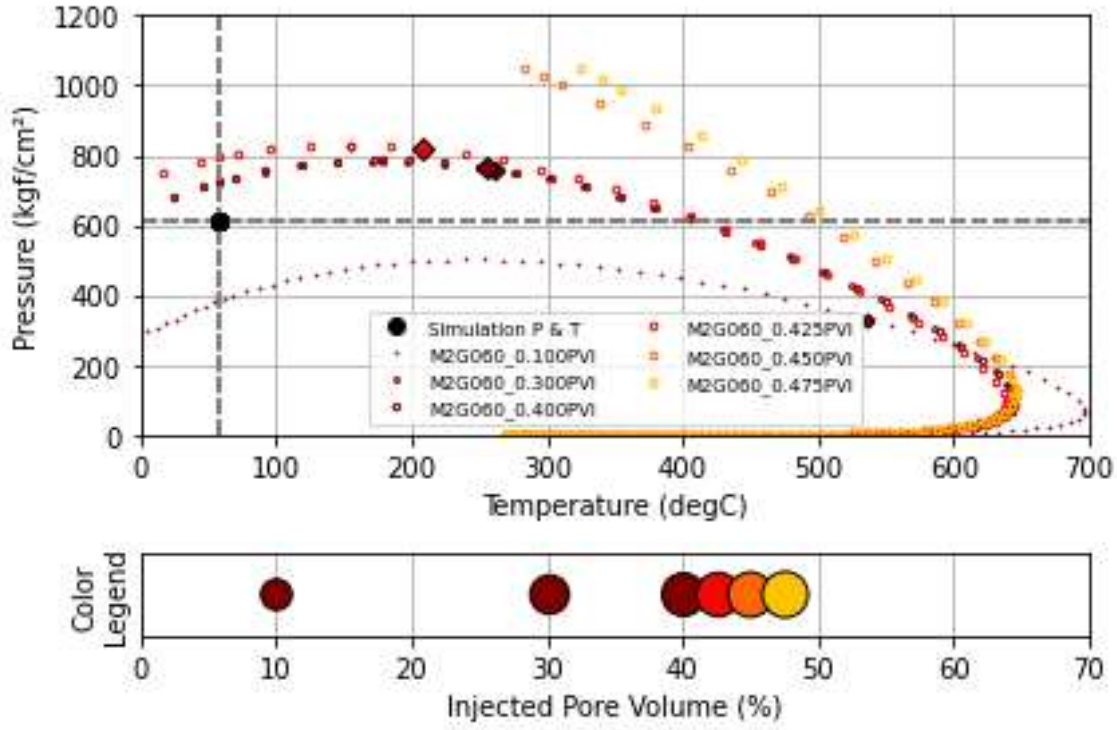

(c) Two-phase envelopes at different IPV for Below MMP2 conditions

Figure 5.28: Two-phase Envelops for Case 1.

Despite the fact that the critical point of Below MMP1 (Figure 5.28b) reaches the reservoir temperature, its pressure is not sufficient to promote a monophasic sweep, as it is located inside the two-phase region.

5.8.2 Case 2: Mix 2 with X-shape Relative Permeability with All Oil Mobile

For the second case, all simulations considered a gas injection composition without CO_2 (Mix2) and an X-shaped relative permeability with all oil mobile, i.e., the "X5" relative permeability (presented in Figure 5.10).

In the above MMP simulation, depicted in Figure 5.28a, a significant reduction in the cricondentherm was observed, which did not replicate in cases below MMP, where the reduction was minor. A similar behavior was also observed in Case 1. In contrast to the previous case, the simulation has entered the two-phase region by a considerable amount (around 150-200 kgf/cm²), since the simulated pressure is approximately 815 kgf/cm² (80MPa). The oscillating trend in the cricondenbar was not observed in any case where the injected composition had no CO_2.

As for the two cases below MMP2, both are simulated with a pressure of 40 MPa (approximately 611 kgf/cm²). The difference between allowing estimation of viscosity (Figure 5.28b) and defining a fixed viscosity for all components (Figure 5.28c) is that

in the former, with a calculated viscosity as a result of molecular interaction between gas and oil, the two-phase envelope starts to enlarge with a smaller proportion of gas injected and reaches a broader region.

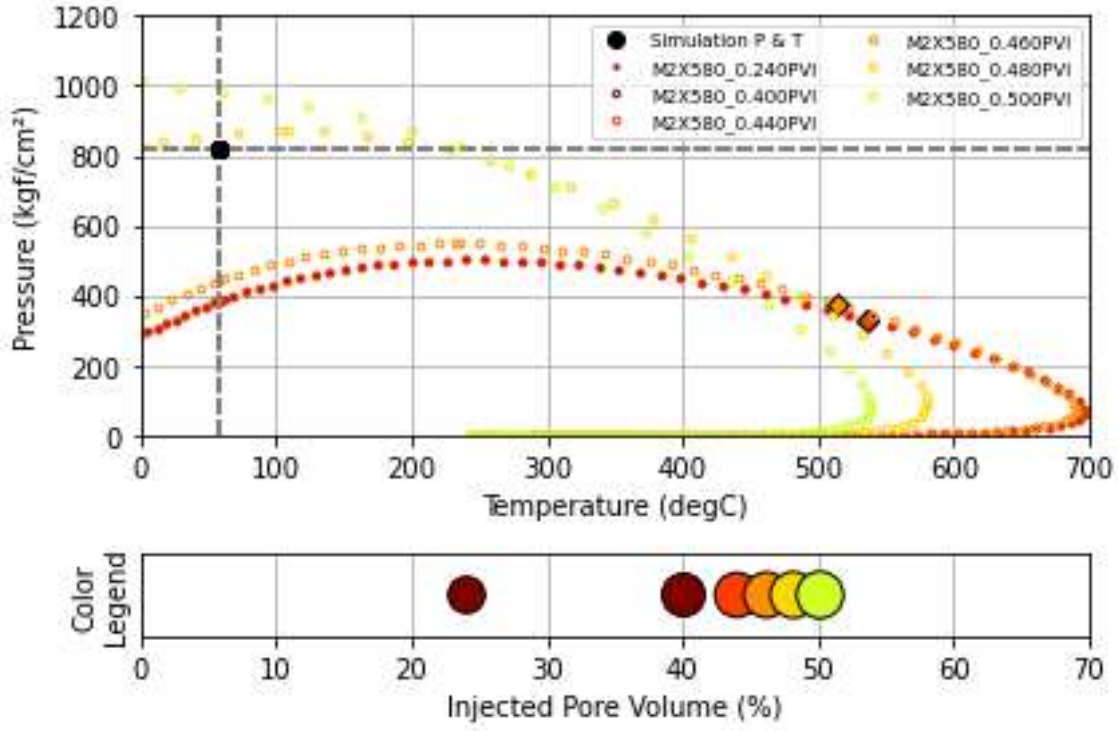

(a) Two-phase envelopes at different IPV for X5 Above MMP2 conditions

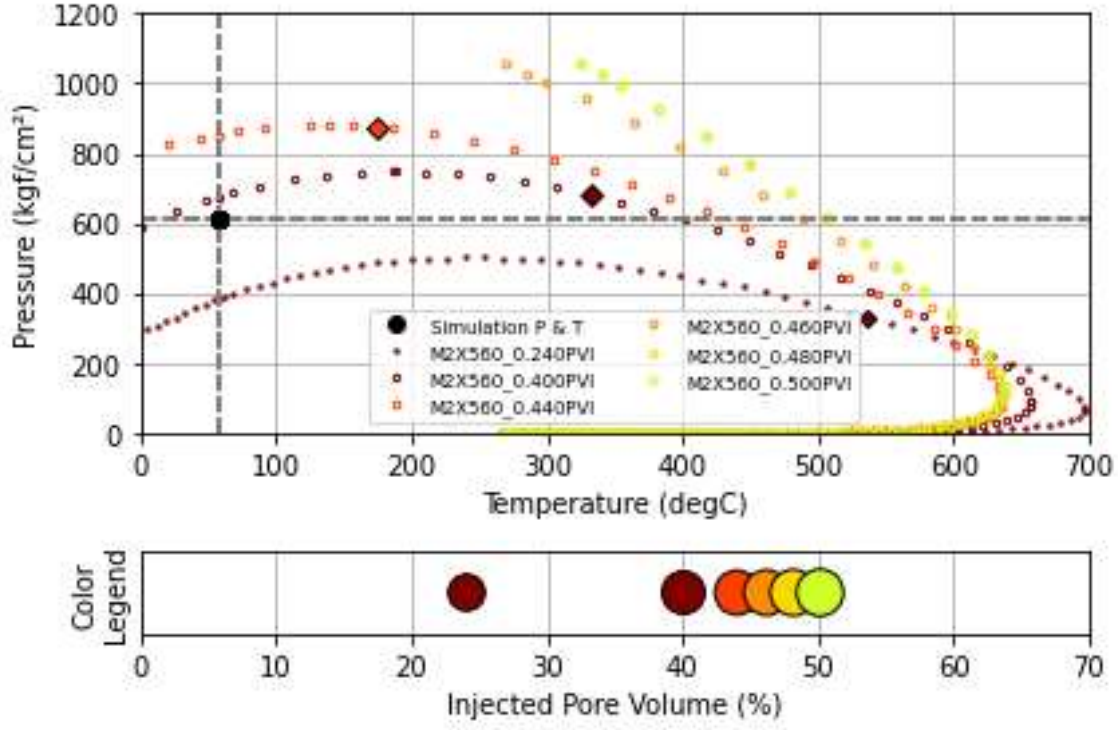

(b) Two-phase envelopes at different IPV for X5 Below MMP2 conditions

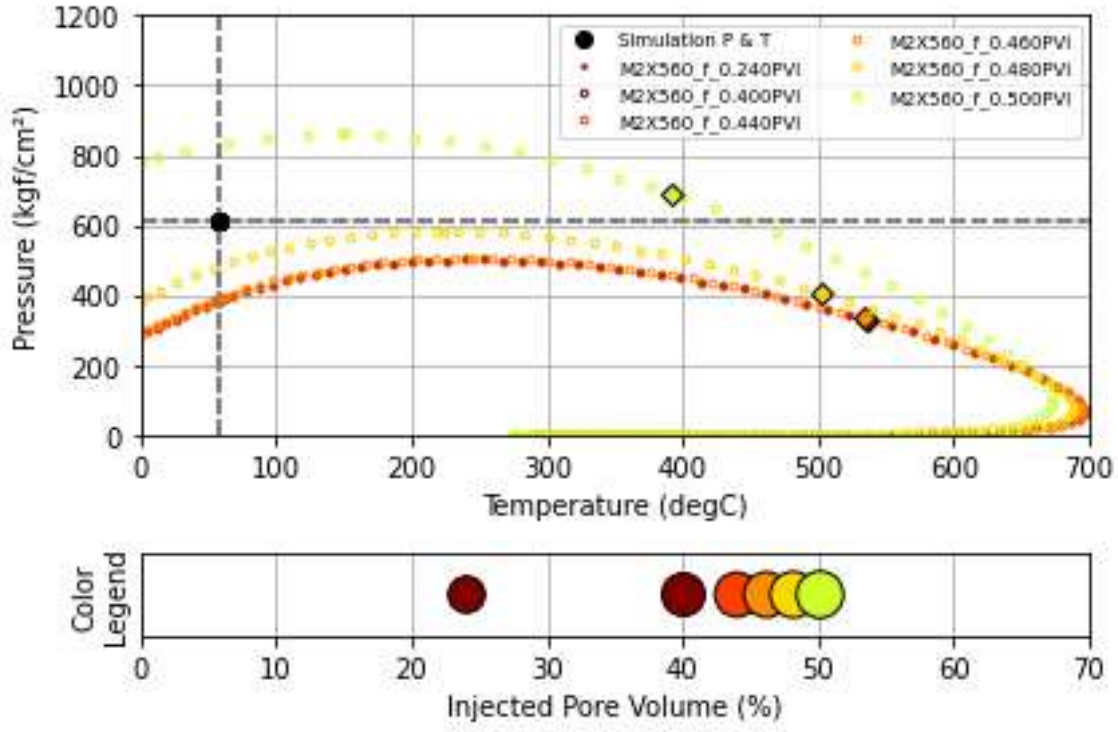

(c) Two-phase envelopes at different IPV for X5 fixed viscosity Below MMP2 conditions

Figure 5.28: Two-phase Envelopes for Case 2 (Mix2 and X5 Relative Permeability).

In the fixed viscosity case (Figure 5.28b), an efficient sweep leads to a more consistent composition due to the proportional mixture of injected gas and oil in front of a shock wave, as the gas does not have greater mobility as a result of X-shape relative permeability and the constant viscosity for both phases. After reaching nearly 50% of IPV, as the monitored composition is in the middle of the 1D reservoir, the envelope starts to enlarge, increasing the cricondenbar.

However, as discussed in Section 5.5, recovery is high in cases with fixed viscosity with all oil mobile in an X-shape relative permeability. Therefore, the increase in the two-phase region occurs after the shock wave has already swept the majority of hydrocarbons. Additionally, since both phases have the same viscosity, the by-passed oil from biphasic equilibrium will eventually be efficiently swept due to convective flow forces, resulting in high recovery.

5.8.3 Case 3: Mix 1 with X-shape Relative Permeability with All Oil Mobile

The third case is analogous to the second one but considers Mix 1 as the injected gas and a simulated pressure of 60 MPa (611 kgf/cm²) for the above MMP1 case and 40 MPa (407 kgf/cm²) for both below MMP1 cases.

The results above MMP1 (Figure 5.28a) show the corresponding two-phase envelope for each IPV evaluated. A significant reduction in cricondentherm and oscillating behavior of cricondenbar is observed. As in the first case, the simulated pressure (horizontal gray dashed line) slightly reaches the saturation line and drainage occurs mainly in the monophasic region.

The unfixed viscosity condition (Figure 5.28b) shows that the cricondentherm and cricondenbar behave the same as in the above MMP conditions. However, the oscillatory behavior of cricondenbar was not observed. As the drainage moves forward, the selected IPV reaches a maximum saturation pressure at reservoir temperature. Since the reservoir pressure is lower, the monitored position in the reservoir is deep inside (more than 200 kgf/cm²) the two-phase region.

In the fixed viscosity condition (Figure 5.28c), the evolution of cricondentherm and cricondenbar as a function of drainage is similar, including the oscillatory behavior of the cricondenbar and the saturation pressure. Similar to case 2, the fixed viscosity condition enters the two-phase region. However, as discussed in the previous section, the drainage is very efficient regarding the hydrocarbon distribution among phases, since both phases' flow interaction behaves linearly with saturation (X-shape relative permeability) and has a constant viscosity, independent of the composition and molecular interaction.

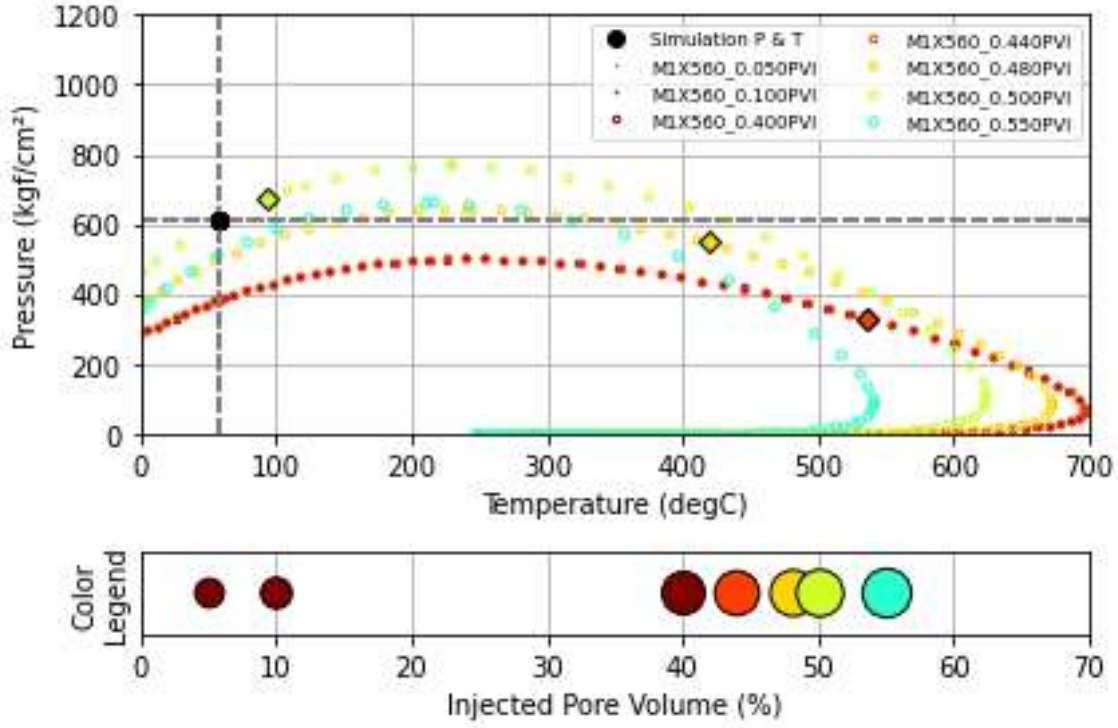

(a) Two-phase envelops at different IPV for X5 Above MMP1 condition

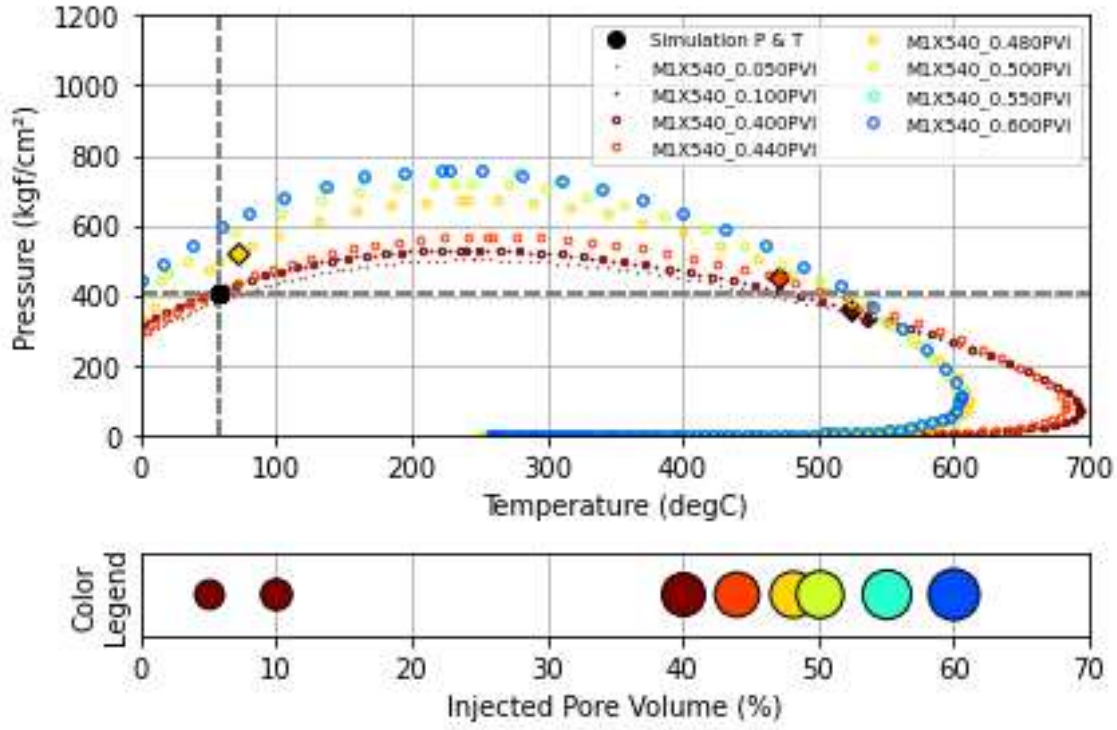

(b) Two-phase envelops at different IPV for X5 below MMP1 condition

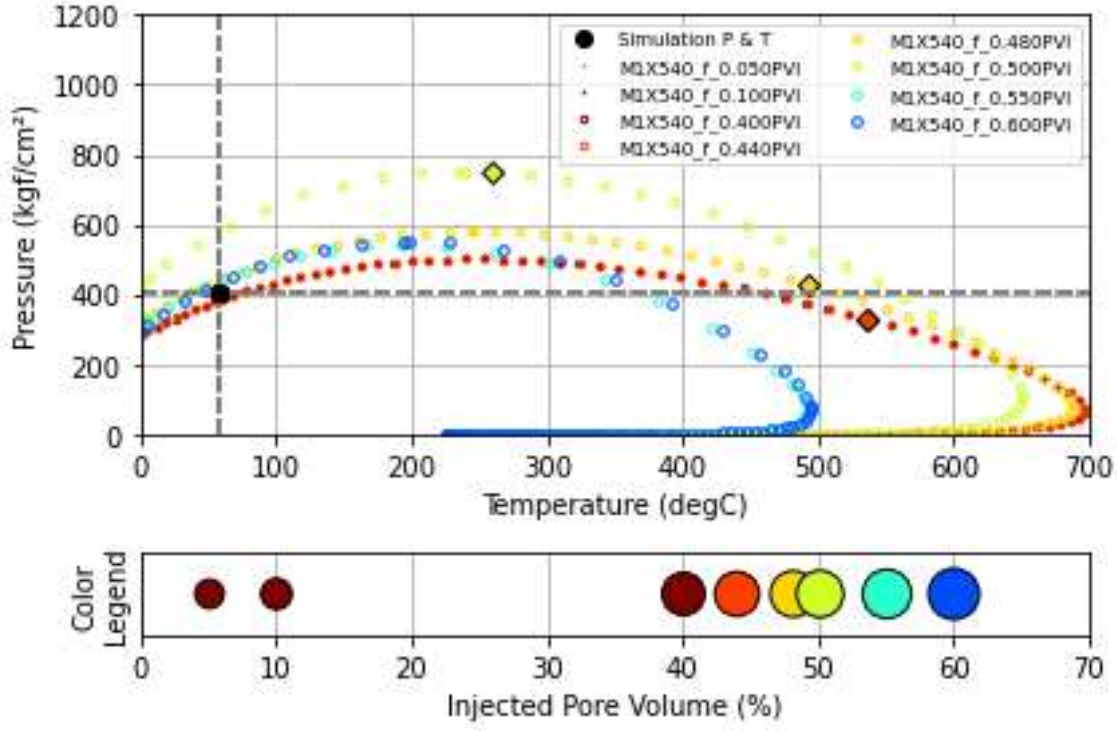

(c) Two-phase envelops at different IPV for X5 fixed viscosity below MMP1 condition

Figure 5.28: Two-phase Envelop for Case 3 (Mix1 and X5 Relative Permeability).

5.8.4 Variation on Saturation Pressure

As discussed in the three previous sections, the saturation pressure exhibited an oscillatory behavior as a function of the amount of gas-oil mixture whenever CO_2 was present in the injected gas.

It is important to note that the simulation considered the producer operating at a constant bottom-hole pressure, which is the same as the initial reservoir pressure. Therefore, the variation of pressure along the reservoir is minimal and does not significantly alter the initial pressure. Another important consideration is thermal equilibrium in the system, so the temperature is constant throughout the reservoir. The only source capable of altering the saturation pressure is flow-driven, which is determined by the resulting global composition in the monitored part of the reservoir as a function of how the gas injection was able to interact and sweep the original oil.

All of the simulations with Mix 1, which contain CO_2 in the composition, can be seen in Figures 5.28a, 5.28b, 5.28g, 5.28h, and 5.28i. The only case with Mix 1 that did not show a reversion in cricondenbar, and therefore, did not present oscillatory behavior in the saturation pressure (or bubble pressure/point), was the case with an X-shape relative permeability with unfixed viscosity (Figure 5.28h).

The same case with the original relative permeability presented a reversion in the reduction of the saturation pressure (5.28b). As the format of the relative permeability is important to capture oscillatory behavior, the X-shape relative permeability was focused on eliminating mutual phase disturbance in flow, and thus it was not a realistic case. Also, despite the fact that this case did not experience a lower saturation pressure as the drainage moved onward, it seemed to reach a maximum after 55% IPV.

The simulation for Mix 2, displayed in Figures 5.28c, 5.28d, 5.28e, and 5.28f, always resulted in an increase in the saturation pressure. The only pseudo-component injected in this composition was methane (with traces of N_2). This component tends to extract light components from the oil as a result of losing light components, so the remaining hydrocarbon composition becomes heavier, resulting in an increase in the saturation pressure necessary to vaporize the remaining light-end. Another relevant fact we observed was the derivative increase in saturation pressure over PVI.

Excluding Figure 5.28d, which is above MMP2 and where the saturation pressure increases little early on, since monitoring is in the middle of the reservoir, recovery is expected to be extremely efficient after this "time", and the composition should be near the injected gas composition. The other cases without CO_2 present a very rapid and aggressive increase in the saturation pressure. In fact, the derivative of the increment is so high, the saturation pressure almost doubles, increasing 300-400 kgf/cm² with a 15-20% increment in the cumulative gas injection. None of these cases present a stabilization similar as seen in Figure 5.28h.

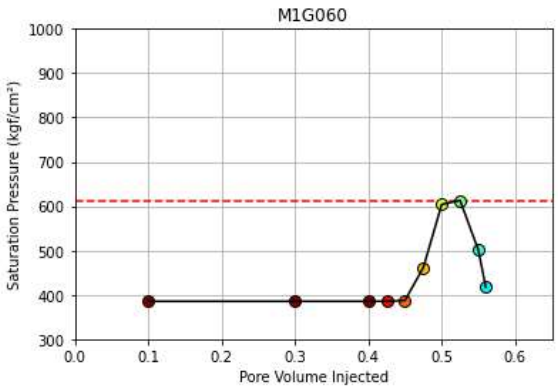

(a) Sat. Pressure for Case1-Above MMP1

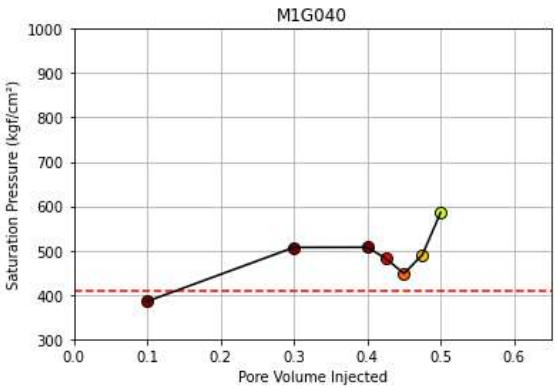

(b) Sat. Pressure for Case1-below MMP1

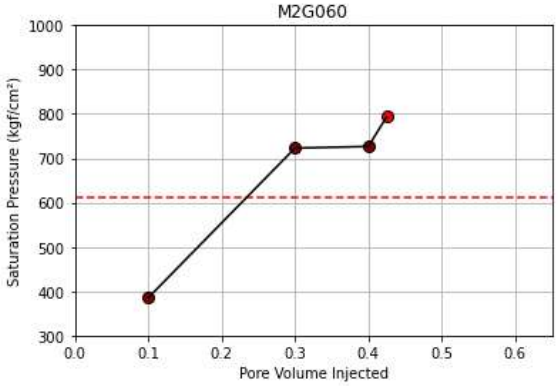

(c) Sat. Pressure for Case1-below MMP2

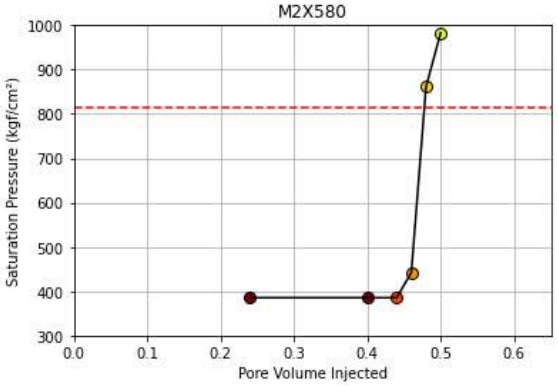

(d) Sat. Pressure for Case2-Above MMP2

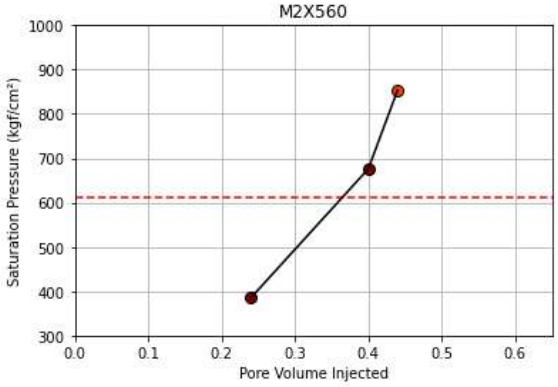

(e) Sat. Pressure for Case2-below MMP2

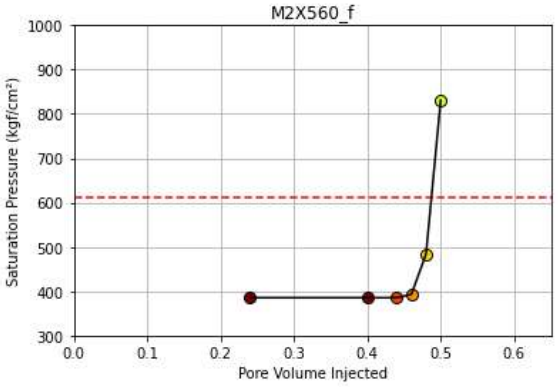

(f) Sat. Pressure for Case2-visc. cte. below MMP2

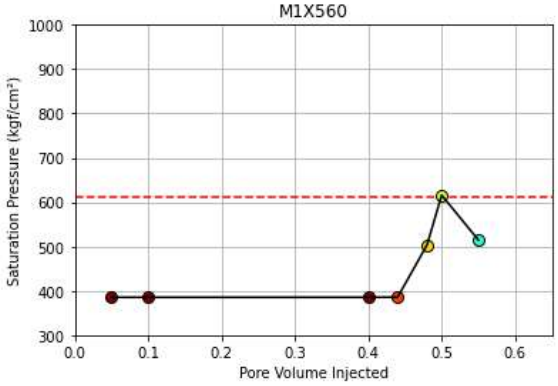

(g) Sat. Pressure for Case 3-Above MMP1

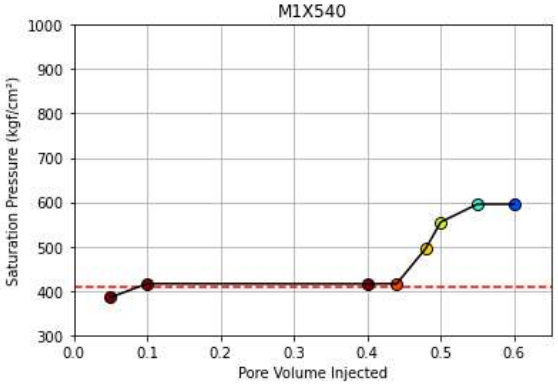

(h) Sat. Pressure for Case 3-below MMP1

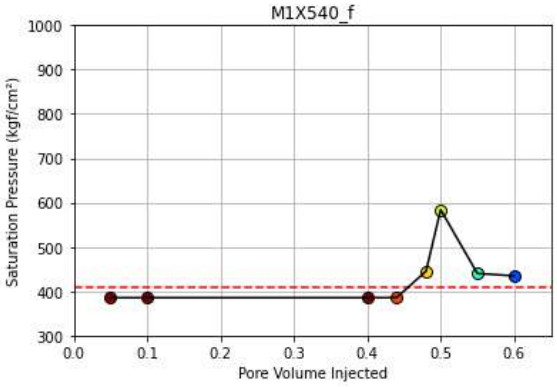

(i) Sat. Pressure for Case 3-visc. cte. below MMP1

Figure 5.28: Saturation Pressure for several IPV in Cases 1,2, and 3.

Being able to track how the composition varies in the reservoir allows for a specific analysis of phase equilibrium that might drive the recovery mechanism. The simulated pressure in the first row of Figure 5.28 was previously defined in the selection of cases for the first section of this chapter, but it could have been a different initial value.

For this analysis, an oscillatory behavior case was selected as an example, such as the one shown in more detail in Figure 5.29, which is happening in Figure 5.28b.

Suppose that this behavior would happen in a simulation with a different initial pressure is very likely, as seen in other cases in Figure 5.28, for instance, 500 kgf/cm². As seen in Figure 5.29, the reservoir would enter the two-phase region around 30% IPV and then exit the biphasic region after 40% IPV and return to the monophasic region just before 50% IPV. This behavior is precisely the condensing/vaporizing mechanism suggested by ZICK (1986), PEDERSEN *et al.* (2006), and many other authors.

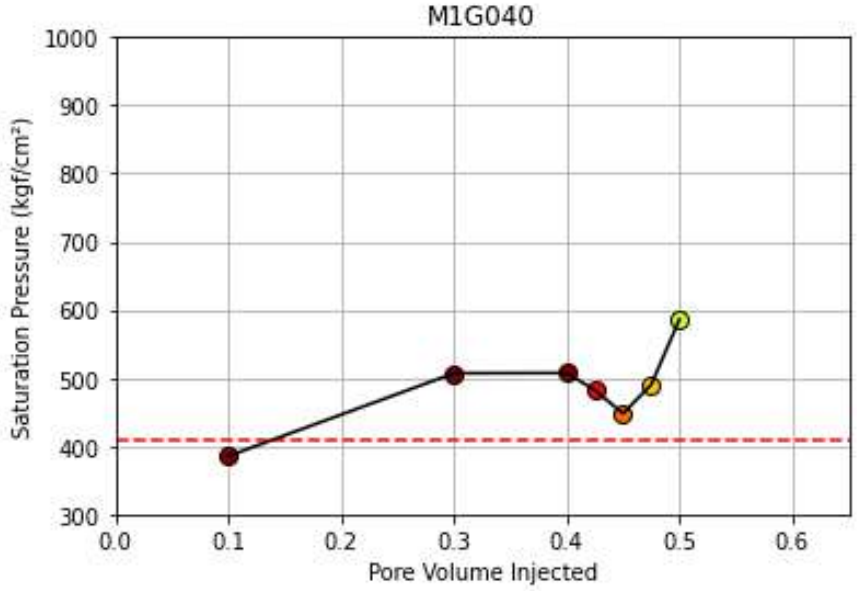

Figure 5.29: Saturation Pressure variation for Case1 Below MMP 1 (Figure 5.28b).

The interpretation of the mechanism suggests that the gas has been enriched by extracting lights and intermediates from the oil adjacent to the injector, resulting in the composition becoming monophasic with the new oil contacted that reached the middle of the reservoir. As previous extraction may have saturated, leaving only heavier oil behind with no lights and intermediates to move to the gas phase, the gas is not enriched enough to be monophasic with oil, resulting in the mixture returning to the two-phase region at 40% IPV. The process repeats itself, with the gas returning to extract more lights/intermediates further in the flow.

Note that this evaluation does not consider miscibility from a thermodynamic perspective, as an analysis of the critical point was not performed, and it is uncertain whether this mixture is monophasic in any proportion or not.

For this evaluation, a P-X analysis was performed on Winprop to evaluate the saturation pressure for ResFluid1 behavior on gas injection, as shown in Figure 5.30. As observed in Figure 5.28, only Mix 1, with CO_2, is capable of a reversal in the tendency of the saturation pressure. A thermodynamic evaluation of miscibility concerns the critical point (little over 440 kgf/cm²), which is around 80% gas. From this pressure onwards, the mixture is assumed to be First Contact Miscibility (FCM).

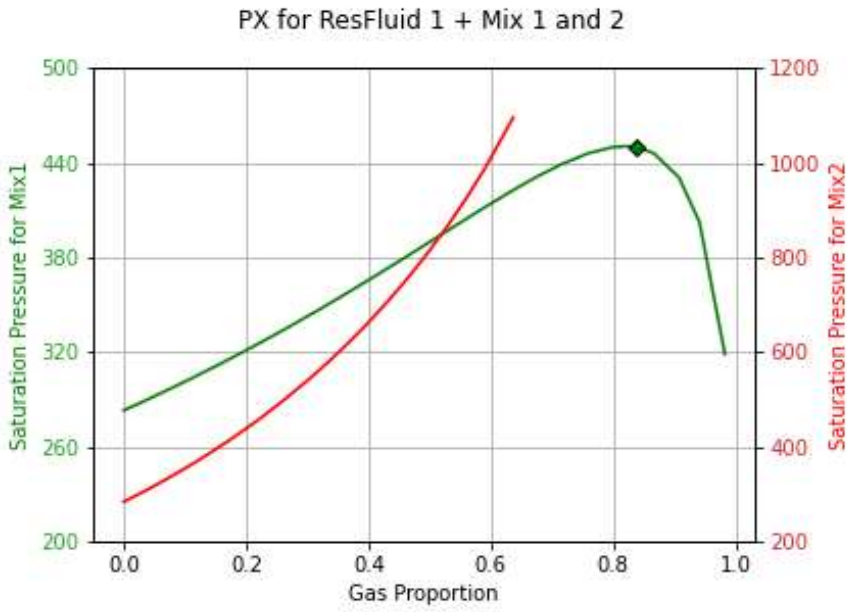

Figure 5.30: P-X analysis for ResFluid1 combined in many proportion with Mix 1 (with CO_2) and Mix 2 (without CO_2.

From the recovery and reservoir engineering aspects, it is important to operate the field and drainage in the monophasic region and, furthermore, to ensure maximum recovery and economic value from the asset. For instance, a 400 kgf/cm² reservoir might deploy an EOR-project to improve recovery, even though it might face a region of bifasic behavior around 70-90% gas mixture, and so it is not a "purely" miscible injection

(miscible in any proportion), even though after some injection, the resulting composition might become miscible (MCM - Multiple Contact Miscibility). This might be the optimum strategy for economical returns on a project.

Another interesting behavior observed in the P-X analysis was the tendency to increase saturation pressure when dealing only with methane. A very steep saturation line might be observed from 40% to 60% gas fraction, increasing the saturation pressure from 600 to more than 1000 kgf/cm², as also observed in the previous experiment (Figure 5.28).

5.9 Consistency in Different Thermodynamic Model

To investigate whether the indicators found are exclusive to ResFluid1 thermodynamic model, a consistency check was performed on ResFluid2 (introduced in Section 4.2.4). As discussed before, this fluid has almost no CO_2 content in its composition and was represented with a completely different model, especially in the binary interaction coefficient (BIC or k_{ij}). The BIC for CO_2 and $C_2 - C_5$ shows a significant difference in the fluid models. Both were set constant for hydrocarbon interaction after the methane group, with the first set to 0.11 and the last set to 0.03, as previously presented in Tables 4.7 and 4.9.

The injected composition without CO_2 was the same as Mix2; however, the composition with the contaminant could not be the same as Mix1 since no MMP could be defined, as previously presented in Figure 4.8. Therefore, the composition for Mix3 was defined as 10% CO_2 and 90% $N_2 - C_1$. The MMP for ResFluid2 and Mix2 ($MMP2^2$) is around 63 MPa, and the MMP for ResFluid2 and Mix3 ($MMP3^2$) is around 66 MPa. This proximity of $MMP2^2$ and $MMP3^2$ may be due to the lack of CO_2 in ResFluid2 content or because of the parameters selected for tuning the EOS, but this phenomenon was not evaluated in this work, and the aim is to evaluate whether the indicators might be found in a different fluid model or not.

The simulations were done only in the original relative permeability, in cases above $MMP2^2$ and $MMP3^2$ (70 MPa) and below $MMP2^2$ and $MMP3^2$ (50 MPa). The recovery factor is presented in Figure 5.31. As expected, cases above MMP had reached a large cumulative production of hydrocarbons, leading to a high recovery factor of nearly 100%, and the cases below MMP could only recover a little over 60%.

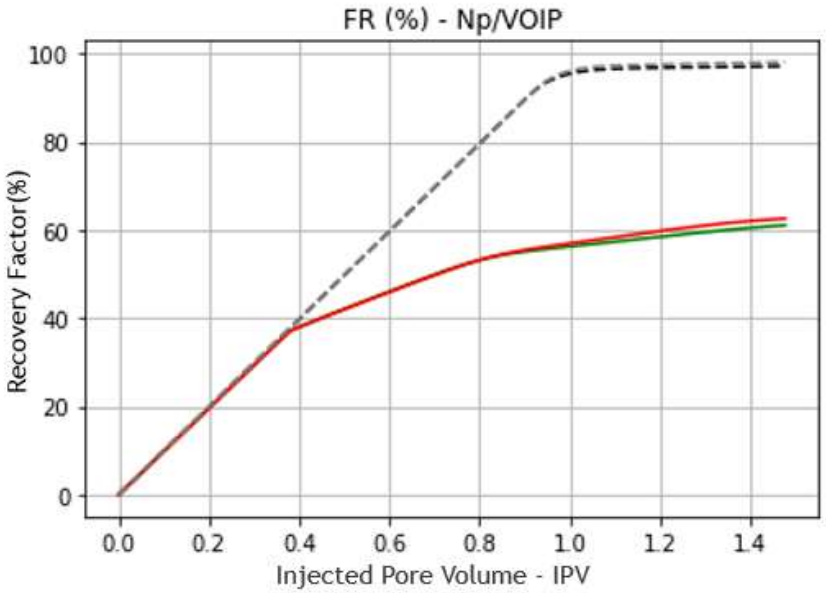

Figure 5.31: Recovery Factor for cases with ResFluid2: (- - - -) Above $MMP2^2$, (——) Below $MMP2^2$, (- - - -) Above $MMP3^2$, (——) Below $MMP3^2$.

Figure 5.32 illustrates the alteration in oil composition as the gas injection proportion to the original volume progresses. The composition alteration for this fluid decreases for the light-ends in oil ($C_6 - C_{12}$) in miscible cases and increases for immiscible cases. An amplified peak is observed for this reservoir fluid, and the indicator is also triggered. For the intermediates ($C_{13} - C_{19}$), an increase followed by a decrease in composition is observed in the miscible condition, while a small decrease is observed in the immiscible condition. For the heavier-ends (C_{20}^{+}), an increase, after a small decrease, in content is observed when miscible displacement is occurring, and only a decrease is noticeable for immiscible displacement.

These results are the same for ResFluid1 (Figure 5.9), with small changes: an amplified peak in the light-ends, a very small decrease barely observable in the immiscible scenario, and a small decrease before the increase in composition. Figure 5.33 shows the indicator triggered.

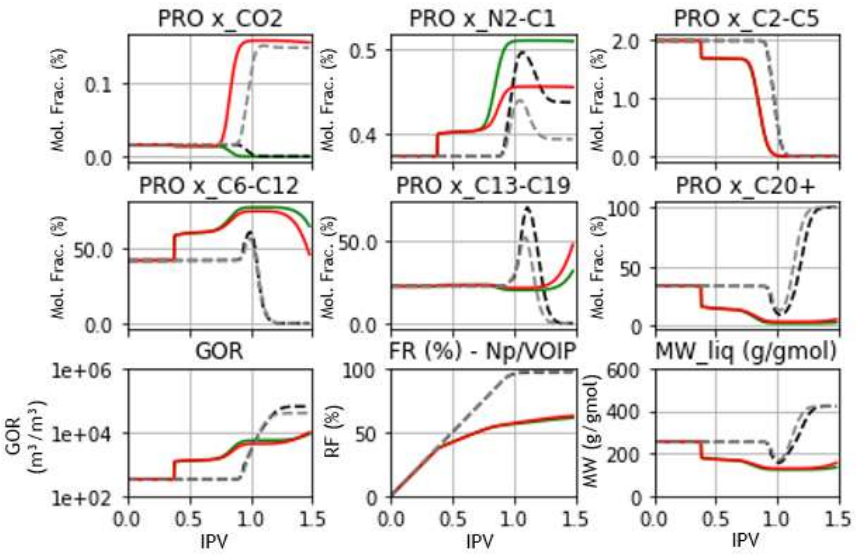

Figure 5.32: Producer oil composition for: (- - - -) Above $MMP2^2$, (——) Below $MMP2^2$, (- - - -) Above $MMP3^2$, (——) Below $MMP3^2$.

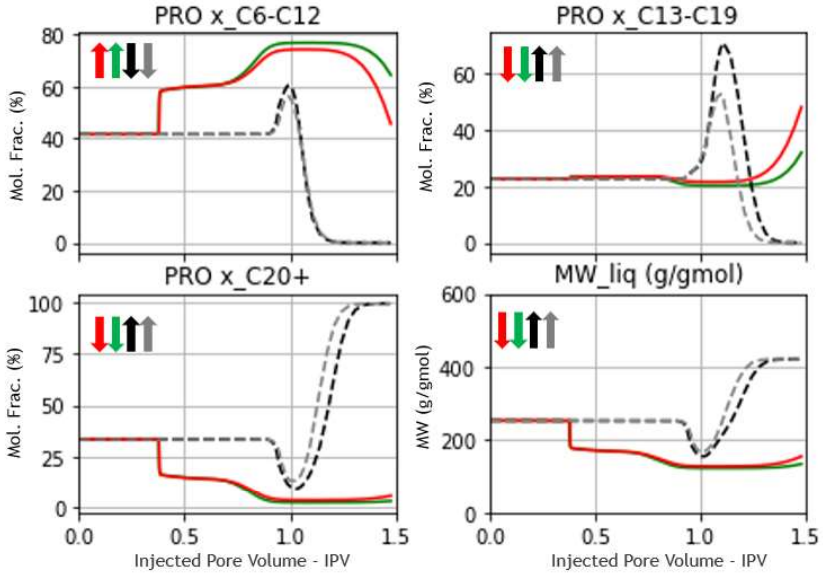

Figure 5.33: Indicator for alteration in oil composition for: (- - - -) Above $MMP2^2$, (——) Below $MMP2^2$, (- - - -) Above $MMP3^2$, (——) Below $MMP3^2$.

Chapter 6

Conclusions and Recommendations

The objective of this study was to evaluate the compositional changes that occur in oil depending on the miscibility of injected gas with oil. To achieve this objective, a series of numerical experiments were conducted using ResFluid 1 and gas composition, as explained in the preceding chapter.

The effects of miscibility on oil composition were determined by analyzing and comparing the outcomes of these experiments. They provide useful insights into the behavior of gas injection in oil systems under miscible and immiscible conditions, which may provide additional information regarding the EOR process and projected reserves.

The results showed that the presence of miscible gas injection led to significant alterations in the chemical composition of the oil. These findings have significant implications for data collection and reservoir surveillance for reservoirs subjected to gas injection.

6.1 Conclusions

The hypothesis that different conditions of miscible displacement modify the oil composition differently has been demonstrated to be correct, as some indicators could be established to distinguish whether immiscible or miscible gas displacement is occurring in the reservoir. Furthermore, the indicators may forecast a very efficient sweep with high recovery.

The indicators for miscibility include a decrease in the light ends and an increase in the intermediates and heavy ends. As oil becomes more dense, its molecular weight likewise increases.

The indicators we discovered were unrelated to reservoir pressure since they occurred in scenarios of miscible gas injection with the same and different pressures, but the immiscible scenario did not. Indicators were also unaffected by changes in

viscosity, relative permeability shape, and mobile oil range since they were submitted without consideration to these specific variations in a variety of scenarios and only activated when pressure surpassed the minimum miscibility pressure.

Nonetheless, in a single instance, indicators were detected even under immiscible conditions. These are the circumstances in which all oil is mobile, the relative permeability is X-shaped, and the viscosity for oil and gas are equal and constant. These modifications aid the sweep and promote a recovery comparable to a miscible state. Evidently, this instance is an abstraction, but it may resemble a flawless mobility control project, such as Foam Assisted WAG, chemical injection, and low-salinity water injection, that increases gas viscosity and reduces disruption of phases and reservoir rock on flow.

In these instances, even below MMP, a great level of recovery was achieved as they were miscible. The investigation of the main mechanism promoting the high recovery was performed to identify if the convective and viscous force of displacement with constant viscosity in both phases or if the molecular interaction of components in gas with oil reached an ideal condition of mixture for phase-equilibrium. It reveals that the dominant process is convective displacement, since in a black oil formulation, with no molecular interaction, recovery was still high, even when no oil swelling was permitted.

In the evaluation of compositional change in reservoir conditions, a two-phase envelope appraisal revealed that conditions were not thermodynamically evaluated as miscible, as the critical point did not reach reservoir temperature in all cases above MMP, but they were "miscible" from a reservoir engineering perspective, i.e., monophasic in the range where drainage occurs as all hydrocarbon remained as a single phase until completely swept since the reservoir pressure was maintained above saturation limit. In other instances, the pressure was below the MMP, the critical point reached reservoir temperature, but reservoir pressure was insufficient to be outside of the two-phase region. In addition, an oscillatory tendency of the cricondenbar resulted in oscillations in saturation pressure with a suitable visual description of the combined vaporization and condensation mechanism of miscible displacement as reported by several authors.

The indicators were also examined in a completely different thermodynamic model of a distinct reservoir fluid, and they were only activated when recovery was high due to a miscibility condition.

This work has led to a greater comprehension of the effect of miscibility on oil composition and its importance in the context of gas injection for enhanced oil recovery and also suggests a simple series of chromatography on stock-tank oil to infer on the miscible scenario at reservoir conditions.

6.2 Recommendations

To further investigate the alteration in oil composition regarding the miscible condition, the following suggestions are made:

1. Evaluate the WAG effect on indicators. A period of water flood might change oil composition differently in bypassed oil if water injection occurs before gas injection and/or might renew gas composition altering phase-equilibrium.

2. Evaluate results in 2D and 3D Reservoir Model and investigate gravity, heterogeneity, and fractures' effect on indicators and recovery.

3. Evaluate results in a more detailed lumped scheme and/or in a completely lumped composition (up to C35+) to evaluate the main pseudocomponents affected by gas displacement.

4. Evaluate indicators in a experiment. In a slim tube test, acquire the dead oil composition throughout the experiment to evaluate the results in laboratory data.

5. Evaluate indicators in the real field. Acquiring dead oil chromatography from the beginning of gas injection might reveal the miscibility condition of gas injection. A combined evaluation with two or more different partition chemical tracers is also desirable.

6. Improve the relative permeability models for miscible conditions using the miscibility indicators based on the composition alteration during simulation.

Bibliography

AARRA, M. G., SKAUGE, A., MARTINSEN, H. A., 2002, "FAWAG: A Breakthrough for EOR in the North Sea", (09). doi: <10.2118/77695-MS>. Availability: <https://doi.org/10.2118/77695-MS>. SPE-77695-MS.

AFZALI, S., REZAEI, N., ZENDEHBOUDI, S., 2018, "A comprehensive review on Enhanced Oil Recovery by Water Alternating Gas (WAG) injection", *Fuel*, v. 227, n. March, pp. 218–246. doi: <10.1016/j.fuel.2018.04.015>. Availability: <https://doi.org/10.1016/j.fuel.2018.04.015>.

AGUILAR, R. A., MCCAIN, W. D., 2002, "An Efficient Tuning Strategy to Calibrate Cubic EOS for Compositional Simulation", v. All Days (09). doi: <10.2118/77382-MS>. Availability: <https://doi.org/10.2118/77382-MS>. SPE-77382-MS.

AHMED, T., 2010, *Reservoir Engineering Handbook*. Elsevier Science. ISBN: 9780080966670. Availability: <https://books.google.com.br/books?id=LXJcG_jwTHAC>.

ARBABI, S., FIROOZABADI, A., 1995, "Near-Critical Phase Behavior of Reservoir Fluids Using Equations of State", *SPE Advanced Technology Series*, v. 3, n. 01 (03), pp. 139–145. doi: <10.2118/24491-PA>. Availability: <https://doi.org/10.2118/24491-PA>.

BERGE, L. I., STENSEN, J. A., CRAPEZ, B., QUALE, E. A., 2002, "SWAG Injectivity Behavior Based on Siri Field Data", (04). doi: <10.2118/75126-MS>. Availability: <https://doi.org/10.2118/75126-MS>. SPE-75126-MS.

BLACKWELL, R., TERRY, W., RAYNE, J., LINDLEY, D., HENDERSON, J., 1960, "Recovery of Oil by Displacements With Water-Solvent Mixtures", *Transactions of the AIME*, v. 219, n. 01 (12), pp. 293–300. doi: <10.2118/1306-G>. Availability: <https://doi.org/10.2118/1306-G>.

BROCK, W., BRYAN, L., 1989, "Summary Results of CO2 EOR Field Tests, 1972-1987". SPE Rocky Mountain Petroleum Technology Conference / Low Permeabil-

ity Reservoirs Symposium. Society of Petroleum Engineers, 03. Availability: <https://doi.org/10.2118/18977-MS>. SPE-18977-MS.

CABRAL, V. F., CASTIER, M., CARDOZO-FILHO, L., 2019, "Classical Models Part 1". In: *Thermodynamics of Phase Equilibria in Food Engineering*, Elsevier, pp. 73–102, oct.

CAUDLE, B., DYES, A., 1958, "Improving Miscible Displacement by Gas-Water Injection", *Transactions of the AIME*, v. 213, n. 01 (12), pp. 281–283. doi: <10.2118/911-G>. Availability: <https://doi.org/10.2118/911-G>.

CAVALCANTE FILHO, J. S. D. A., PIZARRO, J. O. D. S., 2019, "Application of the Convective-Dispersive Equation to Estimate Field Scale Dispersivity based on a Field Scale Numerical Model and Tracer Production Data". v. Day 3 Thu, October 31, 2019, *Offshore Technology Conference Brasil*, 10. Availability: <https://doi.org/10.4043/29736-MS>. D031S035R002.

CHANG, Y. B., 1990, *Development and application of an equation of state compositional simulator*. Ph.D. Thesis, the University of Texas at Austin. Availability: <https://repositories.lib.utexas.edu/handle/2152/80585>.

CHEN, S., LI, H., YANG, D., TONTIWACHWUTHIKUL, P., 2010, "Optimal Parametric Design for Water-Alternating-Gas (WAG) Process in a CO2-Miscible Flooding Reservoir", *Journal of Canadian Petroleum Technology*, v. 49, n. 10 (10), pp. 75–82. doi: <10.2118/141650-PA>. Availability: <https://doi.org/10.2118/141650-PA>.

CHRISTENSEN, J. R., STENBY, E. H., SKAUGE, A., 2001, "Review of WAG Field Experience", *SPE Reservoir Evaluation Engineering*, v. 4, n. 02 (04), pp. 97–106. doi: <10.2118/71203-PA>. Availability: <https://doi.org/10.2118/71203-PA>.

COATS, K. H., 1980, "An Equation of State Compositional Model", *Society of Petroleum Engineers Journal*, v. 20, n. 05 (10), pp. 363–376. doi: <10.2118/8284-PA>. Availability: <https://doi.org/10.2118/8284-PA>.

COREY, A. T., 1954, "The interrelation between gas and oil relative permeabilities", *Producers monthly*, pp. 38–41.

CROGH, N. A., EIDE, K., MORTERUD, S. E., 2002, "WAG Injection at the Statfjord Field, A Success Story". SPE Europec featured at EAGE Conference and Exhibition, 10. Availability: <https://doi.org/10.2118/78348-MS>. SPE-78348-MS.

DAKE, L. P., 2001, *The Practice of Reservoir Engineering (revised edition)*, v. 36. Elsevier.

DARCY, H. P. G., 1856, *Les Fontaines publiques de la ville de Dijon. Exposition et application des principes à suivre et des formules à employer dans les questions de distribution d'eau, etc.* V. Dalamont.

DE FARIAS, M. L. R., 2013, *Recuperação Avançada de Óleos Pesados por Injeção de Emulsões Diluídas em Água.* Ph.D. Thesis, DEM, PUC-RJ. Availability: <https://doi.org/10.17771/PUCRio.acad.23855>.

DEHYADEGARI, E., RABBANI, A. R., 2014, "The Effects of Miscible CO2 Injection on Oil Biomarker Parameters", *Petroleum Science and Technology*, v. 32, n. 23, pp. 2853–2866. doi: <10.1080/10916466.2014.902959>. Availability: <https://doi.org/10.1080/10916466.2014.902959>.

DOS SANTOS, M. P. P. C., 2017, *Modelo de rede de capilares para o estudo do escoamento de gás retrógrado em meios porosos.* Master Thesis, PUC-RJ, Rio de Janeiro. Availability: <https://doi.org/10.17771/PUCRio.acad.32319>.

DYER, S. B., FAROUQ ALI, S. M., 1994, "Linear Model Studies of the Immiscible CO2 WAG Process for Heavy-Oil Recovery", *SPE Reservoir Engineering*, v. 9, n. 02 (05), pp. 107–111. doi: <10.2118/21162-PA>. Availability: <https://doi.org/10.2118/21162-PA>.

ESPOSITO, R. O., ALIJÓ, P. H. R., SCILIPOTI, J. A., TAVARES, F. W., 2017, *Compositional grading in Oil and Gas reservoirs.* Gulf Professional Publishing.

ESPÓSITO, R. O., CASTIER, M., TAVARES, F. W., 2000, "Phase Equilibrium Calculations for Semicontinuous Mixtures Subject to Gravitational Fields", *Industrial & Engineering Chemistry Research*, v. 39, n. 11, pp. 4415–4421. doi: <10.1021/ie000268z>. Availability: <https://doi.org/10.1021/ie000268z>.

FOLSTA, K., CAMARGO, G., ESPÓSITO, R., 2010, "Gas condensate characterization from chromatogram areas and retention times", *Fluid Phase Equilibria*, v. 292, n. 1, pp. 87–95. doi: <https://doi.org/10.1016/j.fluid.2010.02.001>. Availability: <https://www.sciencedirect.com/science/article/pii/S0378381210000683>.

GHARBI, R. B. C., 2003, "Integrated Reservoir Simulation Studies to Optimize Recovery from a Carbonate Reservoir". v. All Days, *SPE Asia Pacific Oil and Gas Conference and Exhibition*, 09. Availability: <https://doi.org/10.2118/80437-MS>. SPE-80437-MS.

GREEN, D. W., WILLHITE, G. P., 1998, *Enhanced oil recovery*, v. 6. Henry L. Doherty Memorial Fund of AIME, Society of Petroleum Engineers.

HERNANDEZ, C., ALVAREZ, C., SAMAN, A., DE JONGH, A., AUDEMARD, N., 2002, "Monitoring WAG Pilot at VLE Field, Maracaibo Lake, by Perfluorocarbon and Fluorined Benzoic Acids Tracers", v. All Days (04). doi: <10.2118/75259-MS>. Availability: <https://doi.org/10.2118/75259-MS>. SPE-75259-MS.

HOLM, L., 1976, "Status of CO2 and Hydrocarbon Miscible Oil Recovery Methods", *Journal of Petroleum Technology*, v. 28, n. 01 (01), pp. 76–84. doi: <10.2118/5560-PA>. Availability: <https://doi.org/10.2118/5560-PA>.

HWANG, R., ORTIZ, J., 1998, "Effect of CO2 flood on geochemistry of McElroy oil", *Organic Geochemistry*, v. 29, n. 1, pp. 485–503. doi: <https://doi.org/10.1016/S0146-6380(98)00057-6>. Availability: <https://www.sciencedirect.com/science/article/pii/S0146638098000576>. Advances in Organic Geochemistry 1997 Proceedings of the 18th International Meeting on Organic Geochemistry Part I. Petroleum Geochemistry.

KOCH, H.A., J., SLOBOD, R., 1957, "Miscible Slug Process", *Transactions of the AIME*, v. 210, n. 01 (12), pp. 40–47. doi: <10.2118/714-G>. Availability: <https://doi.org/10.2118/714-G>.

LAFORCE, T., ORR, F. M., 2008, "Development of Gas/Oil Miscibility in Water and Gas Injection". v. All Days, *SPE Annual Technical Conference and Exhibition*, 09. Availability: <https://doi.org/10.2118/116119-MS>. SPE-116119-MS.

LEWIS, G. N., 1901, "THE LAW OF PHYSICO-CHEMICAL CHANGE", v. 37, n. 3, pp. 48.

LIMA, H. A. T. D. S. M., 2016, *Simulação da Injeção Alternada de Água-Emulsão-Água Considerando Efeitos Capilares em Modelos De Reservatórios Estratificados*. Master Thesis, PUC-RJ. Availability: <https://doi.org/10.17771/PUCRio.acad.28384>.

LOPEZ-ECHEVERRY, J. S., REIF-ACHERMAN, S., ARAUJO-LOPEZ, E., 2017, "Peng-Robinson equation of state: 40 years through cubics", *Fluid Phase Equilibria*, v. 447, pp. 39–71. doi: <https://doi.org/10.1016/j.fluid.2017.05.007>. Availability: <https://www.sciencedirect.com/science/article/pii/S0378381217301851>.

MANRIQUE, E. J., MUCI, V. E., GURFINKEL, M. E., 2007, "EOR Field Experiences in Carbonate Reservoirs in the United States", *SPE Reservoir Evaluation Engineering*, v. 10, n. 06 (12), pp. 667–686. doi: <10.2118/100063-PA>. Availability: <https://doi.org/10.2118/100063-PA>.

MOORTGAT, J., FIROOZABADI, A., LI, Z., ESPÓSITO, R., 2013, "CO2 Injection in Vertical and Horizontal Cores: Measurements and Numerical Simulation", *SPE Journal*, v. 18, n. 02 (04), pp. 331–344. doi: <10.2118/135563-PA>. Availability: <https://doi.org/10.2118/135563-PA>.

MUSKAT, M., MERES, M. W., 1936, "The Flow of Heterogeneous Fluids Through Porous Media", *Physics*, v. 7, n. 9, pp. 346–363. doi: <10.1063/1.1745403>. Availability: <https://doi.org/10.1063/1.1745403>.

MYERS, D., OTHERS, 1999, *Surfaces, Interfaces, and Colloids*, v. 415. Wiley New York.

NING, S. X., MCGUIRE, P. L., 2004, "Improved Oil Recovery in Under-Saturated Reservoirs Using the US-WAG Process", v. All Days (04). doi: <10.2118/89353-MS>. Availability: <https://doi.org/10.2118/89353-MS>. SPE-89353-MS.

PANDA, M., NOTTINGHAM, D., LENIG, D., 2011, "Systematic Surveillance Techniques for a Large Miscible WAG Flood", *SPE Reservoir Evaluation Engineering*, v. 14, n. 03 (05), pp. 299–309. doi: <10.2118/127563-PA>. Availability: <https://doi.org/10.2118/127563-PA>.

PEDERSEN, K. S., FREDENSLUND, A., 1987, "An improved corresponding states model for the prediction of oil and gas viscosities and thermal conductivities", *Chemical Engineering Science*, v. 42, n. 1, pp. 182–186. doi: <https://doi.org/10.1016/0009-2509(87)80225-7>. Availability: <https://www.sciencedirect.com/science/article/pii/0009250987802257>.

PEDERSEN, K. S., CHRISTENSEN, P. L., SHAIKH, J. A., CHRISTENSEN, P. L., 2006, *Phase behavior of petroleum reservoir fluids*. CRC press.

PENG, D.-Y., ROBINSON, D. B., 1976, "A New Two-Constant Equation of State", *Industrial & Engineering Chemistry Fundamentals*, v. 15, n. 1, pp. 59–64. doi: <10.1021/i160057a011>. Availability: <https://doi.org/10.1021/i160057a011>.

PEREIRA, C. G., 2018, "Fundamentals of Phase Equilibria". In: *Thermodynamics of Phase Equilibria in Food Engineering*, Elsevier, pp. 27–71, oct.

PRIVAT, R., JAUBERT, J.-N., 2011, "PPR78, a thermodynamic model for the prediction of petroleum fluid-phase behaviour", *JEEP 2011 - 37th Conference on Phase Equilibria*, (10), pp. 00011. doi: <10.1051/jeep/201100011>.

REDLICH, O., KWONG, J. N. S., 1949, "On the Thermodynamics of Solutions. V. An Equation of State. Fugacities of Gaseous Solutions." *Chemical Reviews*, v. 44,

n. 1, pp. 233–244. doi: <10.1021/cr60137a013>. Availability: <https://doi.org/10.1021/cr60137a013>. PMID: 18125401.

SANTOS, L. O. S. D., 2013, *Development of a multi-formulation compositional simulator*. Ph.D. Thesis, the University of Texas at Austin. Availability: <https://repositories.lib.utexas.edu/handle/2152/21396>.

SHAW, D. J., 1980, *Introduction to colloid and surface chemistry*. Butterworths.

SHIBATA, S. K., SANDLER, S. I., BEHRENS, R. A., 1987, "Phase equilibrium calculations for continuous and semicontinuous mixtures", *Chemical Engineering Science*, v. 42, n. 8, pp. 1977–1988. doi: <https://doi.org/10.1016/0009-2509(87)80144-6>. Availability: <https://www.sciencedirect.com/science/article/pii/0009250987801446>.

SOAVE, G., 1972, "Equilibrium constants from a modified Redlich-Kwong equation of state", *Chemical Engineering Science*, v. 27, n. 6, pp. 1197 – 1203. doi: <https://doi.org/10.1016/0009-2509(72)80096-4>. Availability: <http://www.sciencedirect.com/science/article/pii/0009250972800964>.

STALKUP, F. I., 1983, "Miscible displacement", (1). Availability: <https://www.osti.gov/biblio/5373832>.

THOMAS, F., HOLOWACH, N., ZHOU, X., BENNION, D., BENNION, D., 1994a, "Miscible or Near-Miscible Gas Injection, Which Is Better?" (04). doi: <10.2118/27811-MS>. Availability: <https://doi.org/10.2118/27811-MS>. SPE-27811-MS.

THOMAS, F., ZHOU, X., BENNION, D., BENNION, D., 1994b, "A Comparative Study of RBA, P-x, Multicontact And Slim Tube Results", *Journal of Canadian Petroleum Technology*, v. 33, n. 02 (02). doi: <10.2118/94-02-02>. Availability: <https://doi.org/10.2118/94-02-02>.

THOMAS, F., SHTEPANI, E., IMER, D., BENNION, D., 2002, "How Many Pseudo-Components Are Needed to Model Phase Behaviour?" *Journal of Canadian Petroleum Technology*, v. 41, n. 01 (01). doi: <10.2118/02-01-04>. Availability: <https://doi.org/10.2118/02-01-04>.

WANG, G., PICKUP, G., SORBIE, K., MACKAY, E., 2020, "Detailed Assessment of Compositional and Interfacial Tension Effects on the Fluid Behaviour During Immiscible and Near-Miscible CO2 Continuous and WAG Displacements", *Transport in Porous Media*, v. 131 (02). doi: <10.1007/s11242-019-01368-x>.

WANG, P., POPE, G. A., 2001, “Proper Use of Equations of State for Compositional Reservoir Simulation”, *Journal of Petroleum Technology*, v. 53, n. 07 (07), pp. 74–81. doi: <10.2118/69071-JPT>. Availability: <https://doi.org/10.2118/69071-JPT>.

ZABALOY, M. S., VERA, J. H., 1998, “The Peng-Robinson Sequel. An Analysis of the Particulars of the Second and Third Generations”, *Industrial & Engineering Chemistry Research*, v. 37, n. 5, pp. 1591–1597. doi: <10.1021/ie970654p>. Availability: <https://doi.org/10.1021/ie970654p>.

ZICK, A., 1986, “A Combined Condensing/Vaporizing Mechanism in the Displacement of Oil by Enriched Gases”. v. All Days, *SPE Annual Technical Conference and Exhibition*, 10. Availability: <https://doi.org/10.2118/15493-MS>. SPE-15493-MS.

Appendix A

Procedure for Tuning an EOS

The following list summarizes the approach used for tuning ResFluid1 and ResFluid2 fluids, based on ESPOSITO *et al.* (2017), WANG and POPE (2001), and PEDERSEN *et al.* (2006):

1. **Providing an good estimation for initial parameters**

   (a) Physical Properties:
   Winprop's library and Twu for physical properties and Lee-Kesler for ω (plus fraction).

   (b) Peneloux's volume shift: $c_i/b_i = 0.0887 * ln(M_i) - 0.4668$, for i=1,...,nc
   and $c_{CO_2}/b_{CO_2} = -0.718$

   (c) BIC for C_1:
   $BIC_{C_1-C_n} = 0.2 + 0.0001 * SCN_n$

   (d) BIC for CO_2:
   $BIC_{CO_2-C_n} = 0.1515 - 0.0002 * SCN_n$

   (e) BIC for CO_2 and C_1:
   $BIC_{CO_2-C_1} = 0.15$

   (f) BIC for other component:

   - $BIC_{C_{n,n>2}} = 0.0$

2. **Lumping Pseudo-Components**

   (a) 5 pseudo-component:
   CO_2, $N_2 - C_1$, $C_2 - C_5$, $C_6 - C_{12}$, and $C_{13} - C_{19}$

   (b) Plus fraction (SHIBATA *et al.*, 1987):
   PC_{24}, PC_{44}, and PC_{70} (Res.Fluid 1) and PC_{27} and PC_{60} (Res.Fluid 2)

3. **Grouping data to step-wise fitting approach**

(a) Saturation Pressure + Liquid properties

(b) Gas properties

(c) Miscibility assay (not available)

(d) Viscosity (vapor and liquid phase)

4. **Selecting EOS parameter necessary to fit data**

   (a) Group varying by equal ratios:

      i. P_c, T_c, ω and MW from $C_6 - C_{12}$

      ii. V_{shift} from $N_2 - C_1$

      iii. BIC_{CO_2} from $N_2 - C_1$

      iv. BIC_{C_1} from $C_2 - C_5$

   (b) Regroup plus-fraction P_c into a different group.
   Two groups for PC: lighter and heavier than C19

   (c) Individually regression of plus fraction P_c

   (d) Regroup plus-fraction for T_c

   (e) ...

   (f) Segregate one-by-one plus fraction variable regression

   (g) ...

   (h) Combine two groups for plus-fraction in selected EOS Parameter

   (i) ...

5. **Consistency-check in each step of step before (STEP 4) and for variable range:**

   (a) SCN/MCN increases, T_c, ω, $BIC_{C_1-C_n}$, and MW increases

   (b) SCN/MCN increases, P_c and $BIC_{CO_2-C_n}$ decreases

6. **Evaluate error of all available data and determine the continuation.**

   (a) Error limits suggestions for volumetric/massic/viscosity's data: Below 10% (5% to be rigorous)

   (b) Error limits suggestions for Saturation Pressure/Miscibility Data: Below 5% (1-2% to be rigorous)

7. **Include next grouping data (from STEP 3) if necessary**

Appendix B

Technique for Representing Plus Fraction

Typically, in order to better represent the plus fraction, more than one pseudo-component is necessary. SHIBATA *et al.* (1987) proposed a technique for representing the plus fraction using as many points as desired, by adapting the Gauss-Laguerre Quadrature to the plus fraction representation.

B.1 Mathematical Formulation and Assumptions

The technique consists of assuming that a function is capable of representing the molar composition distribution from the first SCN (η) in the plus fraction to the last one (ϕ), ideally to infinity.

$$\sum_{i=1}^{\eta-1} z_i \; + z_{\eta+} = \sum_{i=1}^{\eta-1} z_i \; + \int_{\eta}^{\phi} F(I)\, dI = 1 \tag{B.1}$$

The first term on the left-hand side of Equation B.1 represents the composition acquired from laboratory chromatography until the last SCN before the plus fraction ($\eta-1$). The function $F(I)$ models the composition distribution on each SCN in the plus fraction. The integral of $F(I)$ from η to ϕ represents the plus fraction.

Many authors have reported that the concentration of components in the plus fraction decreases exponentially with increasing SCN index (SHIBATA *et al.* (1987), PEDERSEN *et al.* (2006), and ESPOSITO *et al.* (2017)). Therefore, the function $F(I)$ is defined by Equation B.2.

$$F(I) = Ce^{-DI} \tag{B.2}$$

Where C and D are adjustable parameters used to fit the distribution of the plus fraction. The integral representing the plus fraction has two constraints: the composition and the molecular weight of the plus fraction. By using an approximation for the molecular weight of heavier components, such as the plus fraction, one can estimate the average SCN carbon of the plus fraction ($\overline{I}$), for example using Equation B.3.

$$MW = 14I - 4 \tag{B.3}$$

The 14 multiplied by I considers the increment of 14g/mol for each carbon added, 12 g/mol for each carbon plus 1 g/mol for each hydrogen atom on paraffinic molecules. The subtraction of 4 considers the presence of some aromatic structures, as they contain fewer hydrogen per carbon atom than paraffin.

The integrals for plus fraction are defined as Equation B.4 for the composition, and this integral is set to unity since a multiplication of plus fraction composition on both sides forces it to match laboratory data. Also, since it represents the molar composition distribution, a multiplication by I results in $\overline{I}$ (Equation B.5), as it represents a mixing rule of molecular weight.

$$\int_{\eta}^{\phi} Ce^{-DI}\,dI = 1 \tag{B.4}$$

$$\int_{\eta}^{\phi} ICe^{-DI}\,dI = \overline{I} \qquad \frac{\int_{\eta}^{\phi} F(I)MW(I)\,dI}{\int_{\eta}^{\phi} F(I)\,dI} = \overline{MW_{+}} \tag{B.5}$$

It is impractical to work until infinity, as it will exceed the recommended range for empirical correlation and computational limits. Many authors suggest a range from 70-100. SHIBATA *et al.* (1987) states that components with more than 70 carbon atoms are statistically unlikely in the majority of oils. PEDERSEN *et al.* (2006) proposes an upper limit of 80 carbon atoms, which is considered in this work.

Integration of Equation B.4 results in:

$$\int_{\eta}^{\phi} Ce^{-DI}\,dI = 1 \qquad \text{since: } \int e^{ax}\,dx = \frac{e^{ax}}{a}$$

$$C\left[\frac{e^{-DI}}{-D}\right]\Bigg|_{\eta}^{\phi} = 1$$

$$C\left[\frac{e^{-D\phi}-e^{-D\eta}}{-D}\right]=1$$

$$\frac{C}{D}(e^{-D\eta}-e^{-D\phi})=1$$

$$C=\frac{D}{e^{-D\eta}-e^{-D\phi}} \tag{B.6}$$

Integration of Equation B.5 results in:

$$\int_{\eta}^{\phi} ICe^{-DI}\,dI=\overline{I} \qquad \text{since: } \int xe^{ax}\,dx=e^{ax}\left(\frac{ax-1}{a}\right)$$

$$C\left[e^{-DI}\left(\frac{-DI-1}{D^2}\right)\right]\Bigg|_{\eta}^{\phi}=\overline{I}$$

$$C\left[e^{-D\phi}\left(\frac{-D\phi-1}{D^2}\right)-e^{-D\eta}\left(\frac{-D\eta-1}{D^2}\right)\right]=\overline{I}$$

Replacing Eq. B.6

$$\frac{D}{(e^{-D\eta}-e^{-D\phi})}\left[e^{-D\phi}\left(\frac{-D\phi-1}{D^2}\right)-e^{-D\eta}\left(\frac{-D\eta-1}{D^2}\right)\right]=\overline{I}$$

$$\frac{\eta e^{-D\eta}}{(e^{-D\eta}-e^{-D\phi})}+\frac{e^{-D\eta}}{D(e^{-D\eta}-e^{-D\phi})}-\frac{\phi e^{-D\phi}}{(e^{-D\eta}-e^{-D\phi})}-\frac{e^{-D\phi}}{D(e^{-D\eta}-e^{-D\phi})}=\overline{I}$$

Coupling second and forth terms and adding/subtracting and multiplying/dividing the new terms:

$$\frac{(e^{-D\eta}-e^{-D\phi})}{D(e^{-D\eta}-e^{-D\phi})}+\frac{\eta e^{-D\eta}}{(e^{-D\eta}-e^{-D\phi})}-\eta-\frac{\phi e^{-D\phi}}{(e^{-D\eta}-e^{-D\phi})}=\overline{I}-\eta$$

$$\frac{1}{D}+\frac{\eta e^{-D\eta}}{(e^{-D\eta}-e^{-D\phi})}-\frac{\eta(e^{-D\eta}-e^{-D\phi})}{(e^{-D\eta}-e^{-D\phi})}-\frac{\phi e^{-D\phi}}{(e^{-D\eta}-e^{-D\phi})}=\overline{I}-\eta$$

$$\frac{1}{D}+\frac{\eta e^{-D\eta}-\eta e^{-D\eta}+\eta e^{-D\phi}-\phi e^{-D\phi}}{(e^{-D\eta}-e^{-D\phi})}=\overline{I}-\eta$$

$$\frac{1}{D}+\frac{(\eta-\phi)e^{-D\phi}e^{D\eta}}{(e^{-D\eta}-e^{-D\phi})e^{D\eta}}=\overline{I}-\eta$$

$$\frac{1}{D}-\frac{(\phi-\eta)e^{-D(\phi-\eta)}}{(1-e^{-D(\phi-\eta)})}=\overline{I}-\eta$$

Applying a constant defined as $\Delta = D(\phi - \eta)$ (SHIBATA *et al.*, 1987):

$$\frac{1}{\Delta} - \frac{e^{-\Delta}}{1 - e^{-\Delta}} = \frac{\overline{I} - \eta}{\phi - \eta} \tag{B.7}$$

For a given molecular weight for the plus fraction, one can calculate $\overline{I}$ from Equation B.3. Also, by defining the upper and lower integration limits of the distribution, Equation B.7 can be solved for Δ. Then, using $\Delta = D(\phi - \eta)$ and Equation B.6, one can obtain the values of D and C. Now, the generation of the pseudo-components for representing the plus fraction can be performed using the Gauss-Laguerre Quadrature procedure.

B.2 Analytical Solutions for Integrals in Gauss-Laguerre Quadrature

For n integration points, the quadrature technique of Gaussian integration yields an exact value for an integral of a polynomial of order *2n-1* or lower, and an approximate value for other functions. The methodology states that the integral of a weighted function (in this case, a polynomial function weighted by an exponential) can be calculated by a weighted sum of the function values evaluated at quadrature points.

$$J = \int_a^b W(x)F(x)\,dx = \sum_{i=1}^{n} w_i F(z_i) \tag{B.8}$$

Where the location of quadrature points is obtained by solving for w_i and z_i in the sequence of equations that results from substituting polynomials of order 0 up to $2n-1$ in Equation B.8. The Gauss-Laguerre solution is specific when $a = 0$, $b = \infty$, and $W(x) = e^{-x}$. The integral in our problem is:

$$\int_\eta^\phi e^{-DI} G(I)\,dI \tag{B.9}$$

To operate equations in terms of Gauss-Laguerre format, a variable change is needed.

Been: $z = D(I - \eta)$ and $I = \frac{z}{D} + \eta$

For I=η $z = D(\eta - \eta) = 0$

For I=ϕ $z = D(\phi - \eta) = \Delta$

The derivative: $dz = DdI$

$$\int_\eta^\phi e^{-DI} G(I)\, dI = \int_0^\Delta \left(\frac{e^{\frac{\eta}{D}}}{D}\right) e^{-z} G(z)\, dz \quad \text{omitting the constant} = \int_0^\Delta e^{-z} G(z)\, dz$$

As the integral has an analytic solution to obtain the quadrature points and weights, there are *2n* unknowns, which are the quadrature points and weights. To obtain these unknowns, the function G(z) is set to z^j with *j=0,1,2,...,2n-1* to obtain a set of *2n* equations.

$$\int_0^\Delta e^{-z} z^j\, dz = \sum_{i=1}^{n} w_i z_i^j \qquad j = 0, 1, ..., 2n-1 \tag{B.10}$$

For a set of 2 quadrature points, the linear system becomes:

$$\begin{aligned}
&\int_0^\Delta e^{-z} z^0\, dz = 1 - e^{-\Delta} && = \sum_{i=1}^{n=2} w_i z_i^0 = w_1 + w_2 && \text{j=0}\\
&\int_0^\Delta e^{-z} z^1\, dz = 1 - (\Delta + 1) e^{-\Delta} && = \sum_{i=1}^{n=2} w_i z_i^1 = w_1 z_1 + w_2 z_2 && \text{j=1}\\
&\int_0^\Delta e^{-z} z^2\, dz = 2 - (\Delta^2 + 2(\Delta + 1)) e^{-\Delta} && = \sum_{i=1}^{n=2} w_i z_i^2 = w_1 z_1^2 + w_2 z_2^2 && \text{j=2}\\
&\int_0^\Delta e^{-z} z^3\, dz = 6 - (\Delta^3 + 3\Delta^2 + 6(\Delta + 1)) e^{-\Delta} && = \sum_{i=1}^{n=2} w_i z_i^3 = w_1 z_1^3 + w_2 z_2^3 && \text{j=3}
\end{aligned}$$

Through the results of the four integrals for 2 quadrature points, one might notice that besides the first one for *j=0*, the integral results are based on previous results. The integral results in a convenient format, highlighted in blue, are shown below:

$$\begin{aligned}
&\int_0^\Delta e^{-z} z^0\, dz = -e^{-z}\Big|_0^\Delta && = 1 - e^{-\Delta}\\
&\int_0^\Delta e^{-z} z^1\, dz = -(z+1) e^{-z}\Big|_0^\Delta && = -\Delta e^{-\Delta} + (1 - e^{-\Delta})\\
& && = 1 - (\Delta + 1) e^{-\Delta}
\end{aligned}$$

$$\int_0^{\Delta} e^{-z} z^2\, dz = -z^2 e^{-z}\Big|_0^{\Delta} + 2\int_0^{\Delta} z^1 e^{-z}\, dz \qquad = -\Delta^2 e^{-\Delta} + 2(1-(\Delta+1)e^{-\Delta})$$

$$= 2-(\Delta^2+2(\Delta+1))e^{-\Delta}$$

$$\int_0^{\Delta} e^{-z} z^3\, dz = -z^3 e^{-z}\Big|_0^{\Delta} + 3\int_0^{\Delta} z^2 e^{-z}\, dz \qquad = -\Delta^3 e^{-\Delta} + 3(2-(\Delta^2+2(\Delta+1))e^{-\Delta})$$

$$= 6-(\Delta^3+3\Delta^2+6(\Delta+1))e^{-\Delta}$$

This fact is based on the solution for a polynomial coupled with an exponential function:

Since: $$\int x^n e^{cx}\, dx \qquad = \frac{1}{c}x^n e^{cx} - \frac{n}{c}\int x^{n-1} e^{cx}\, dx$$

as $n = j$, $x = z$, and $c = -1$ $$= -z^j e^{-z} + j\int z^{j-1} e^{-z}\, dz$$

For our case, a computational convenient format is related

$$Integral(j) = \int_0^{\Delta} e^{-z} z^j\, dz = 1 - e^{-\Delta} \qquad j = 0 \tag{B.11a}$$

$$Integral(j) = \int_0^{\Delta} e^{-z} z^j\, dz = -\Delta^j e^{-\Delta} + Integral(j-1) = \qquad j = 1,...,2n-1 \tag{B.11b}$$

B.3 Computational Coding for Gauss-Laguerre Quadrature Points

With laboratory data for molar composition and molecular weight of the plus fraction, the determination of the lower and upper integration limits, and the number of quadrature points, the problem can determine the quadrature points by solving the nonlinear system for Δ and the linear system for z_i and w_i.

Once solved, as the z_i values relate to the composition and w_i values relate to the SCN number for each quadrature point, a reverse variable change must be performed to find the composition and molecular weight for each quadrature point.

$$\text{Molar Composition}_{I-quadrature} = z_i z_{C+} \tag{B.12}$$

$$\text{Molecular Weight}_{I-quadrature} = 14 I_{quadrature} - 4 = 14\left(\frac{w_i}{D} + \eta\right) - 4 \tag{B.13}$$

The code procedure developed follows this simplified scheme:

1. Input $MW_{+fraction}$, $z_{+fraction}$, Lower and upper carbon limits (η and ϕ),and number of quadrature points desired
2. Perform a single Newton-Raphson procedure in Equation B.7 as a function (subtracting right-hand term and equalling too zero) in and its analytic derivative
3. Calculate analytically all integrals from Gauss-Laguerre integrals from Equations B.11a and B.11b
4. Performing a Newton-Raphson routine to estimate z_i and w_i
   (a) Initial guess for w_i as a random number between [0-1], normalized to sum up unity
   (b) Initial guess for z_i with an increasing constant increment until reaching Δ
   (c) Subtracting Integrals results in both sides of Equation B.10 to treat it as a function, as Integrals might be considered as a constant, analytical defined in item 3.
   (d) Taken derivative for w_i and z_i of this function to assemble Jacobian matrix
   (e) Calculate increments of w_i and z_i, using inverse of Jacobian Matrix, if determinant is larger than 0.01, or Moore–Penrose inverse if not (for stability propose).
   (f) Check condition for increment to keep physical meaning, since w_i must be greater than zero and z_i must be between zero and Δ
      - reduce increment that violate previous statements by 50% if occurs in first 50 iteration
      - reduce increment by a factor of 25/interaction number if occurs after 50th iteration
5. Validate results for w_i and z_i with analytical Integrals (Eq. B.11a and B.11b)
6. Calculate Molar Composition and Molecular Weight for quadrature points using Equation B.13
7. Perform logging and printing routines

For example, the code developed for ResFluid1 with 4 quadrature points and integration limits, as suggested by ESPÓSITO *et al.* (2000), ranging from 19.5 to 80.5, results in the following output:

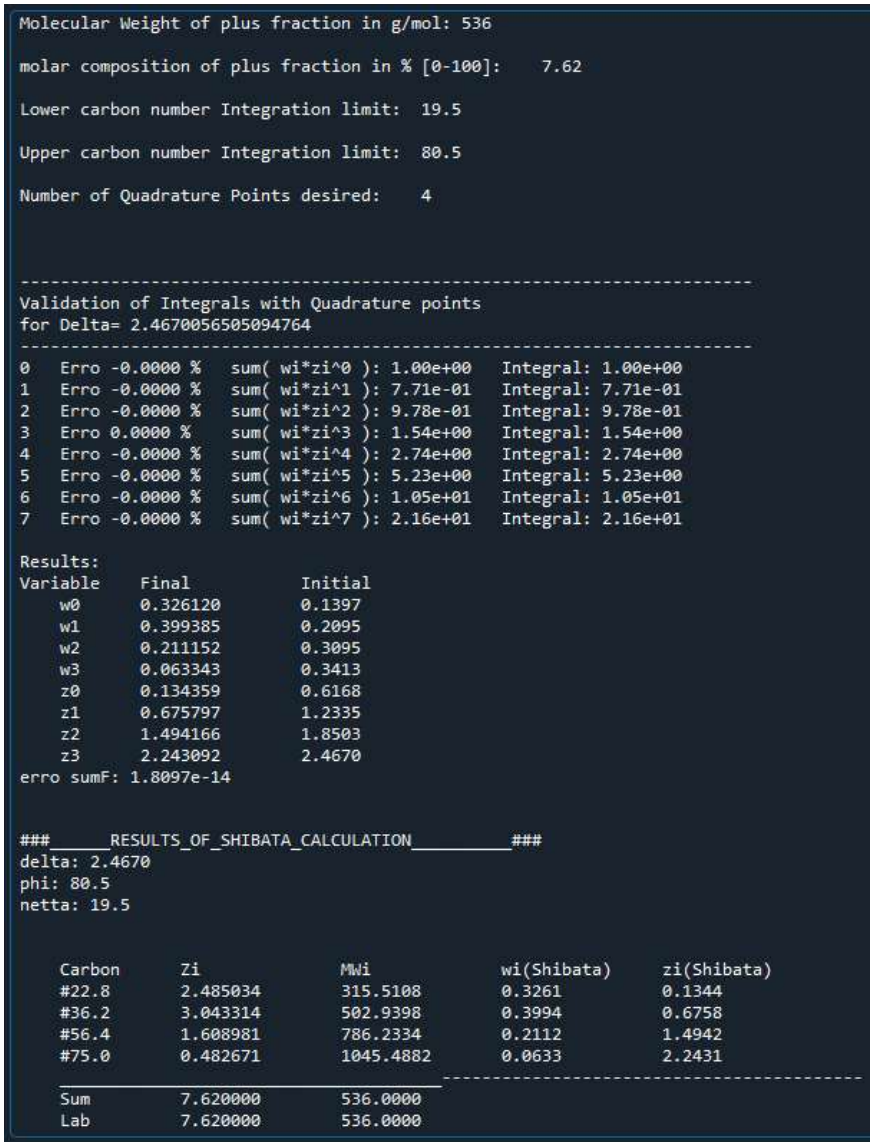

Figure B.1: Results of Program Develop for ResFluid1 and 4 Quadrature Points

The coding, develop in Python 3.8.3, for previous scheme are share above.

```
import numpy as np
import copy
log=[]

##########################################Input data
MW_plus=float(input('Molecular Weight of plus fraction in g/mol:'))
Zi_plus=float(input('molar composition of plus fraction in %
    [0-100]:'))
netta=float(input('Lower carbon number Integration limit:'))
phi=float(input('Upper carbon number Integration limit:'))
I=(MW_plus+4)/14    #Number of continuous carbon to MMW+
pontos=int(input('Number of Quadrature Points desired:'))
w_z,comp_f,NroC_f,MW_f,delta=Shibata_calc(I,netta,phi,pontos,
    MW_plus,Zi_plus)
```

```
#w_z: variable with solution for Shibata wi's & zi's
#comp_f: Composition of each quadrature point
#NroC_f: Number of Carbon of each quadrature point
#MW_f: Molecular Weight of each quadrature point
################################################
```

Listing B.1: Start of Program

```
def Shibata_calc(I,netta,phi,pontos,MW_plus,Zi_plus):
    ###############Delta and Integrals for Laguerre-Gauss
   Quadrature
    delta,log_D=calc_delta(I, netta, phi)
    del log_D

    INT=Quadrature_Integral(delta,pontos)
    #Normalization of first integral (wi sum up 1)
    INT=INT/INT[0]

    ###############Initial guess
    wi=sorted(np.random.rand(pontos))
    wi=wi/np.sum(wi)
    zi=sorted(np.random.rand(pontos)*delta)   #z=D(I-netta) delta=D
   (phi-netta)

    for i in range(pontos):
        zi[i]=(i+1)*delta/pontos

    x=[]
    x.extend(wi) #### x= 1st half is wi's
    x.extend(zi) #### X= 2nd half is zi's

    ###############Quadrature points calculation of wi's and zi's
    xcalc,log_NR=NewtonRaphson(INT,x,10000,1e-10,delta)
    log.extend(log_NR)
    del log_NR

    ###############Sort zi&wi from Zi_min to Zi_max
    z_w_aux = sorted(zip(xcalc[pontos:], xcalc[:pontos]))
    zi_order=[item[0] for item in z_w_aux]
    wi_order=[item[1] for item in z_w_aux]
    z=np.zeros(2*pontos)
    for i in range(pontos):
        z[i]=wi_order[i]
        z[i+pontos]=zi_order[i]

    ###############Validation with analytic integrals
    print('\n\n')
```

```
    Check(delta,INT,z,x)
    log_CK=Check_log(delta,INT,z,x)
    log.extend(log_CK)
    del log_CK

    ###############Save Log file
    log.extend(['\n'])
    log_Result=Print_result(delta,z,1)
    log.extend(log_Result)
    del log_Result

    F=F_NR(INT,z)
    print('erro sumF: %.4e'% np.sum(np.abs(F)))

    D=delta/(phi-netta)
    zi_f=z[:pontos]*Zi_plus
    C_f=z[pontos:]/D+netta
    MWi_f=14*C_f-4

    PrintlastTable(delta,phi, netta,C_f,zi_f,MWi_f,z)
    log_LastTable=LoglastTable(delta,phi, netta,C_f,zi_f,MWi_f,z)
    log.extend(['\n'])
    log.extend(log_LastTable)
    del log_LastTable

    f = open("Shibata.log",'w')
    f.write('\n'.join(log))
    f.close()
    return z,zi_f,C_f,MWi_f,delta
```

Listing B.2: Main function for Quadrature Points

```
def calc_delta(I,netta,phi):
    logging=[]
    logging.extend(['
   ------------------------------------------------------------'])
    logging.extend(['Newton-Raphson Iteration for DELTA Estimation
   :\n'          \
            + '\t\tdelta_new=delta_old-F/dF \n'
              \
            +'\nF=1/delta-exp(-delta)/(1-exp(-delta)\n'
              \
            +'dF=-1/delta^2+[exp(-delta)*(1-exp(-delta)+'
              \
            +'exp(-2*delta)]/(1-exp(-delta))^2'
              \
            +'\n\nMax iteration: 1000 tMax delta: 1e-8\n'
              \
```

```
            +'
    ------------------------------------------------------------'])
     deltai=1
     ITERMAX=1000
     TOL=1e-8
     for i in range(ITERMAX):
         F=((1/deltai)-np.exp(-deltai)/(1-np.exp(-deltai)))-(I-netta
    )/(phi-netta)
         dF=-1/deltai-(-(1-np.exp(-deltai))*np.exp(-deltai)- \
                       np.exp(-2*deltai))/((1-np.exp(-deltai))**2)
         ddelta=-F/dF
         deltai=deltai+ddelta
         if ddelta<TOL:
             logging.extend(['\n\t\tConvergence Reached ' + \
                             'in iteration:%.0i' % i + \
                             '\n\t\t\tDelta i: %.8e' % deltai + "\n\
    t\t\t/\Delta: %.2e" % ddelta])
             break
         logging.extend(["\t*iteration:%.0i" % i + \
                         "\tDelta i: %.8e" % deltai + "\t/\Delta %.2
    e" % ddelta])
         if i==ITERMAX-1:
             logging.extend(['Max iteration limit reached without
    convergence'+  \
                             ' in Delta calculation\n Iteration %.0i
    ' % ITERMAX + \
                                 '/\delta %.8f' % ddelta + 'Tol %.2f
    ' % TOL])
             logging.extend(['\n
    ------------------------------------------------------------'\
                  +'\nERROR in Newton-Raphson Iteration for DELTA
    Estimation\n'  \
                  +'
    ------------------------------------------------------------\n\n'])
     logging.extend(['\n
    ------------------------------------------------------------'\
         +'\nEnd of Newton-Raphson Iteration for DELTA Estimation\n'
      \
         +'------------------------------------------------------------\
    n\n'])
     return deltai,logging

def NewtonRaphson(Integrals,x0,N,TOL,delta):
     logging=[]
     logging.extend(['\n
    ------------------------------------------------------------'])
     logging.extend(["Newton-Raphson Iteration for wi's and zi's'\
```

```
    ndx=-J^-1*F" \
                        +"\nMax iteration %.0i" % N + '\tMax dx:%.3e' %
     TOL])
     logging.extend(['
    ----------------------------------------------------------'])
     k=0
     z=copy.deepcopy(x0)
     pontos=int(len(x0)/2)
     #**********************
     aux_x=''
     aux_dx=''
     for i in range(2*pontos):
         aux_x+='\tnewx%.0i' % (i+1)
         aux_dx+='\tdx%.0i'% (i+1)
     text='iteration\tSum(F)\tmax dx\t|DetJ|\tSingular\tx_eval'
     text+=aux_dx+ aux_x
     # print(text)
     logging.extend([text])
     auxValue='%2.0i' % k # initial iteration
     auxValue+='\t-\t-\t-\t-\t-'
     auxValue+= '\t'+'\t'.join(["{:10.2f}".format(elem) for elem in
    [0]*pontos*2])
     auxValue+= '\t'+'\t'.join(["{:10.2f}".format(elem) for elem in
    z])
     logging.extend([auxValue])
     while (k<N):
         s=0
         k+=1
         F=F_NR(Integrals,z)
         dF=J_NR(z)
         #Newton-Raphson
         DetJ=np.abs(np.linalg.det(dF))
         if DetJ<1e-2:    #very close to singular matrix
             dz = -np.linalg.pinv(dF).dot(F)
             s=1
         else:
             dz = -np.linalg.inv(dF).dot(F)
#**********************
         #condition max and min value for dx
         dz,condwz,log_condwz=LimitesZiWi(z,dz,delta,k)
         z=z+dz
#**********************
# ---------Print of Xis-----
         auxValue='%2.0i' % k #iteration
         auxValue+='\t%4.2e' % np.sum(np.abs(F)) #maxdz
         auxValue+='\t%4.2e' % np.max(np.abs(dz)) #maxdz
         auxValue+='\t%.2e' % DetJ #deter
```

```
        auxValue+='\t%.0i' % s #singular
        auxValue+='\t%.0i' % condwz #x condition
        auxValue+= '\t'+'\t'.join(["{:10.2e}".format(elem) for elem
    in dz])
        auxValue+= '\t'+'\t'.join(["{:10.5f}".format(elem) for elem
    in z])
        logging.extend([auxValue])
        plot_cond=0
        if condwz==1 and plot_cond==1:
            logging.extend([log_condwz])
# --------Print of Xis-------
        if (np.max(np.abs(dz)) < TOL):
            logging.extend(['\n\t\t\tTolerance reached in %.0i' % k
    \
                + ' iteration\n
    ------------------------------------------------------------------'
    \
                +"\nEnd of Newton-Raphson Iteration for wi's and zi
    's Estimation\n"\
                +'
    ------------------------------------------------------------------\
    n\n'])
            return z, logging
        elif N-k==1:
            print("Max Iteration reached w/o convergence in NR for
    wi's and zi's \n")
            print('\tMaximum dz: %10.2e' %np.max(np.abs(dz)))
            print('\tMaximum Error:%10.2e'%np.max(np.abs(F)))
            if np.max(np.abs(dz))>1e-4 and np.max(np.abs(F))>1e-4:
                z=z*np.nan
            logging.extend(['\n
    ------------------------------------------------------------------'
    \
                           +"\nERROR of Newton-Raphson Iteration
    for wi's and zi's Estimation\n"\
                           +'
    ------------------------------------------------------------------\
    n\n'])
            return z, logging


def F_NR(Integrals,x):
    pontos=np.int(len(Integrals)/2)
    y=np.zeros(pontos*2)
    for j in range(2*pontos):
        aux=0
        for i in range(pontos):
```

```
            aux=x[i]*x[i+pontos]**j+aux
        y[j]=aux-Integrals[j]
    return y

def J_NR(x):
    pontos=np.int(len(x)/2)
    y=np.zeros((pontos*2,pontos*2))
    for j in range(2*pontos):
        for i in range(pontos):
            y[j,i]=x[i+pontos]**j
            y[j,i+pontos]=j*x[i]*x[i+pontos]**(j-1)
    return y

def LimitesZiWi(z,dz,delta,k):
##########Conditioniting for next iteration
### Since sum(wi)=1 due to 1st integral and must be positive -
   physical meaning
### Also, max value for any zi is delta and min is zero.
        auxValue=''
        znew=z+dz
        dz1=copy.deepcopy(dz)
        condwz=0
        pontos=int(len(z)/2)
        if np.min(znew[:pontos])<0 or np.max(znew[:pontos])>1 \
            or np.min(znew[pontos:])<0 or np.max(znew[pontos:])>
   delta:
            zmax=[1]*pontos
            zmax.extend([delta]*pontos)
            dz_maxPos=np.array(zmax)-np.array(z) #max dz positive
            dz_minNeg=np.array(z)*-1             #min dz negative

            c_pos=dz_maxPos-np.array(dz)    #if negative is too
   large
            d_neg=-np.array(dz)-dz_minNeg    #if negative is too
   large

            if c_pos.min()<0 or d_neg.min()<0:
                condwz=1
                if k<10:
                    factor=0.5
                else:
                    factor=5/k #reducing factor to look in
   neihboorhood
                for i in range(pontos*2):
                    ##if dz is bigger than possible, it will take
   factor% of possibe
                    if dz[i]>dz_maxPos[i]:
```

```
                        dz1[i]=dz_maxPos[i]*factor
                    if dz[i]<dz_minNeg[i]:
                        dz1[i]=dz_minNeg[i]*factor
            #### Log for dx from Newton-Raphson
            auxValue+='\t\t\t\t\t'
            auxValue+= '\t'+'\t'.join(["{:10.2f}".format(elem) for
    elem in dz])
            auxValue+= '\t'+'\t'.join(["{:10.2f}".format(elem) for
    elem in z+dz])
        return dz1, condwz, auxValue

def Check(delta,Integrals,fin,ini):
    print('
    ------------------------------------------------------------------------
    ')
    print('Validation of Integrals with Quadrature points')
    print('for Delta=',delta)
    print('
    ------------------------------------------------------------------------
    ')
    pontos=np.int(len(ini)/2)
    for j in range(2*pontos):
        deltaInte=F_NR(Integrals,fin)
        print(j,'\tErro %.4f' % (100*deltaInte[j]/Integrals[j]),'%\
    t','sum( wi*zi^%.0f' %j,'): %.2e' % (deltaInte[j]+Integrals[j]),
    '\tIntegral: %.2e' % Integrals[j])
    print('\nResults:')
    print('Variable \tFinal \t\t\tInitial') #\tTrue')
    for i in range(2*pontos):
        if i<pontos:
            text= '\tw' + str(i) + '\t\t%.6f' % + fin[i] + '\t\t%.4
    f' % + ini[i]   #+ '\t\t%.4f' % + gab[i]
        else:
            text= '\tz' + str(np.int(i-pontos)) + '\t\t%.6f' % +
    fin[i] +'\t\t%.4f' % + ini[i] #+ '\t\t%.4f' % + gab[i]
        print(text)

def Check_log(delta,Integrals,fin,ini):
    logging=[]
    logging.extend(['
    ------------------------------------------------------------------------\
    n' \
        +'Validation of Integrals with Quadrature points' \
        +'\nfor Delta=%.5f' % delta \
        +'\n
    ------------------------------------------------------------------------
    '])
```

```
    pontos=np.int(len(fin)/2)
    for j in range(2*pontos):
        deltaInte=F_NR(Integrals,fin)
        logging.extend([str(j) +'\tErro\t %.4f' % (100*deltaInte[j
   ]/Integrals[j]) +'%' \
                +"\tsum( wi*zi^%.0f" %j +'): \t%.2e' % (deltaInte[j
   ]+Integrals[j]) \
                +'\tIntegral:\t %.2e' % Integrals[j]])
    logging.extend(['\nResults: \nVariable \tFinal \t\t\tInitial'])
    for i in range(2*pontos):
        if i<pontos:
            logging.extend(['\tw' + str(i) + '\t\t%.6f' % + fin[i]
   + '\t\t%.4f' % + ini[i]])
        else:
            logging.extend(['\tz' + str(np.int(i-pontos)) + '\t\t
   %.6f' % + fin[i] +'\t\t%.4f' % + ini[i]])
    return logging


def Print_result(delta,fin, head):
    logging=[]
    pontos=np.int(len(fin)/2)
    aux_val='%.3f' % delta
    aux_val_wi=''
    if head==1:
        aux_text='Delta'
        aux_text_wi=' '
        for i in range(pontos):
            aux_text+='\tz%.0i' % (i+1)
            aux_text_wi+='\tw%.0i' % (i+1)
        aux_text+=aux_text_wi
        logging.extend(['\n\n\n\n'])
        logging.extend(['------------------------'])
        logging.extend([aux_text])
    for i in range(pontos):
        aux_val+='\t%.4f' % fin[i+pontos]
        aux_val_wi+='\t%.4f' % fin[i]
    aux_val+=aux_val_wi
    logging.extend([aux_val])
def PrintlastTable(delta,phi, netta,C_f,zi_f,MWi_f,z):
    print('\n\n###______RESULTS_OF_SHIBATA_CALCULATION__________###
   ')
    print('delta: %.4f' % delta)
    print('phi: %.1f' % phi)
    print('netta: %.1f' % netta)
    print('\n\n\tCarbon \t\tZi \t\t\t\tMWi \t\t\twi(Shibata) \tzi(
   Shibata)') #\tTrue')
```

```
    for i in range(pontos):
            text= '\t#' + str(np.round(C_f[i],1)) + '\t\t%.6f' % +
   zi_f[i] + '\t\t%.4f' % + MWi_f[i] + '\t\t%.4f' % + z[i] + '\t\t\
   t%.4f' % + z[i+pontos]
            print(text)
    print('\t_____________________________________
   ____________________________________________')
    text= '\tSum\t\t\t' + '%.6f' % + np.sum(zi_f) + '\t\t%.4f' % +
   (np.sum(zi_f*MWi_f)/np.sum(zi_f))   #+ '\t\t%.4f' % + gab[i]
    print(text)
    text= '\tLab\t\t\t' + '%.6f' % + Zi_plus + '\t\t%.4f' % +
   MW_plus   #+ '\t\t%.4f' % + gab[i]
    print(text)

def LoglastTable(delta,phi, netta,C_f,zi_f,MWi_f,z):
    logging=[]
    logging.extend(['\n\n'])
    logging.extend(['###
   ______RESULTS_OF_SHIBATA_CALCULATION__________###'])
    logging.extend(['delta: %.4f' % delta])
    logging.extend(['phi: %.1f' % phi])
    logging.extend(['netta: %.1f' % netta])
    logging.extend(['\n\n'])
    logging.extend(['\tCarbon \t\tZi \t\t\t\tMWi \t\t\twi(Shibata)
   \tzi(Shibata)']) #\tTrue')
    for i in range(pontos):
            text= '\t#' + str(np.round(C_f[i],1)) + '\t\t%.6f' % +
   zi_f[i] + '\t\t%.4f' % + MWi_f[i] + '\t\t%.4f' % + z[i] + '\t\t\
   t%.4f' % + z[i+pontos]
            logging.extend([text])
    logging.extend(['\t_____________________________________
   ____________________________________________'])
    text= '\tSum\t\t\t' + '%.6f' % + np.sum(zi_f) + '\t\t%.4f' % +
   (np.sum(zi_f*MWi_f)/np.sum(zi_f))   #+ '\t\t%.4f' % + gab[i]
    logging.extend([text])
    text= '\tLab\t\t\t' + '%.6f' % + Zi_plus + '\t\t%.4f' % +
   MW_plus   #+ '\t\t%.4f' % + gab[i]
    logging.extend([text])
    return logging
```

Listing B.3: Auxilary Function for Quadrature Points Calculation